East Tennessee State University

Digital Commons @ East Tennessee State University

ETSU Faculty Works

Faculty Works

7-1-2021

New Asian and Nearctic Hypechiniscus species (Heterotardigrada: Echiniscidae) signalize a pseudocryptic horn of plenty

Piotr Gasiorek
Uniwersytet Jagielloński

Artur Oczkowski
Uniwersytet Jagielloński

Brian Blagden
Uniwersytet Jagielloński

Reinhardt M. Kristensen
Statens Naturhistoriske Museum

Paul J. Bartels
Warren Wilson College

See next page for additional authors

Follow this and additional works at: https://dc.etsu.edu/etsu-works

Citation Information

Gasiorek, Piotr; Oczkowski, Artur; Blagden, Brian; Kristensen, Reinhardt M.; Bartels, Paul J.; Nelson, Diane R.; Suzuki, Atsushi C.; and Michalczyk, Łukasz. 2021. New Asian and Nearctic Hypechiniscus species (Heterotardigrada: Echiniscidae) signalize a pseudocryptic horn of plenty. *Zoological Journal of the Linnean Society*. Vol.192(3). 794-852. https://doi.org/10.1093/zoolinnean/zlaa110 ISSN: 0024-4082

This Article is brought to you for free and open access by the Faculty Works at Digital Commons @ East Tennessee State University. It has been accepted for inclusion in ETSU Faculty Works by an authorized administrator of Digital Commons @ East Tennessee State University. For more information, please contact digilib@etsu.edu.

New Asian and Nearctic Hypechiniscus species (Heterotardigrada: Echiniscidae) signalize a pseudocryptic horn of plenty

Copyright Statement

© 2020 The Linnean Society of London, Zoological Journal of the Linnean Society, 2021, 192, 794–852 794 Zoological Journal of the Linnean Society, 2021, 192, 794–852. With 29 figures. This is an Open Access article distributed under the terms of the Creative Commons AttributionNonCommercial License (http://creativecommons.org/licenses/by-nc/4.0/), which permits non-commercial re-use, distribution, and reproduction in any medium, provided the original work is properly cited. For commercial re-use, please contact journals.permissions@oup.com

Creative Commons License

This work is licensed under a Creative Commons Attribution-NonCommercial 4.0 International License

Creator(s)

Piotr Gasiorek, Artur Oczkowski, Brian Blagden, Reinhardt M. Kristensen, Paul J. Bartels, Diane R. Nelson, Atsushi C. Suzuki, and Łukasz Michalczyk

This article is available at Digital Commons @ East Tennessee State University: https://dc.etsu.edu/etsu-works/9549

Zoological Journal of the Linnean Society, 2021, **192**, 794–852. With 29 figures.

New Asian and Nearctic *Hypechiniscus* species (Heterotardigrada: Echiniscidae) signalize a pseudocryptic horn of plenty

PIOTR GĄSIOREK[1*], ARTUR OCZKOWSKI[1], BRIAN BLAGDEN[1], REINHARDT M. KRISTENSEN[2], PAUL J. BARTELS[3], DIANE R. NELSON[4], ATSUSHI C. SUZUKI[5] and ŁUKASZ MICHALCZYK[1*]

[1]*Institute of Zoology and Biomedical Research, Jagiellonian University, Gronostajowa 9, 30–387 Kraków, Poland*
[2]*Natural History Museum of Denmark, University of Copenhagen, Universitetsparken 15, Copenhagen Ø DK-2100, Denmark*
[3]*Department of Biology, Warren Wilson College, Asheville, NC 28815, USA*
[4]*Department of Biological Sciences, East Tennessee State University, Johnson City, TN 37614, USA*
[5]*Department of Biology, Keio University, Yokohama 223–8521, Japan*

Received 15 June 2020; revised 18 August 2020; accepted for publication 25 August 2020

The cosmopolitan echiniscid genus *Hypechiniscus* contains exclusively rare species. In this contribution, by combining statistical morphometry and molecular phylogeny, we present qualitative and quantitative aspects of *Hypechiniscus* diversity, which remained hidden under the two purportedly cosmopolitan species: *H. gladiator* and *H. exarmatus*. A neotype is designated for *H. gladiator* from Creag Meagaidh (Scotland), and an informal re-description is provided for *H. exarmatus* based on animals from Creag Meagaidh and the Isle of Skye (Inner Hebrides). Subspecies/forms of *H. gladiator* are suppressed due to the high developmental variability of the *cirrus dorsalis*. At the same time, four species of the genus are described: ***H. daedalus* sp. nov.** from Roan Mountain and the Great Smoky Mountains (Southern Appalachian Mountains, USA), ***H. flavus* sp. nov.** and ***H. geminus* sp. nov.** from the Yatsugatake Mountains (Honshu, Japan), and ***H. cataractus* sp. nov.** from the Malay Archipelago (Borneo and the Moluccas). Dorsal and ventral sculpturing, together with morphometric traits, are shown to be the key characters that allow for the phenotypic discrimination of species within the genus. Furthermore, the morphology of *Hypechiniscus* is discussed and compared to that of the most similar genera, *Pseudechiniscus* and *Stellariscus*. Finally, a diagnostic key to all recognized *Hypechiniscus* species is provided.

ADDITIONAL KEYWORDS: convergence – crypsis – DNA barcoding – species delimitation – taxonomic drawing.

INTRODUCTION

Progress in tardigrade classification is hampered by a history of deceptive pitfalls. Many species that were once considered cosmopolitan and extremely variable are no longer seen as such [see Bertolani & Rebecchi (1993) for the oldest example in the literature based on the genus *Macrobiotus* and the gradually amassed evidence for other taxa: Claxton (1998) for *Minibiotus*, Faurby *et al*. (2011) for *Echiniscoides*, Lisi (2011) for *Doryphoribius*, Michalczyk *et al*. (2012) for *Milnesium*, Gąsiorek *et al*. (2016, 2018a) for *Hypsibius* and *Mesocrista*, Guidetti *et al*. (2016, 2019) for *Richtersius* and *Paramacrobiotus*, Stec *et al*. (2018) for *Ramazzottius*, Santos *et al*. (2019) for *Batillipes* and Cesari *et al*. (2020) for *Pseudechiniscus*]. On the other hand, other species do appear to be widely distributed and morphologically variable [see Cesari *et al*. (2016) for

*Corresponding authors. E-mail: piotr.lukas.gasiorek@gmail.com; LM@tardigrada.net
[Version of record, published online 11 December 2020; http://zoobank.org/ urn:lsid:zoobank.org:pub:A8DBCFD2-DAA6-44D3-A2E9-974C7575039C]

© 2020 The Linnean Society of London, *Zoological Journal of the Linnean Society*, 2021, **192**, 794–852
This is an Open Access article distributed under the terms of the Creative Commons Attribution-NonCommercial License (http://creativecommons.org/licenses/by-nc/4.0/), which permits non-commercial re-use, distribution, and reproduction in any medium, provided the original work is properly cited. For commercial re-use, please contact journals.permissions@oup.com

Downloaded from https://academic.oup.com/zoolinnean/article/192/3/794/6030998 by guest on 18 April 2022

Acutuncus and Gąsiorek *et al*. (2019a) for *Echiniscus*]. Advancement in our understanding of tardigrade intraspecific variability (Kosztyła *et al*., 2016; Gąsiorek *et al*., 2019b; Jackson & Meyer, 2019; Morek *et al*., 2019) and the utilization of species delimitation methods (Stec *et al*., 2018; Cesari *et al*., 2020) was possible thanks to the acquisition of molecular data (Cesari *et al*., 2009, 2013). In short, DNA barcoding has disembroiled systematic doubts concerning tardigrade lineages that had accumulated over decades of classical taxonomy (Jørgensen *et al*., 2018).

In this paper, we investigate the genus *Hypechiniscus* Thulin, 1928, yet another case of undisclosed tardigrade diversity within the class Heterotardigrada. *Hypechiniscus* was distinguished from *Echiniscus*, along with *Bryodelphax*, by differences in the dorsal plate morphology (Thulin, 1928). This genus was at first represented by two species, *H. gladiator* (Murray, 1905) (with a single centrodorsal cirrus) and *H. exarmatus* (Murray, 1907) (without the cirrus), described from Scotland and the adjacent Shetland Islands in the beginning of the 20th century. Despite the clear morphological difference in the state of the centrodorsal cirrus, *H. exarmatus* was long considered a form of *H. gladiator* until Kristensen (1987) elevated it to a species rank based on the morphology of claw spurs (smaller in *H. exarmatus* and larger in *H. gladiator*) and habitat preferences (soil and aquatic niches vs. mosses, respectively). Nearly seven decades after the erection of *H. gladiator*, Robotti (1972) described *H. papillifer* from Italy (originally *Echiniscus papillifer*), and Iharos (1973) described three forms of *H. gladiator* from North Korea, now recognized as subspecies: *bigladii*, *fissigladii* and *spinulosa*. In the light of the findings on the ontogenetic and interpopulation variability of heterotardigrades (Gąsiorek *et al*. 2019b; Santos *et al*. 2019), these three subspecies are questionable. The most recently delineated species, *H. fengi* Sun & Li, 2013, was discovered in China. Thus, the genus currently comprises four species, including one divided into four subspecies. *Hypechiniscus* is distributed worldwide, but its records are rare and scattered (McInnes, 1994). *Hypechiniscus papillifer* and *H. fengi* are known only from their type localities, whereas the two oldest species, *H. gladiator* and *H. exarmatus*, each have been reported from different zoogeographic realms (Palaearctic, Nearctic and Australasia), which may suggest that these two taxa represent species complexes.

By combining morphological, morphometric (statistical) and genetic analyses we identify four new species, formally re-describe the nominal species for the genus, provide descriptions of the remaining known species, amend the generic diagnosis, and invalidate the superfluous subspecies/forms. The cuticular sculpturing of *Hypechiniscus* is reviewed and demonstrated as being of crucial significance in the identification of species, as was discovered in other heterotardigrade groups (e.g. Kristensen & Hallas, 1980; Dastych *et al*., 1998; Grobys *et al*., 2020). Given that the genus shares many morphological similarities with the genus *Pseudechiniscus* Thulin, 1911, which was recently revised from multiple perspectives (Cesari *et al*., 2020; Grobys *et al*., 2020; Tumanov, 2020), and because key problems associated with their taxonomy are similar, we compare the two taxa with each other and with *Stellariscus* Gąsiorek *et al*., 2018c, a potential sister-genus of *Hypechiniscus*. Finally, a diagnostic key to all currently recognized species of *Hypechiniscus* is provided.

MATERIAL AND METHODS

Sampling, data collection and terminology

More than 500 individuals of *Hypechiniscus* were extracted from 21 moss and lichen samples collected throughout the world [details in Table 1; see Stec *et al*. (2015) for the extraction protocol]. After extraction, the animals were divided into three groups to be used in different analyses: (1) qualitative and quantitative morphology investigated with light contrast microscopy (LCM), specifically phase contrast (PCM) and Nomarski differential interference contrast microscopy (NCM), (2) qualitative morphology with scanning electron microscopy (SEM) and (3) DNA sequencing. The terminology for sclerotized structures follows Kristensen (1987), with the reservation that the 'dorsomedian cirrus', i.e. the synapomorphy of some *Hypechiniscus* spp., is termed herein as '*cirrus dorsalis*', consisting of the base and a flexible flagellum. The *gladiator* group is the taxonomic term embracing all *Hypechiniscus* spp. with *cirrus dorsalis*, whereas the *exarmatus* morphogroup includes all *Hypechiniscus* spp. without *cirrus dorsalis*.

Abbreviations used for scientific institutions: CU, University of Catania, Italy. NMNS, National Museum of Nature and Science, Japan. NMS, National Museum of Scotland, UK. UJ, Jagiellonian University, Poland. NHMD, Natural History Museum of Denmark, Denmark.

Establishing the neotype series for *Hypechiniscus gladiator*

Murray (1905) did not designate a type series for *H. gladiator*, but the four individuals (and an exuvia without the *cirrus dorsalis*, thus presumably representing *H. exarmatus*) isolated from the samples he collected from Loch Morar – subsequently mounted on slides and deposited in the Royal Scottish Museum in Edinburgh (Morgan, 1977) – constitute the material used by Murray (1907). However, because Loch Ness was clearly designated as the type locality in Murray (1905), animals from Loch Morar cannot serve as

Downloaded from https://academic.oup.com/zoolinnean/article/192/3/794/6030998 by guest on 18 April 2022

Table 1. List of populations used in integrative analyses. Types of analyses: (LCM) imaging and morphometry in PCM/NCM, (SEM) imaging in SEM, (DNA) DNA sequencing. Number in each analysis indicates how many specimens were utilized in a given method (a, adults; v, exuvia; j, juveniles; l, larvae)

Species	Sample code	Coordinates altitude	Locality	Sample type	Collector	Analyses		
						LCM	SEM	DNA
Hypechiniscus daedalus	US.036	36°07'17"N 82°05'37"W 1239 m a.s.l.	USA, Tennessee, Roan Mountain	moss from tree bark	Diane Nelson	6a + 1j	–	3a
	US.041	35°35'13"N 83°04'31"W 1514 m a.s.l.	USA, North Carolina, Purchase Knob	moss from tree trunk	Nate Gross, Mackenzie McClay	10a + 1l	4a	3a
Hypechiniscus geminus	JP.006	35°56'32"N 138°20'46"E 2510 m a.s.l.	Japan, Mt. Amigasa	moss from rocks and fallen tree trunks	Atsushi C. Suzuki	33a + 5j + 2l	2a	ca. 30a
Hypechiniscus gladiator	GB.033	57°08'49"N 4°40'42"W 20 m a.s.l.	Scotland, Loch Ness, Fort Augustus	moss from rock off the lake shore	Brian Blagden	55a + 4v + 11j + 1l	30a	10a
	GB.058	56°57'33.03"N 4°34'04.5"W 624 m a.s.l.	Scotland, Creag Meagaidh, Lochan a' Choire	moss from rock	Brian Blagden	34a + 4j	10a	4a
	GB.110	57°15'04.9"N 6°16'11.3"W 107 m a.s.l.	Scotland, Inner Hebrides, Isle of Skye	moss from rock	Brian Blagden	13a	–	-
	IS.019	64°15'59"N 21°04'46"W 122 m a.s.l.	Iceland, Thingvellir	moss from soil	Małgorzata Mitan, Małgorzata Osielczak	48a	–	4a
	IT.116	45°28'59"N 7°22'17"E 1854 m a.s.l.	Italy, Lago di Teleccio	moss from rock	Piotr Gąsiorek, Witold Morek	2a	–	–
	IT.132	45°28'47"N 7°22'22"E 1709 m a.s.l.	Italy, Vallone di Piantonetto	moss from rock	Piotr Gąsiorek, Witold Morek	2a	–	–
	SE.018	56°40'01"N 16°36'12"E 33 m a.s.l.	Sweden, Öland, Gråborg	moss from rock	Reinhardt M. Kristensen	4a	–	–

Downloaded from https://academic.oup.com/zoolinnean/article/192/3/794/6030998 by guest on 18 April 2022

Table 1. Continued

Species	Sample code	Coordinates altitude	Locality	Sample type	Collector	Analyses		
						LCM	SEM	DNA
Hypechiniscus cataractus	ID.865	0°39'52"N 127°24'19"E 1561 m a.s.l.	Indonesia, Moluccas, Tidore, Gunung Kiematubu	moss from tree bark	Piotr Gąsiorek	3a	–	–
	ID.870	0°39'51"N 127°24'31"E 1368 m a.s.l.	Indonesia, Moluccas, Tidore, Gunung Kiematubu	moss from tree bark	Piotr Gąsiorek	1a	–	1a
	ID.874	0°39'55"N 127°24'38"E 1211 m a.s.l.	Indonesia, Moluccas, Tidore, Gunung Kiematubu	moss and lichen from tree bark	Piotr Gąsiorek	3a	–	1a
	MY.041	4°57'N 118°09'E 700–800 m a.s.l.	Malaysia, Borneo, Sabah, Gunung Silam	moss from tree bark	Piotr Gąsiorek	4a	–	2a
	MY.802	1°43'27"N 110°28'16"E 67 m a.s.l.	Malaysia, Borneo, Sarawak, Bako Peninsula	moss from tree bark	Piotr Gąsiorek, Artur Oczkowski	16a + 4j	–	–
	MY.803	1°43'27"N 110°28'16"E 67 m a.s.l.	Bako Peninsula, Sarawak, Borneo, Malaysia	moss from tree bark	Piotr Gąsiorek, Artur Oczkowski	9a + 2j	–	–
	MY.805	1°43'29"N 110°28'10"E 90 m a.s.l.	Bako Peninsula, Sarawak, Borneo, Malaysia	moss from soil	Piotr Gąsiorek, Artur Oczkowski	18a + 3j	10a	6a
Hypechiniscus exarmatus	GB.061	56°57'03"N 4°36'09"W 1100 m a.s.l.	Scotland, Creag Meagaidh	lichen from rock	Brian Blagden	7a	–	1a
	GB.110	57°15'04.9"N 6°16'11.3"W 107 m a.s.l.	Scotland, Inner Hebrides, Isle of Skye	moss from rock	Brian Blagden	6a	–	1a
Hypechiniscus flavus	JP.006	35°56'32"N 138°20'46"E 2510 m a.s.l.	Japan, Mt. Amigasa	moss from rocks and fallen tree trunks	Atsushi C. Suzuki	10a + 4j	4a	ca. 30a
	JP.008	36°03'31"N 138°20'43"E 2127 m a.s.l.	Japan, Mugikusa Pass	moss from rocks and fallen tree trunks	Atsushi C. Suzuki	54a + 20j + 1l	4a	–

Downloaded from https://academic.oup.com/zoolinnean/article/192/3/794/6030998 by guest on 18 April 2022

syntypes and a neotype needs to be established. In accordance with the International Code of Zoological Nomenclature (1999), the neotype and the new type (neotype) locality (Scotland, Creag Meagaidh) are designated on the following grounds: the description of the species in question is vague and both phenotypic and genotypic characters need to be redefined, allowing an unambiguous identification of the taxon (art. 75.3.1–3), the type series does not exist (art. 75.3.4), the neotype corresponds with the original description (art. 75.3.5), one of the populations used in the redescription was collected precisely at the type locality chosen by Murray (art. 75.3.6) and the neotype is deposited in a recognized scientific institution (art. 75.3.7). Even though the GB.033 population is geographically closer to the original type locality, we chose Creag Meagaidh, which is *c.* 20 km southwards, as the new type locality for *H. gladiator,* because specimens representing the population GB.058 (Creag Meagaidh) are preserved in a better condition, allowing us to designate a good-quality specimen for the neotype. Nevertheless, the population GB.033 (Loch Ness) is included in the redescription as an additional locality, because we confirm that populations originating from both places are conspecific.

Attempts to redescribe *Hypechiniscus exarmatus* and *Hypechiniscus papillifer*

We undertook sampling in the Shetland Islands, the type locality of *H. exarmatus* (Mainland, Northmaven, Ronas Hill; see Murray, 1907), but without success. Consequently, a designation of a neotype for this species was not possible as we could not ascertain whether the populations from the Hebrides and mainland Scotland represent the same species as from the Shetland Islands. We also sampled in the vicinity of Lago di Teleccio (Vallone di Piantonetto, Graian Alps, Italy), the type locality of *H. papillifer* (Robotti, 1972), yet again with a negative outcome.

Microscopy and imaging

Specimens for light microscopy and morphometry were first air-dried on microscope slides, subsequently mounted in a small drop of Hoyer's medium to ensure they were fully stretched, and finally examined under a Nikon Eclipse 50i PCM associated with a Nikon Digital Sight DS-L2 digital camera and Olympus BX 51 NCM. Specimens for imaging in the SEM were prepared according to Stec *et al*. (2015) and examined in Versa 3D DualBeam SEM at the ATOMIN facility of the Jagiellonian University. All figures were assembled in Corel Photo-Paint X8. For deep structures that could not be fully focused in a single LCM photograph, a series of seven to ten images was taken every *c.* 0.2 mm of vertical focusing and then assembled manually in Corel Photo-Paint into a single deep-focus image. General schematics of the dorsal and ventral cuticle for all *Hypechiniscus* spp. were drawn, based on observations of optimally stretched and dorsoventrally oriented specimens under 1000× magnification in LCM.

Morphometry and statistics

All measurements were performed using PCM. Sample size was adjusted following recommendations by Stec *et al*. (2016) wherever the number of individuals was sufficiently high. Structures were measured only when oriented properly and not broken or deformed. Body length was measured from the anterior to the posterior end of the body, excluding the hind legs. The *sp* index is the ratio of the length of a given structure to the length of the scapular plate (Dastych, 1999). The *bs* index is the ratio between the body length and the maximal body width, only when a specimen is fully relaxed and oriented dorsoventrally (Gąsiorek *et al*., 2018c). Morphometric data were handled using the Echiniscoidea v.1.2 template available from the Tardigrada Register, https://tardigrada.net/register (Michalczyk & Kaczmarek, 2013). Fifteen standard absolute traits were measured and one relative trait (cirrus *A* length/body length ratio) was calculated for adult females and males of all analysed species of *Hypechiniscus*. *Hypechiniscus exarmatus* was excluded from interspecific comparisons due to an insufficient number of individuals. To allow for a comparison of all species of the *gladiator* and *exarmatus* groups, the length of *cirrus dorsalis* was not considered in the principal component analysis (PCA), which was performed in RStudio (RStudio Team, 2015) with the prcomp function. To completely eliminate body-size effects, Thorpe normalizations are required (Bartels *et al*., 2011), but sample sizes for some species did not allow for this approach. Therefore, to minimize allometric effects, PCA included only the *sp* values, with the exception of the body and scapular plate lengths. Approximately 13% (♀♀) and 15% (♂♂) of the measurements could not be made due to unfavourably oriented structures (mostly claw spurs). To avoid losing sample size for the other traits, the missing data were replaced by the median values of each variable within a given population, which for small datasets is usually similar to using mean values (Refaat, 2007). To account for divergent dimensions of the measured traits, all variables were scaled to unit variance and zero mean. The results were visualized using the package ggfortify (v.0.4.1; Tang *et al*., 2016). As the first and the second principal components, comprising cephalic appendages and claws, explained the predominant portion of variance (65% for ♀♀ and 63% for ♂♂), they were chosen for one-way ANOVA tests followed by post-hoc Tukey's testing to check for morphometric differences between the species. The assumptions relating to homogeneity

Downloaded from https://academic.oup.com/zoolinnean/article/192/3/794/6030998 by guest on 18 April 2022

of variances and the normality of distributions were checked by applying Levene's and Shapiro–Wilk tests, respectively, using car package (Fox & Weisberg, 2011). In all cases, the assumptions of ANOVA were met ($P >> 0.05$), with the exclusion of the *cirrus internus* length for ♂♂, for which the variances were always heterogeneous, irrespective of discarded outliers. The Benjamini–Hochberg correction was applied to the α-level to account for multiple testing. Box plot charts were generated using the package ggpubr (https://CRAN.R-project.org/package=ggpubr).

Genotyping and phylogenetics

DNA was extracted from individual animals following a Chelex 100 resin (Bio-Rad) extraction method (Casquet *et al*., 2012; Stec *et al*., 2015). Four DNA fragments were sequenced: the small ribosome subunit 18S rRNA, the large ribosome subunit 28S rRNA, the internal transcribed spacer ITS1 and the cytochrome *c* oxidase subunit I *COI*. Despite trying various sets of primers (LCO1490+HCO2198, LCO1490+HCOoutout, jjLCO1490+jjHCO2198 and bcdF01+bcdR04), only for *H. exarmatus* were we able to sequence the *COI*. All fragments were amplified and sequenced according to the protocols described in Stec *et al*. (2015); primers and original references for specific PCR programmes are listed in Table 2. GenBank accession numbers for all species are provided in Table 3. The sequences 18S rRNA, 28S rRNA and ITS1 were aligned with sequences (MW077138–40) for *Acanthechiniscus islandicus* (Richters, 1904) as the outgroup, using the Q-INS-i strategy in MAFFT v.7 (Katoh *et al*., 2002; Katoh & Toh, 2008). The aligned fragments were edited and checked manually in BioEdit with the gaps left intact.

ModelFinder (Kalyaanamoorthy *et al*., 2017) under the Akaike information criterion (AIC) and corrected AIC (AICc) were used to find the best substitution models for three predefined partitions (Chernomor *et al*., 2016). The programme indicated the following models: K2P+G4 (18S rRNA), TIM2e+I (28S rRNA) and TVM+F+I (ITS1). Maximum likelihood (ML) topologies were constructed using IQ-TREE (Nguyen *et al*., 2015; Trifinopoulos *et al*., 2016). The strength of support for the internal nodes of the ML construction was measured using 1000 ultrafast bootstrap replicates (Hoang *et al*., 2018).

Table 2. Primers and references for specific protocols for amplification of the four DNA fragments sequenced in the study

DNA fragment	Primer name	Primer direction	Primer sequence (5'-3')	Primer source	PCR programme*
18S rRNA	18S_Tar_Ff1	forward	AGGCGAAACCGCGAATGGCTC	Stec *et al*. (2017)	Zeller (2010)
	18S_Tar_Rr2	reverse	CTGATCGCCTTCGAACCTCTAACTTTCG	Gąsiorek *et al*. (2017)	
28S rRNA	28S_Eutar_F	forward	ACCCGCTGAACTTAAGCATAT	Gąsiorek *et al*. (2018b)	Mironov *et al*. (2012)
	28SR0990	reverse	CCTTGGTCCGTGTTTCAAGAC	Mironov *et al*. (2012)	
ITS1	ITS1_Echi_F	forward	CCGTCGCTACTACCGATTGG	Gąsiorek *et al*. (2019a, b)	Wełnicz *et al*. (2011)
	ITS1_Echi_R	reverse	GTTCAGAAAACCCTGCAATTCACG		
COI	LCO1490	forward	GGTCAACAAATCATAAAGATATTGG	Folmer *et al*. (1994)	Michalczyk *et al*. (2012)
	HCO2198	reverse	TAAACTTCAGGGTGACCAAAAAATCA		

* All PCR programmes are also provided in Stec *et al*. (2015).

Table 3. GenBank accession numbers for the *Hypechiniscus* spp. analysed in this work, bold font indicates new sequences

Species	18S rRNA	28S rRNA	ITS1	*COI*
Hypechiniscus gladiator	**MT809239–43**	**MT809202–3**	**MT809191–4**	–
Hypechiniscus exarmatus	**MT809238**	**MT809201**	**MT809190**	**MT801042**
Hypechiniscus daedalus	**MT809236–7**	**MT809199–200**	**MT809186–9**	–
*Hypechiniscus flavus**	HM193377	HM193394	–	HM193410
*Hypechiniscus geminus**	HM193378	HM193395	–	HM193411
Hypechiniscus cataractus	**MT809232–5**	**MT809195–8**	**MT809179–85**	–

*Sequences of *H. flavus* and *H. geminus* were reported in Jørgensen *et al*. (2011) as belonging to *H. exarmatus* and *H. gladiator*, respectively.

© 2020 The Linnean Society of London,

Downloaded from https://academic.oup.com/zoolinnean/article/192/3/794/6030998 by guest on 18 April 2022

Using PartitionFinder v.2.1.1 (Lanfear *et al.*, 2016) under the AIC, the best substitution model and partitioning scheme was chosen for posterior phylogenetic analysis. As the best-fit partitioning scheme, PartitionFinder suggested the retention of three separately predefined partitions, and the best-fit models were: GTR+I+G (18S rRNA) and GTR+I (28S rRNA, ITS1). Bayesian inference (BI) marginal posterior probabilities were calculated using MrBayes v.3.2 (Ronquist & Huelsenbeck, 2003). Random starting trees were used and the analysis was run for ten million generations, sampling the Markov chain every 1000 generations. An average standard deviation of split frequencies of < 0.01 was used as a guide to ensure the two independent analyses had converged. TRACER v.1.3 (Rambaut *et al.*, 2014) was then used to ensure Markov chains had reached stationarity and to determine the correct 'burn-in' for the analysis, which was the first 10% of generations. The ESS values were greater than 200 and the consensus tree was obtained after summarizing the resulting topologies and discarding the 'burn-in'. All final consensus trees were viewed and visualized by FigTree v.1.4.3 available from https://tree.bio.ed.ac.uk/software/figtree.

Data deposition

Raw morphometric data underlying the description of the new species are deposited in the Tardigrada Register under www.tardigrada.net/register/0071.htm (*H. gladiator*), www.tardigrada.net/register/0072.htm (*H. daedalus*), www.tardigrada.net/register/0073.htm (*H. flavus*), www.tardigrada.net/register/0074.htm (*H. geminus*) and www.tardigrada.net/register/0075.htm (*H. cataractus*). DNA sequences are deposited in GenBank.

RESULTS

Phylogenetic position and phylogeny of *Hypechiniscus*

The concatenated 18S rRNA+28S rRNA+ITS1 phylogenetic reconstructions reveal congruent topologies in both BI and ML (Figs. 1–2), corroborating the monophyly of *Hypechiniscus* and the position

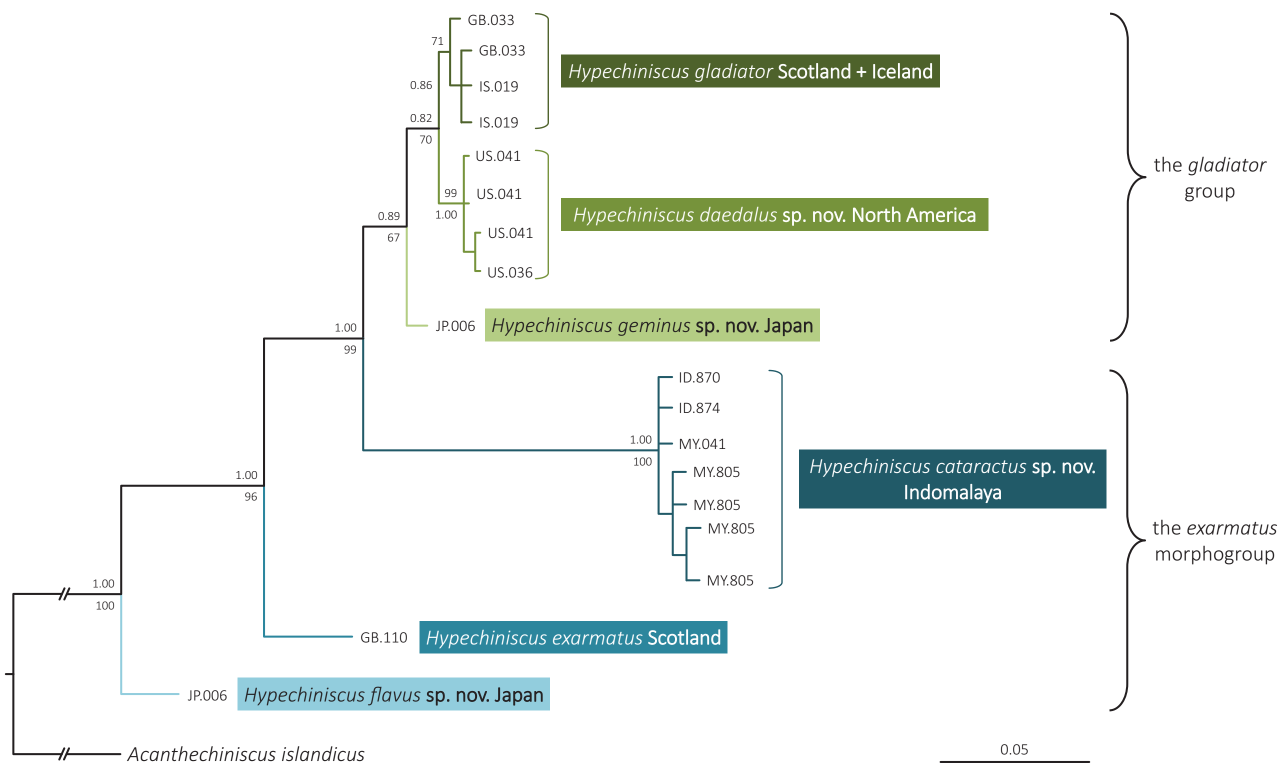

Figure 1. The concatenated 18S rRNA+28S rRNA+ITS1 consensus Bayesian phylogenetic tree of the six *Hypechiniscus* spp. analysed in this study; with *Acanthechiniscus islandicus* (Richters, 1904) as the outgroup. *Hypechiniscus gladiator* is represented by two populations: GB.033 and IS.019, as the population GB.058 was characterized by identical haplotypes as GB.033. Branch support is given as BI posterior probability values above branches and ML bootstrap values below branches. Maximum likelihood tree shared the topology with BI analysis.

Downloaded from https://academic.oup.com/zoolinnean/article/192/3/794/6030998 by guest on 18 April 2022

of the genus as a sister-taxon to *Testechiniscus*, *Diploechiniscus* and *Echiniscus*-like genera, as inferred in other recent echiniscid phylogenies (Gąsiorek & Michalczyk, 2020a; Fig. 2).

The three analysed species of the *gladiator* group form a clade (Fig. 1). The *exarmatus* group is paraphyletic with respect to the monophyletic *gladiator* group. The Palaearctic *H. gladiator* and new Nearctic species *H. daedalus* are the most closely related taxa. The new species *H. flavus*, exhibiting a unique yellow body coloration, is the sister-taxon to all other sequenced *Hypechiniscus* spp., which are whitish.

Species descriptions

Phylum: Tardigrada Doyère, 1840

Class: Heterotardigrada Marcus, 1927

Order: Echiniscoidea Richters, 1926

Family: Echiniscidae Thulin, 1928

Genus: *Hypechiniscus* Thulin, 1928

The *Hypechiniscus gladiator* group

Species: Hypechiniscus daedalus Gąsiorek, Oczkowski, Bartels, Nelson, Kristensen & Michalczyk, sp. nov.

Zoobank registration: 99D4BB97-5668-4C96-BBE3-CAB4FB52EA39.

Echiniscus gladiator; Durham (North Carolina, USA); Higgins (1960)

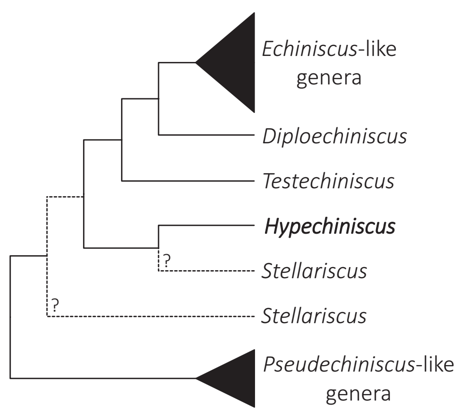

Figure 2. Phylogenetic position of *Hypechiniscus* in the crown-group Echiniscidae. The hypothetical position of *Stellariscus* based on the morphological and molecular analyses of Gąsiorek *et al.* (2018c), Cesari *et al.* (2020) and Gąsiorek & Michalczyk (2020a).

E. (*Hypechiniscus*) *gladiator*; Giles and Grayson County (Virginia, USA); Riggin (1962)

E. (*H.*) *gladiator*; Roan Mountain (Tennessee, North Carolina, USA); Nelson (1975)

H. gladiator; Spruce Mountain (West Virginia, USA); Tarter & Nelson (1990)

H. gladiator; Monongahela National Forest (West Virginia, USA); Tarter & Nelson (1994)

H. gladiator; Roan Mountain (Tennessee, USA); Guidetti *et al.* (1999)

H. gladiator; Great Smoky Mountains (Tennessee, North Carolina, USA); Bartels & Nelson (2007), Nelson & Bartels (2007, 2013), Nelson *et al.* (2020)

(Fig 3–6, 26C; Tables 4–5)

Description

Females (i.e. from the third instar onwards; measurements and statistics in Table 4): Body whitish and stout (Figs 3A, C, 4), with spheroid or ovoid black eyes, persisting also after mounting. Elongated, dactyloid cephalic papillae (secondary clavae) and (primary) clavae (Figs 3A, C, 5A, B); peribuccal cirri without cirrophores (Fig. 5B). Cirrus *A* short, with cirrophore (Figs 3A, 5A). Long *cirrus dorsalis* with a triangular base inserted posterior to median plate 2 (Figs 3A, C, 4), the flagellum occasionally subdivided into two cirri.

Dorsal plates poorly sclerotized, with the *Pseudechiniscus*-type sculpturing, that is endocuticular pillars protruding through the epicuticle and visible as densely packed dark dots in PCM (Fig. 3A), bumps in NCM (Fig. 3C) or weakly elevated protrusions (granules) in SEM (Fig. 26C). Epicuticular ornamentation in the form of ridges visible in LCM and SEM (Figs 3A, C, 4, 26C). Generally, the sculpture is well-developed and evident in LCM. The cephalic plate is large and pentapartite, with two small anterior portions, a central keel-like portion and two larger trapezoid portions (Figs 3A, 4A, 5A). The cervical (neck) plate is not visible in LCM, indistinctly merged with the anterior margin of the scapular plate in SEM (Fig. 5A). The scapular plate falsely divided in two parts by a central longitudinal suture and by numerous epicuticular ridges (Figs 3A, 4A, 5A, 6A). Three median plates, all pseudobipartite, falsely subdivided by transverse sutures (Fig. 6A) and with six pairs of lateral intersegmental platelets flanking their borders (Figs 3A, 4A, 6A). Two pairs of large segmental plates without marginal incisions, but with a complicated system of epicuticular ornamentation giving an impression of false subdivisions (Figs 3A, 6A). Caudal (terminal) plate large, with long incisions (Figs 3A, 4A, 6A).

Ventral cuticle with a clear species-specific pattern of ornamentation reaching the lateroventral sides of the body (Figs 3A, 4B). Ornamentation composed of epicuticular thickenings and endocuticular pillars of

Downloaded from https://academic.oup.com/zoolinnean/article/192/3/794/6030998 by guest on 18 April 2022

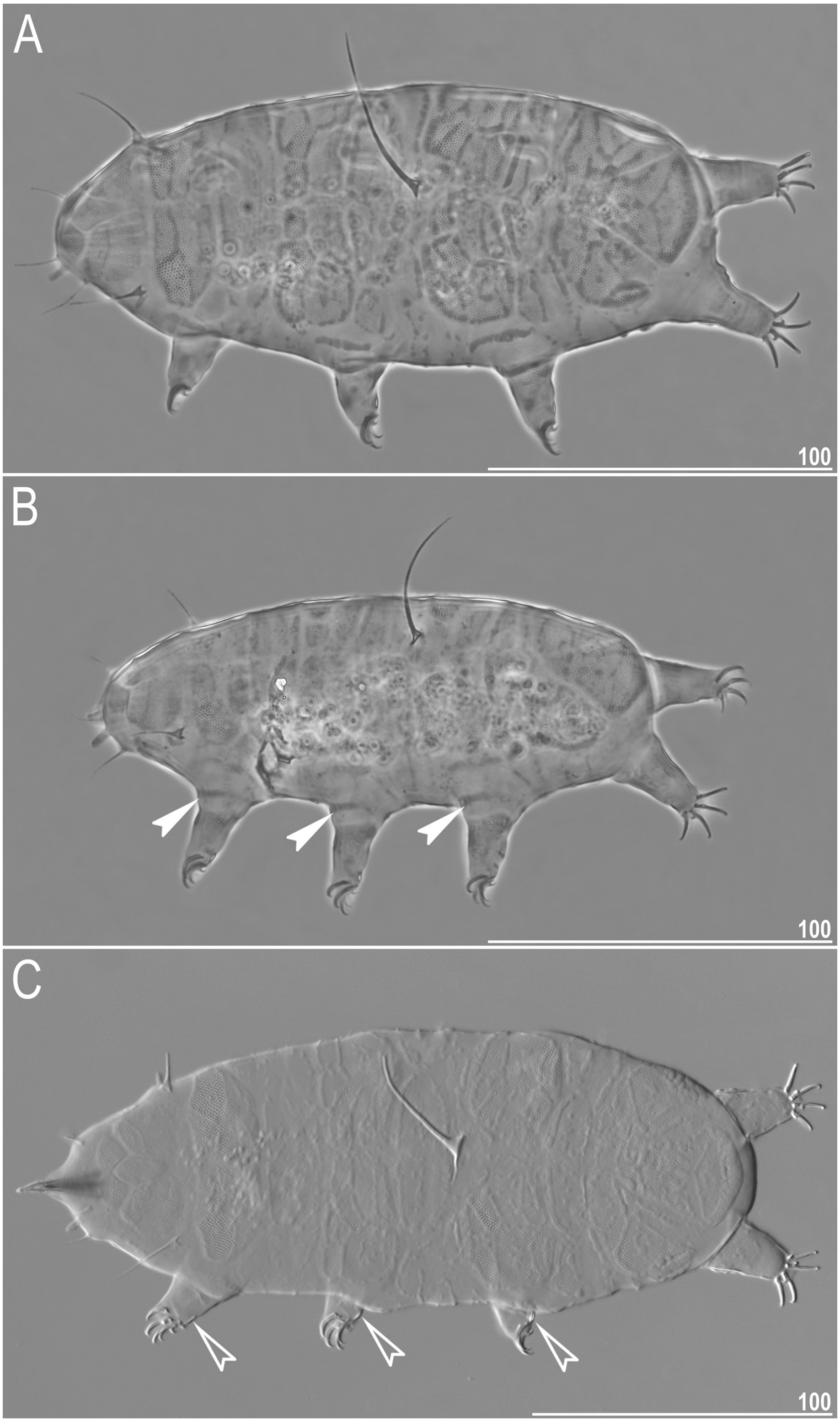

Figure 3. Habitus of *Hypechiniscus daedalus* (LCM): A, holotype (♀), dorsal view (PCM); B, allotype (♂), dorsolateral view (PCM), filled arrowheads indicate pulvini; C, paratype (♀), dorsal view (NCM), empty arrowheads indicate distal, sclerotized portions of legs. All scale bars = 100 µm.

Downloaded from https://academic.oup.com/zoolinnean/article/192/3/794/6030998 by guest on 18 April 2022

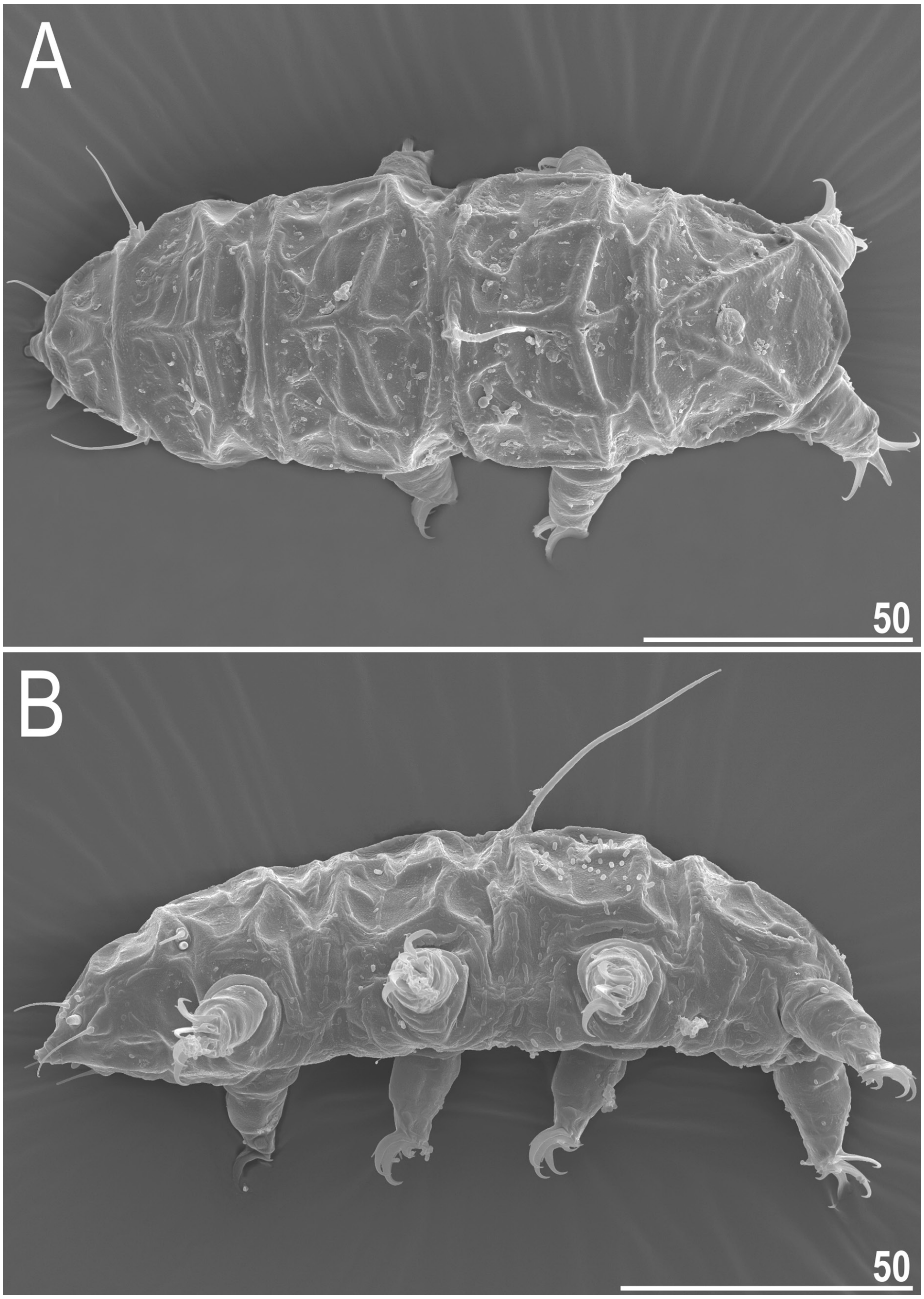

Figure 4. Habitus of *Hypechiniscus daedalus* (SEM): A, paratype (♀), dorsal view; B, paratype (♀), lateral view. All scale bars = 50 µm.

variable sizes, which are tightly arranged and closely adjacent to each other (Figs 4B, 6B). The largest and most evident pillars occur between legs II and legs III, and in the gonoporal zone, where pillars are densely aggregated and form pseudoplates. Subcephalic zone with a pair of large pseudoplates, and the subcervical area with a slender columnar or pedestal shaped aggregation or plate (Fig. 6B). Sexpartite gonopore placed between legs III and legs IV and a trilobed anus between legs IV.

Pedal plates and dentate collar IV absent, instead large belts of pillars are present on the outer central part of each leg (Fig. 5D). Weak pulvini present on all

Downloaded from https://academic.oup.com/zoolinnean/article/192/3/794/6030998 by guest on 18 April 2022

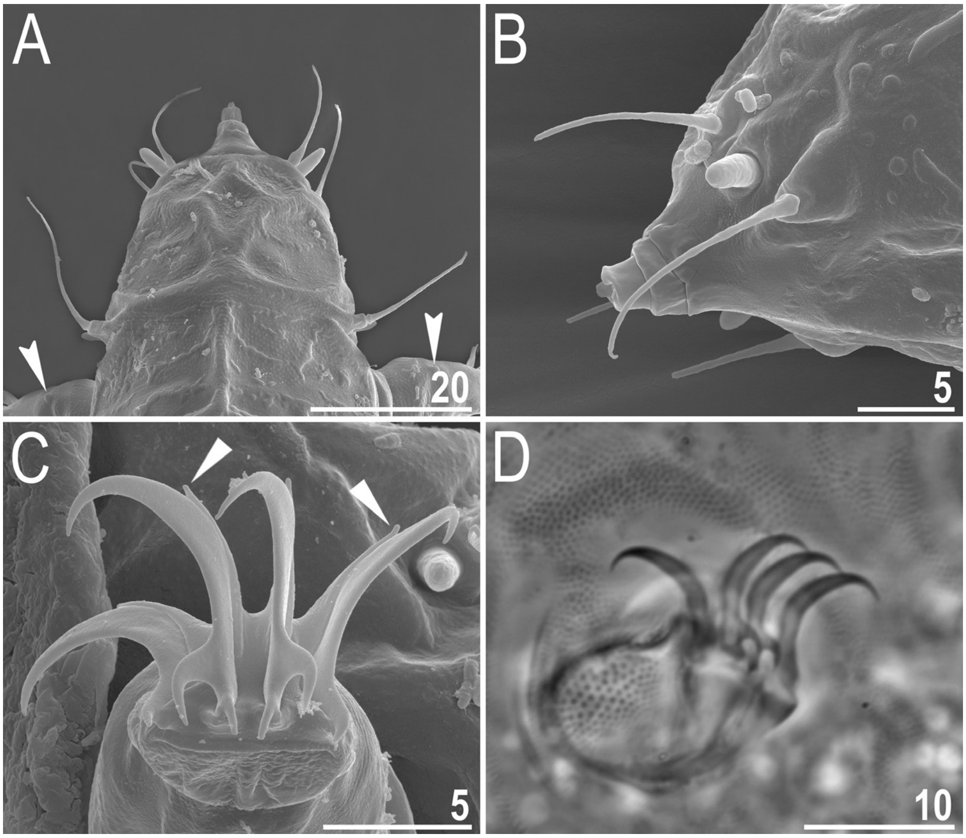

Figure 5. Morphological details of *Hypechiniscus daedalus*: A, cephalic region, incised arrowheads indicate rudimentary papillae I (SEM); B, peribuccal cirri and cephalic papilla in close-up (SEM); C, claws I, arrowheads indicate pseudoaccessory points (SEM); D, claws II (PCM). All scale bars in μm.

legs. Markedly sclerotized areas present at the inner side of each leg below the claws (Fig. 3C). A small papilla on leg I present and visible in SEM (Fig. 5A); a papilla on leg IV present (Fig. 4A). Claws I–IV of equal heights. External claws on all legs smooth (Fig. 5C–D). Internal claws with massive spurs positioned at *c.* one-quarter of the claw height and strongly bent downwards. Fragments of upwardly bent epicuticle formed as pseudoaccessory points on all claws (visible only in SEM; Fig. 5C, arrowheads).

Males (i.e. from the second instar onwards; measurements and statistics in Table 5): Except for the circular gonopore, no sexual dimorphism was observed (compare Fig. 3B with Figs 3A, C). The *bs* ratios for males and females largely overlap (0.35–0.43 in *N* = 8 ♂♂ vs. 0.38–0.43 in *N* = 6 ♀♀).

Juveniles (i.e. the second instar, sexually immature females): No qualitative differences with respect to adults, except for lack of the gonopore. Shorter than adults (165 μm in length, scapular plate length 20.7 μm). Lengths of cephalic appendages: *cirrus internus* 12.1 μm, *cirrus externus* 16.2 μm, cirrus *A* 21.4 μm. *Cirrus dorsalis* length: 65.9 μm. Claw heights: 9.0–9.2 μm.

Larvae (i.e. the first instar): Dorsal sculpturing weakly developed, but epicuticular ornamentation present. Gonopore and anus absent. Shorter than juveniles and adults, body 122 μm in length, scapular plate length 10.9 μm. Lengths of cephalic appendages: *cirrus internus* 4.3 μm, cephalic papilla 3.7 μm, *cirrus externus* 7.8 μm, clava 4.0 μm, cirrus *A* 9.4 μm. *Cirrus dorsalis* length: 24.4 μm. Claw heights: 5.9–7.1 μm.

Eggs: One or two round, white eggs per exuvia were found.

Genetic markers: 18S rRNA was characterized by two haplotypes with minor differences between them (*p*-distance = 0.2%). One haplotype was detected in the 28S rRNA and three in the ITS1 (0.1–0.2%); see Table 3 for details.

Downloaded from https://academic.oup.com/zoolinnean/article/192/3/794/6030998 by guest on 18 April 2022

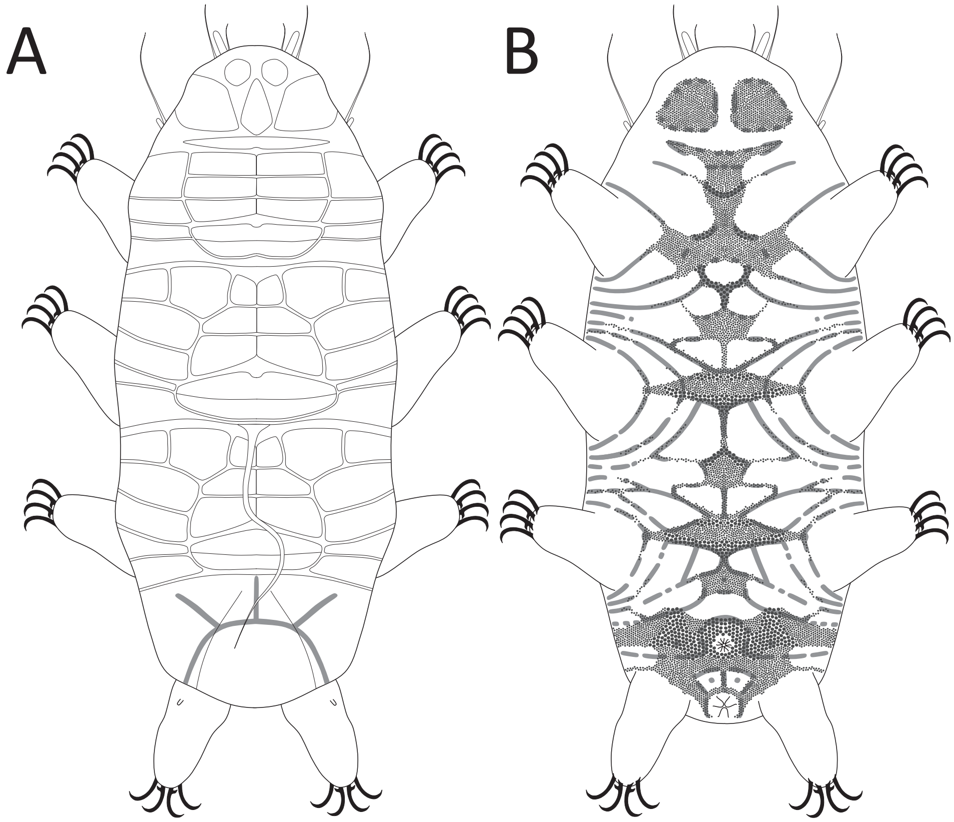

Figure 6. Schematic morphology of *Hypechiniscus daedalus*: A, dorsum; B, venter.

Type material: Holotype (adult female, slide US.041.02), allotype (adult male, slide US.041.02) and 16 paratypes (8♀♀, 6♂♂, 1 juvenile, 1 larva). Slides US.041.01–2 (3♀♀, 2♂♂, 1 larva) deposited in UJ, slide US.041.05 deposited in NHMD (3♀♀, 2♂♂), slide US.036.18 deposited in NMS (1♀, 2♂♂) and slides US.036.19–20 (2♀♀, 1♂, 1 juvenile) deposited in CU.

Type locality: 35°35'13"N, 83°04'31"W, 1514 m a.s.l.: USA, North Carolina, Purchase Knob (see Supporting Information, Fig. S1); deciduous forest; moss from tree trunk. The species was accompanied by other echiniscids: *Claxtonia mauccii* (Ramazzotti, 1956), *Echiniscus virginicus* Riggin, 1962 and *Pseudechiniscus brevimontanus* Kendall-Fite & Nelson, 1996.

Additional locality: 36°07'17"N, 82°05'37"W, 1239 m a.s.l.: USA, Tennessee, Roan Mountain, (see Supporting Information, Fig. S2); deciduous forest; moss from beech tree (*Fagus grandifolia* Ehrh.) bark.

Etymology: From Latin *daedalus* = artfully, subtly formed. The name refers to the sophisticated ventral pattern in the new species. An adjective in the nominative singular.

Phenotypic differential diagnosis: The species is separated from the *exarmatus* group by having a *cirrus dorsalis* and it differs from the remaining members of the *gladiator* group:

- *H. fengi* by the presence of papilla IV, identifiable in LCM (papilla IV not observable in LCM in *H. fengi*).
- *H. geminus* by having median plates 1–2 falsely subdivided into anterior and posterior portions by sutures (clearly unipartite median plates in *H. geminus*; compare Fig. 6A with Fig. 10A).
- *H. gladiator* by both clear epicuticular ridges and endocuticular pillars visible in LCM (only endocuticular pillars visible in LCM in *H. gladiator*; compare Fig. 3 with Fig. 11).
- *H. papillifer* by having smooth external claws (claws with secondary spurs directed upwards in *H. papillifer*) and lacking papillae on legs II–III.

Downloaded from https://academic.oup.com/zoolinnean/article/192/3/794/6030998 by guest on 18 April 2022

Table 4. Measurements (in µm) of selected morphological structures of the adult females of *Hypechiniscus daedalus* (type series) mounted in Hoyer's medium. *N*, number of specimens/structures measured; RANGE refers to the smallest and the largest structure among all measured specimens; SD, standard deviation; *sp*, the proportion between the length of a given structure and the length of the scapular plate

CHARACTER	*N*	RANGE		MEAN		SD		Holotype	
		µm	*sp*	µm	*sp*	µm	*sp*	µm	*sp*
Body length	7	180 – 239	*882* – *1062*	200	*963*	20	*55*	196	*942*
Scapular plate length	8	18.1 – 22.5	–	20.4	–	1.5	–	20.8	–
Head appendages lengths									
Cirrus internus	7	9.0 – 14.4	*47.9* – *70.1*	12.0	*59.3*	2.0	*7.7*	11.2	*53.8*
Cephalic papilla	8	5.8 – 6.8	*26.7* – *36.2*	6.5	*31.9*	0.4	*2.7*	6.7	*32.2*
Cirrus externus	8	13.5 – 18.7	*71.8* – *88.6*	16.7	*81.9*	1.7	*5.5*	16.1	*77.4*
Clava	8	4.0 – 5.7	*21.2* – *26.1*	4.9	*24.1*	0.6	*2.0*	4.4	*21.2*
Cirrus *A*	8	14.7 – 25.9	*73.1* – *115.1*	20.5	*100.1*	3.4	*13.7*	20.8	*100.0*
Cirrus *A*/Body length ratio	7	7% – 12%	–	10%	–	2%	–	11%	–
Body appendages lengths									
Cirrus C^d	7	36.7 – 71.6	*186.3* – *324.0*	52.8	*261.1*	12.0	*47.3*	51.5	*247.6*
Papilla on leg IV length	5	3.2 – 4.0	*16.2* – *19.9*	3.6	*17.9*	0.3	*1.3*	3.7	*17.8*
Claw I heights									
Branch	7	8.8 – 10.2	*44.0* – *51.8*	9.5	*47.3*	0.6	*3.2*	9.2	*44.2*
Spur	5	1.9 – 2.5	*9.0* – *12.4*	2.2	*10.5*	0.3	*1.3*	2.0	*9.6*
Spur/branch height ratio	5	20% – 25%	–	22%	–	2%	–	22%	–
Claw II heights									
Branch	8	8.9 – 10.8	*45.3* – *53.0*	9.9	*48.7*	0.5	*2.8*	9.7	*46.6*
Spur	8	1.8 – 2.7	*8.5* – *13.2*	2.2	*10.9*	0.3	*1.6*	2.7	*13.0*
Spur/branch height ratio	8	17% – 28%	–	22%	–	3%	–	28%	–
Claw III heights									
Branch	8	8.8 – 10.3	*45.8* – *51.2*	9.7	*47.8*	0.6	*2.0*	10.3	*49.5*
Spur	6	1.9 – 2.4	*9.6* – *11.5*	2.2	*10.5*	0.2	*0.8*	2.4	*11.5*
Spur/branch height ratio	6	20% – 23%	–	22%	–	1%	–	23%	–
Claw IV heights									
Branch	8	9.1 – 11.6	*50.2* – *57.7*	10.8	*53.2*	0.8	*2.5*	11.3	*54.3*
Spur	1	2.0 – 2.0	*10.6* – *10.6*	2.0	*10.6*	?	*?*	?	*?*
Spur/branch height ratio	1	20% – 20%	–	20%	–	?	–	?	–

Downloaded from https://academic.oup.com/zoolinnean/article/192/3/794/6030998 by guest on 18 April 2022

Table 5. Measurements (in µm) of selected morphological structures of the adult males of *Hypechiniscus daedalus* (type series) mounted in Hoyer's medium. *N*, number of specimens/structures measured; RANGE refers to the smallest and the largest structure among all measured specimens; SD, standard deviation; *sp*, the proportion between the length of a given structure and the length of the scapular plate

CHARACTER	*N*	RANGE						MEAN		SD		Allotype	
		µm			*sp*			µm	*sp*	µm	*sp*	µm	*sp*
Body length	8	153	–	213	*812*	–	*1009*	172	*900*	18	*76*	166	*869*
Scapular plate length	8	16.1	–	21.1		–		19.2	–	1.9	–	19.1	–
Head appendages lengths													
Cirrus internus	7	9.0	–	16.2	*43.7*	–	*78.2*	11.8	*62.2*	2.7	*14.1*	9.3	*48.7*
Cephalic papilla	8	5.9	–	8.0	*31.8*	–	*41.2*	6.8	*35.6*	0.7	*3.5*	6.1	*31.9*
Cirrus externus	8	12.3	–	20.9	*64.4*	–	*99.1*	15.9	*82.6*	2.9	*10.8*	12.3	*64.4*
Clava	8	3.8	–	6.6	*19.3*	–	*32.7*	5.1	*26.7*	1.0	*4.1*	4.5	*23.6*
Cirrus *A*	8	13.7	–	25.3	*71.7*	–	*119.9*	19.3	*100.7*	3.3	*16.3*	13.7	*71.7*
Cirrus *A*/Body length ratio	8	8%	–	12%		–		11%	–	1%	–	8%	–
Body appendages lengths													
Cirrus C^{d}	8	40.5	–	64.5	*206.1*	–	*390.9*	49.2	*259.2*	9.1	*61.6*	40.5	*212.0*
Papilla on leg IV length	6	2.8	–	3.7	*14.7*	–	*19.9*	3.3	*17.6*	0.4	*1.8*	2.8	*14.7*
Claw I heights													
Branch	7	7.2	–	10.7	*43.8*	–	*50.7*	8.8	*46.2*	1.1	*2.7*	8.5	*44.5*
Spur	7	1.4	–	2.2	*7.9*	–	*10.7*	1.8	*9.3*	0.3	*1.0*	1.5	*7.9*
Spur/branch height ratio	7	18%	–	24%		–		20%	–	2%	–	18%	–
Claw II heights													
Branch	8	6.8	–	9.5	*42.2*	–	*47.3*	8.7	*45.2*	1.0	*1.9*	8.8	*46.1*
Spur	6	1.3	–	1.8	*6.8*	–	*10.9*	1.6	*8.8*	0.2	*1.5*	1.3	*6.8*
Spur/branch height ratio	6	15%	–	24%		–		19%	–	3%	–	15%	–
Claw III heights													
Branch	8	7.2	–	10.3	*43.1*	–	*48.8*	8.8	*45.9*	1.0	*2.3*	8.6	*45.0*
Spur	8	1.4	–	2.5	*7.3*	–	*11.8*	1.7	*9.1*	0.4	*1.6*	1.4	*7.3*
Spur/branch height ratio	8	16%	–	24%		–		20%	–	3%	–	16%	–
Claw IV heights													
Branch	7	7.6	–	11.4	*46.2*	–	*54.4*	9.8	*51.5*	1.4	*3.4*	10.0	*52.4*
Spur	2	1.6	–	1.8	*9.1*	–	*9.7*	1.7	*9.4*	0.1	*0.4*	?	*?*
Spur/branch height ratio	2	18%	–	20%		–		19%	–	1%	–	?	–

Downloaded from https://academic.oup.com/zoolinnean/article/192/3/794/6030998 by guest on 18 April 2022

Genetic differential diagnosis: Uncorrected *p*-distances between *H. daedalus* and other species are as follows:

- 18S rRNA: from 0.2% (*H. gladiator*, MT809194) to 4.1% (*H. flavus*, HM193377).
- 28S rRNA: from 0.5% (*H. gladiator*, MT809202–3) to 5.0% (*H. cataractus*, MT809195–8).
- ITS1: from 2.4% (*H. gladiator*, MT809192, MT809194) to 18.2% (*H. cataractus*, MT809184).

Genetically verified geographic distribution: Nearctic: USA.

Species: Hypechiniscus fengi Sun & Li, 2013

Shortened and corrected version of the original description

Females (i.e. from the third instar onwards): Body 171–222 µm in length, colourless or very light yellow. Eyespots almost invisible. Cephalic appendages lengths: *cirrus internus* 10.4–13.0 µm, cephalic papilla 5.7–7.5 µm, *cirrus externus* 12.1–21.6 µm, clava 5.1–6.8 µm, and cirrus *A* 19.7–25.8 µm. *Cirrus dorsalis* 25.8–30.0 µm long, arising posteriorly to m2. Dorsal plates poorly sclerotized, sometimes indistinct, with the *Pseudechiniscus*-type sculpturing, i.e. fine endocuticular pillars protruding through the epicuticle and visible as densely packed dark dots in PCM. Dorsal armour consists of pentapartite cephalic plate, narrow cervical (neck plate), scapular plate, median plates m1–3 (false divisions of m2–3 into two parts resulting from the presence of longitudinal sutures) and caudal (terminal) plate with incisions. Lateral intersegmental platelets present laterally to m1 and m2. Ventral sculpturing pattern unknown. Pedal (leg) plates, patches of granulation and papillae absent or not visible under LCM on all legs. Claws 9.6–12.4 µm long. Robust spurs pointed downwards present on internal claws; small, sharp spurs usually present at bases of external claws IV. Sexpartite rosette gonopore.

Males (i.e. from the second instar onwards): Sexual dimorphism not specified, but evidenced by the smaller body size (133–180 µm). Cephalic appendages lengths: *cirrus internus* 4.6–13.7 µm, cephalic papilla 5.1–8.7 µm, *cirrus externus* 12.1–20.6 µm, clava 5.8–8.2 µm and cirrus *A* 18.1–24.4 µm. *Cirrus dorsalis* 16.2–32.2 µm long. Claws 8.2–12.1 µm long. Circular gonopore.

Phenotypic differential diagnosis: The species is separated from the *exarmatus* group by having a *cirrus dorsalis* and it differs from the remaining members of the *gladiator* group by lacking papilla IV (or papilla IV not identifiable under LCM).

Species: Hypechiniscus geminus Gąsiorek, Oczkowski, Suzuki, Kristensen & Michalczyk, sp. nov.

Zoobank registration: 492E0FCD-A39E-4B90-AC7A-2914BC8582E4.

Echiniscus (*Hypechiniscus*) *gladiator*; Mt. Sara (Ehime Prefecture, Japan); Morikawa (1951)

E. gladiator; Toyama Prefecture (Japan); Utsugi *et al*. (1995)

E. gladiator; Mt. Tanzawa (Kanagawa Prefecture, Japan); Utsugi & Hiraoka (1997)

H. gladiator; Mt. Amigasa (Nagano Prefecture, Japan); Jørgensen *et al*. (2011)

(Figs 7–10, 26E; Tables 6–8)

Description

Females (i.e. from the third instar onwards; measurements and statistics in Table 6): Body translucent to light flesh-coloured (Fig. 7) and stout (Fig. 8A, D), with spheroid or ovoid black eyes, persisting also after mounting. Elongated, dactyloid cephalic papillae (secondary clavae) and (primary) clavae (Fig. 8A, D); peribuccal cirri without cirrophores. Cirrus *A* short, with the cirrophore. Long *cirrus dorsalis* with a triangular base inserted posteriorly to the median plate 2 (Fig. 8A, D), flagellum sometimes subdivided into two *cirri*.

Dorsal plates poorly sclerotized, with the *Pseudechiniscus*-type sculpturing, i.e. endocuticular pillars protruding through the epicuticle and visible under PCM as faint, minute, densely packed dark dots on the scapular, segmental and caudal plates (Fig. 8A, B), as densely packed bumps on analogous parts of the armour under NCM (Fig. 8C) or as weakly elevated protrusions (granules) in SEM (Fig. 26E). Generally, the pillars are poorly developed and scarcely visible in LCM. Solid, continuous epicuticular ridges present along the margins of all plates and developed as folds subdividing some plates (Figs 8A, 26E). Cephalic plate large and pentapartite, with two small, anterior portions, a central, keel-like portion and two larger trapezoid posterior portions (Figs 8B, C, 10A). The cervical (neck) plate, not visible in LCM, indistinctly merged with the anterior margin of the scapular plate. The scapular plate uniform (Fig. 10A). Three median plates, all weakly outlined and unipartite (Figs 8A, 10A), with three pairs of lateral intersegmental platelets flanking their borders. Two pairs of large segmental plates without any incisions or sutures

Downloaded from https://academic.oup.com/zoolinnean/article/192/3/794/6030998 by guest on 18 April 2022

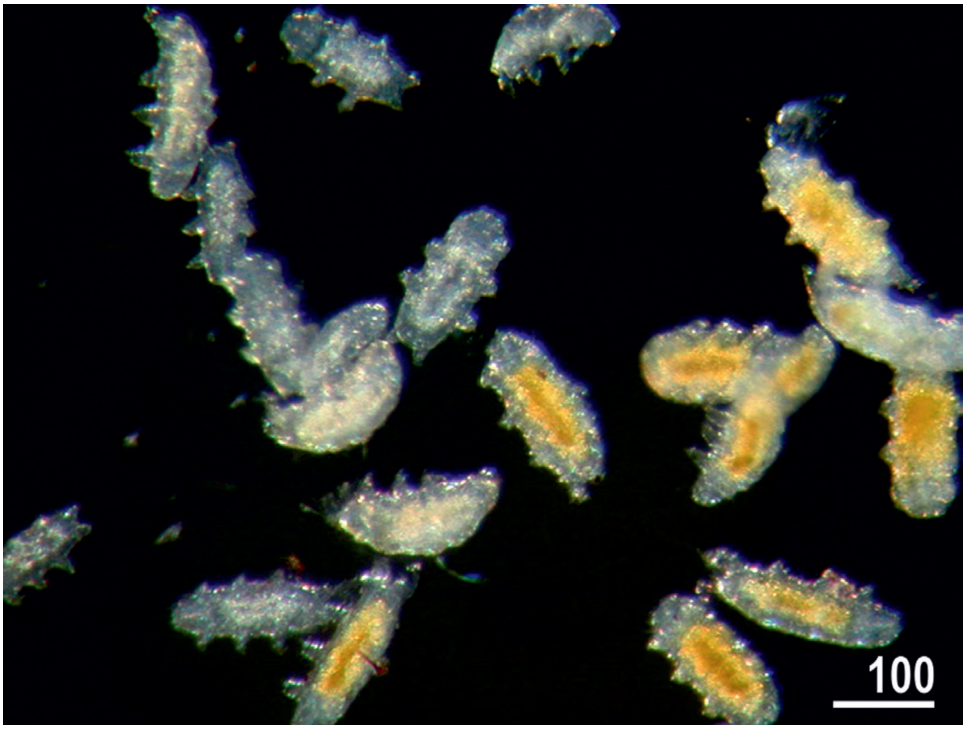

Figure 7. Two Japanese species isolated *in vitro*: white *Hypechiniscus geminus* on the left, and yellow *Hypechiniscus flavus* on the right. Scale bar = 100 μm.

(Fig. 10A). Caudal (terminal) plate large, with long incisions (Figs 8D, 10A).

Ventral cuticle with a clear species-specific pattern of ornamentation that does not extend to the lateroventral margins of the body (Figs 8D, 10B). Ornamentation composed of endocuticular pillars of approximately uniform size. Additionally, large linear epicuticular thickenings sparsely distributed on the venter and discrete from the endocuticular pillars at its lateral sides. Pillars form two column-like shapes: the first extending from the subcervical zone towards the posterior bases of legs I, and the second beginning slightly anterior to legs II and ending at the anterior bases of legs III. The largest aggregation of pillars is in the gonoporal area, however these do not form pseudoplates (Fig. 10B). Sexpartite gonopore placed between legs III and IV and a trilobed anus between legs IV.

Pedal plates, pulvini and dentate collar IV absent (Fig. 8A, D). Belts of pillars present centrally on each leg (Fig. 9A). Poorly sclerotized areas present on the inner side of each leg below the claws. A small spine or papilla on leg I absent and a papilla on leg IV present (Fig. 8D). Claws I–IV of equal heights. External claws on all legs smooth (Fig. 9). Internal claws with spurs of moderate size positioned at *c.* one-quarter of the claw height and strongly bent downwards. Fragments of epicuticle formed as upwardly pointing pseudoaccessory points on all claw branches (visible only in SEM; Fig. 9B, arrowhead).

Males (i.e. from the second instar onwards; measurements and statistics in Table 7): Epicuticular ornamentation in the form of grey ridges may be less obvious than in females (Fig. 8B), but still evident in NCM (Fig. 8C). Suture-like pseudodivision of the scapular plate occasionally present (Fig. 8B). Sexual dimorphism expressed only in the shape of the gonopore. The *bs* ratios overlap (0.29–0.40 in $N = 12$ ♂♂ vs. 0.35–0.42 in $N = 13$ ♀♀).

Juveniles (i.e. the second instar, sexually immature females; measurements and statistics in Table 8): Except for the lack of the gonopore, no qualitative differences with respect to adult females were observed. Body size equal to that of the shortest adult female.

Larvae (i.e. the first instar; measurements and statistics in Table 8): Dorsal sculpturing weakly developed, thus larvae may appear unarmoured (*Oreella*-like). Gonopore and anus absent. Minute and shorter than juveniles.

Eggs: One or two round, white eggs per exuvia were found.

Downloaded from https://academic.oup.com/zoolinnean/article/192/3/794/6030998 by guest on 18 April 2022

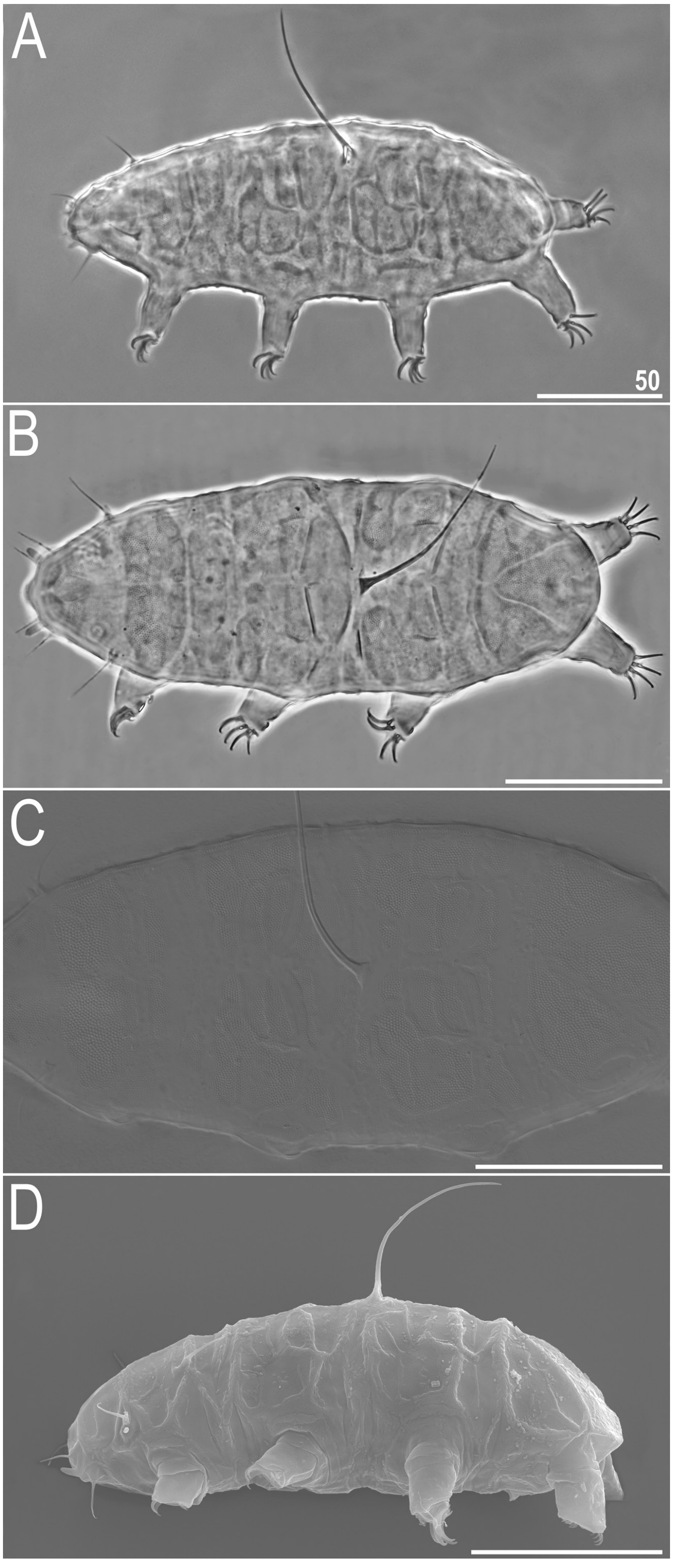

Figure 8. Habitus of *Hypechiniscus geminus*: A, holotype (♀), dorsolateral view (PCM); B, allotype (♂), dorsal view (PCM); C, paratype (♂), dorsal view (NCM); D, paratype (♀), lateral view (SEM). All scale bars = 50 µm.

Downloaded from https://academic.oup.com/zoolinnean/article/192/3/794/6030998 by guest on 18 April 2022

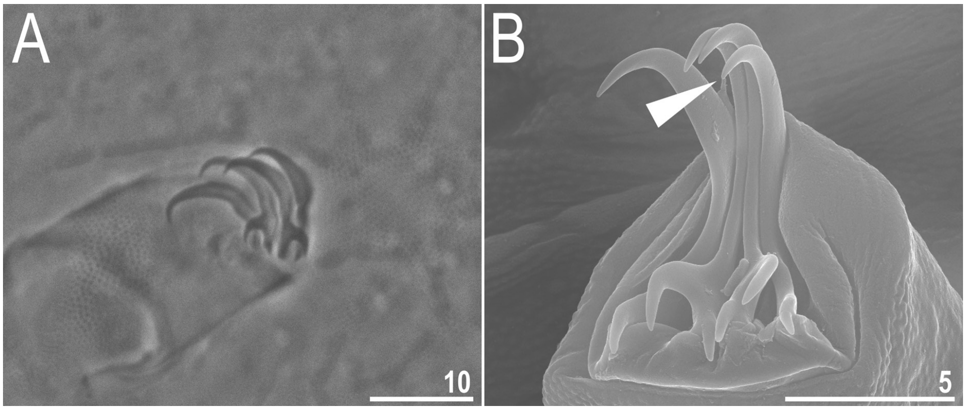

Figure 9. Claws of *Hypechiniscus geminus*: A, claws III (PCM); B, claws II, arrowhead indicates pseudoaccessory point (SEM). All scale bars in μm.

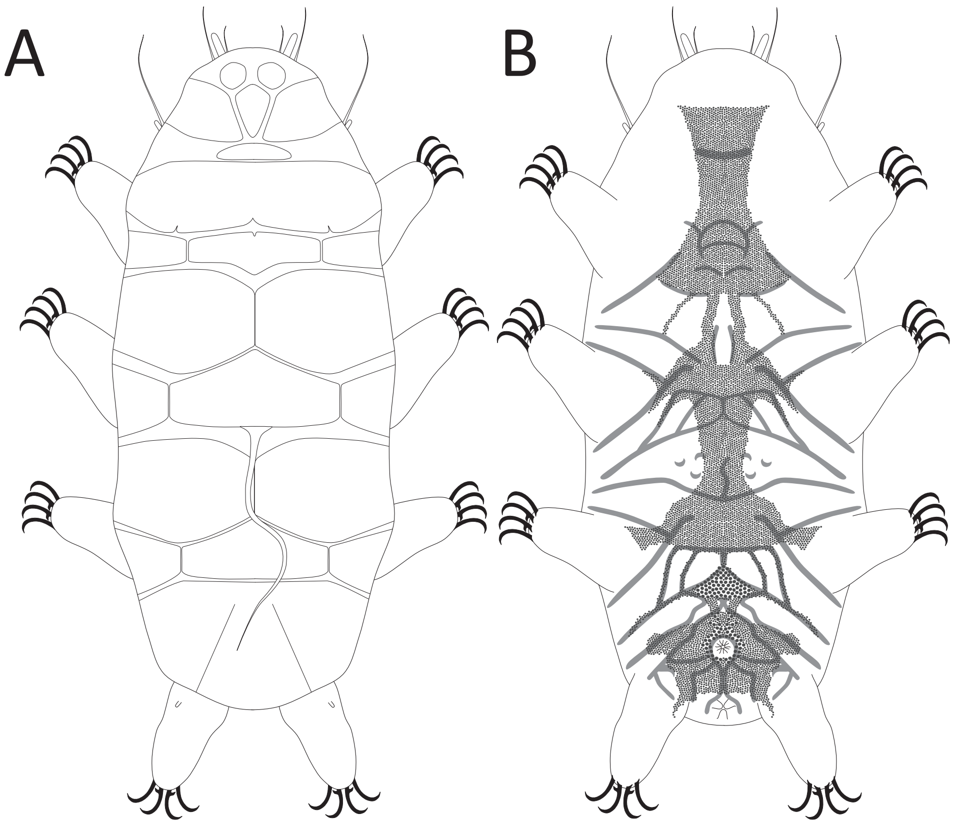

Figure 10. Schematic depiction of morphology of *Hypechiniscus geminus*: A, dorsum; B, venter.

Genetic markers: Single haplotypes were reported for 18S rRNA, 28S rRNA and *COI* in Jørgensen *et al.* (2011).

Type material: Holotype (adult female, slide JP.006.05), allotype (adult male, slide JP.006.11) and 38 paratypes (15♀♀, 16♂♂, 5 juveniles, 2 larvae on slides JP.006.02, 04–19). Slides JP.006.07–19 (11♀♀, 15♂♂, 2 juveniles, 2 larvae) deposited in UJ, slide JP.006.02 deposited in NHMD (1 juvenile), JP.006.04 (2♀♀) deposited in CU and slides JP.006.05–6 (3♀♀, 2♂♂, 2 juveniles) deposited in NMNS.

Downloaded from https://academic.oup.com/zoolinnean/article/192/3/794/6030998 by guest on 18 April 2022

Table 6. Measurements (in μm) of selected morphological structures of the adult females of *Hypechiniscus geminus* (type series) mounted in Hoyer's medium. *N*, number of specimens/structures measured; RANGE refers to the smallest and the largest structure among all measured specimens; SD, standard deviation; *sp*, the proportion between the length of a given structure and the length of the scapular plate

CHARACTER	*N*	RANGE		MEAN		SD		Holotype	
		μm	*sp*	μm	*sp*	μm	*sp*	μm	*sp*
Body length	15	173 – 216	*739* – *977*	196	*880*	16	*67*	209	*897*
Scapular plate length	15	18.6 – 24.9	–	22.4	–	1.9	–	23.3	–
Head appendages lengths									
Cirrus internus	8	6.7 – 11.4	*32.8* – *55.4*	9.4	*43.3*	1.5	*8.0*	?	*?*
Cephalic papilla	15	4.9 – 6.8	*21.3* – *33.3*	5.9	*26.6*	0.6	*3.3*	6.5	*27.9*
Cirrus externus	11	10.9 – 15.3	*49.0* – *70.3*	13.4	*58.5*	1.4	*5.8*	14.0	*60.1*
Clava	13	4.1 – 5.6	*18.5* – *29.0*	4.9	*22.0*	0.4	*2.8*	5.0	*21.5*
Cirrus *A*	11	16.7 – 22.9	*71.7* – *100.5*	19.5	*85.3*	2.1	*9.2*	16.7	*71.7*
Cirrus *A*/Body length ratio	11	8% – 12%	–	10%	–	1%	–	8%	–
Body appendages lengths									
Cirrus C^d	15	41.0 – 72.7	*184.2* – *321.5*	57.7	*258.1*	9.5	*40.4*	72.7	*312.0*
Papilla on leg IV length	8	2.4 – 3.4	*10.7* – *14.0*	2.9	*12.8*	0.4	*1.3*	2.5	*10.7*
Claw I heights									
Branch	15	8.7 – 11.4	*41.8* – *57.0*	10.2	*45.5*	0.8	*3.9*	10.9	*46.8*
Spur	12	1.5 – 2.0	*6.3* – *9.7*	1.7	*7.6*	0.2	*0.9*	1.8	*7.7*
Spur/branch height ratio	12	13% – 19%	–	17%	–	2%	–	17%	–
Claw II heights									
Branch	14	8.7 – 11.6	*41.6* – *56.5*	10.1	*45.7*	0.8	*4.0*	11.6	*49.8*
Spur	10	1.4 – 2.0	*6.7* – *8.6*	1.7	*7.4*	0.2	*0.6*	2.0	*8.6*
Spur/branch height ratio	10	14% – 19%	–	16%	–	1%	–	17%	–
Claw III heights									
Branch	15	8.7 – 11.3	*40.2* – *54.3*	10.1	*45.3*	0.8	*3.6*	11.1	*47.6*
Spur	9	1.3 – 2.2	*5.4* – *9.2*	1.6	*7.2*	0.3	*1.0*	1.6	*6.9*
Spur/branch height ratio	9	13% – 19%	–	16%	–	2%	–	14%	–
Claw IV heights									
Branch	15	9.5 – 12.4	*45.0* – *61.8*	11.1	*49.8*	0.8	*4.1*	12.3	*52.8*
Spur	7	1.5 – 2.1	*6.7* – *8.8*	1.8	*7.8*	0.2	*0.8*	1.9	*8.2*
Spur/branch height ratio	7	14% – 19%	–	16%	–	2%	–	15%	–

Downloaded from https://academic.oup.com/zoolinnean/article/192/3/794/6030998 by guest on 18 April 2022

Table 7. Measurements (in µm) of selected morphological structures of the adult males of *Hypechiniscus geminus* (type series) mounted in Hoyer's medium. *N*, number of specimens/structures measured; RANGE refers to the smallest and the largest structure among all measured specimens; SD, standard deviation; *sp*, the proportion between the length of a given structure and the length of the scapular plate

CHARACTER	*N*	RANGE						MEAN		SD		Allotype	
		µm			*sp*			µm	*sp*	µm	*sp*	µm	*sp*
Body length	14	128	–	199	*645*	–	*938*	172	*837*	19	*80*	159	*791*
Scapular plate length	14	15.7	–	23.4		–		20.6	–	1.9	–	20.1	–
Head appendages lengths													
Cirrus internus	10	6.4	–	9.1	*34.1*	–	*44.3*	8.0	*40.0*	0.8	*3.2*	8.9	*44.3*
Cephalic papilla	12	4.5	–	6.8	*23.0*	–	*33.2*	5.9	*28.9*	0.7	*3.0*	5.7	*28.4*
Cirrus externus	12	8.4	–	14.2	*51.6*	–	*71.1*	11.8	*57.3*	1.6	*6.4*	10.6	*52.7*
Clava	11	3.5	–	5.4	*18.8*	–	*26.7*	4.4	*21.9*	0.5	*2.2*	4.0	*19.9*
Cirrus *A*	13	14.3	–	21.4	*69.1*	–	*105.9*	16.6	*81.6*	2.1	*10.6*	14.6	*72.6*
Cirrus *A*/Body length ratio	13	8%	–	12%		–		10%	–	1%	–	9%	–
Body appendages lengths													
Cirrus C^{d}	14	28.0	–	70.3	*138.6*	–	*312.4*	48.0	*233.5*	10.3	*46.0*	49.1	*244.3*
Papilla on leg IV length	7	1.7	–	3.4	*10.8*	–	*17.8*	2.7	*13.8*	0.7	*2.6*	2.5	*12.4*
Claw I heights													
Branch	14	7.1	–	10.8	*39.7*	–	*51.5*	9.5	*46.3*	0.9	*3.2*	8.6	*42.8*
Spur	8	1.1	–	1.8	*5.8*	–	*8.9*	1.5	*7.4*	0.2	*1.1*	1.5	*7.5*
Spur/branch height ratio	8	12%	–	18%		–		16%	–	2%	–	17%	–
Claw II heights													
Branch	14	6.8	–	10.5	*39.3*	–	*50.2*	9.4	*45.6*	0.9	*3.4*	8.2	*40.8*
Spur	6	1.1	–	1.5	*5.8*	–	*7.5*	1.3	*6.8*	0.2	*0.6*	1.5	*7.5*
Spur/branch height ratio	6	12%	–	18%		–		15%	–	2%	–	18%	–
Claw III heights													
Branch	13	7.2	–	10.6	*40.2*	–	*50.5*	9.6	*46.7*	0.9	*2.8*	8.5	*42.3*
Spur	10	1.2	–	1.6	*5.5*	–	*7.6*	1.5	*7.0*	0.1	*0.6*	?	*?*
Spur/branch height ratio	10	12%	–	17%		–		15%	–	1%	–	?	–
Claw IV heights													
Branch	14	7.5	–	11.5	*39.7*	–	*56.4*	10.4	*50.3*	1.0	*4.2*	10.4	*51.7*
Spur	4	1.4	–	1.7	*6.9*	–	*7.5*	1.5	*7.2*	0.1	*0.3*	1.5	*7.5*
Spur/branch height ratio	4	14%	–	18%		–		15%	–	2%	–	14%	–

Downloaded from https://academic.oup.com/zoolinnean/article/192/3/794/6030998 by guest on 18 April 2022

Table 8. Measurements (in µm) of selected morphological structures of the juveniles and larvae of *Hypechiniscus geminus* (type series) mounted in Hoyer's medium. *sp*, the proportion between the length of a given structure and the length of the scapular plate

CHARACTER	Juvenile 1		Juvenile 2		Larva 1		Larva 2	
	µm	*sp*	µm	*sp*	µm	*sp*	µm	*sp*
Body length	178	*967*	186	*964*	116	*1045*	111	*782*
Scapular plate length	18.4	–	19.3	–	11.1	–	14.2	–
Head appendages lengths								
Cirrus internus	6.6	*35.9*	6.5	*33.7*	3.7	*33.3*	4.3	*30.3*
Cephalic papilla	5.5	*29.9*	5.0	*25.9*	3.6	*32.4*	3.6	*25.4*
Cirrus externus	?	*?*	13.2	*68.4*	5.6	*50.5*	5.7	*40.1*
Clava	3.9	*21.2*	4.8	*24.9*	2.6	*23.4*	3.0	*21.1*
Cirrus *A*	13.8	*75.0*	15.7	*81.3*	7.8	*70.3*	7.3	*51.4*
Cirrus *A*/Body length ratio	8%	–	8%	–	7%	–	7%	–
Body appendages lengths								
Cirrus C^d	47.1	*256.0*	56.4	*292.2*	20.7	*186.5*	25.1	*176.8*
Papilla on leg IV length	2.6	*14.1*	2.8	*14.5*	?	*?*	?	*?*
Claw I heights								
Branch	7.7	*41.8*	9.0	*46.6*	6.3	*56.8*	6.4	*45.1*
Spur	1.5	*8.2*	1.5	*7.8*	1.0	*9.0*	1.2	*8.5*
Spur/branch height ratio	19%	–	17%	–	16%	–	19%	–
Claw II heights								
Branch	8.3	*45.1*	8.7	*45.1*	5.6	*50.5*	5.7	*40.1*
Spur	?	*?*	1.4	*7.3*	1.1	*9.9*	1.1	*7.7*
Spur/branch height ratio	?	–	16%	–	20%	–	19%	–
Claw III heights								
Branch	8.8	*47.8*	9.2	*47.7*	6.0	*54.1*	6.4	*45.1*
Spur	1.7	*9.2*	1.5	*7.8*	1.0	*9.0*	1.2	*8.5*
Spur/branch height ratio	19%	–	16%	–	17%	–	19%	–
Claw IV heights								
Branch	9.5	*51.6*	9.6	*49.7*	6.4	*57.7*	6.7	*47.2*
Spur	?	*?*	1.6	*8.3*	1.3	*11.7*	1.0	*7.0*
Spur/branch height ratio	?	–	17%	–	20%	–	15%	–

Type locality: 35°56'32"N, 138°20'46"E, 2510 m a.s.l.: Japan, Honshu, Mount Amigasa (see Supporting Information, Fig. S3); Japanese stone pine [*Pinus pumila* (Pall.) Regel] zone; moss from rocks and fallen tree trunks. The species was accompanied by *H. flavus*, *Stellariscus pseudelegans* (Séméria, 1994) and a *Pilatobius* sp. nov.

Etymology: From Latin *geminus* = twin. The name has a twofold sense as the new species was found in the company of *H. flavus*, and it is the sister-species of *H. gladiator*. An adjective in the nominative singular.

Phenotypic differential diagnosis: The species is separated from the *exarmatus* group by having the *cirrus dorsalis* and it differs from the remaining members of the *gladiator* group:

- *H. gladiator* by clear epicuticular ridges visible in LCM as grey elements overlapping with pillars (only endocuticular pillars visible in LCM in *H. gladiator*; compare Fig. 8 with Fig. 11).
- *H. papillifer* by having smooth external claws (with secondary spurs directed upwards in *H. papillifer*) and lacking papillae on legs II–III.

Genetic differential diagnosis: Uncorrected *p*-distances between *H. geminus* and other species are as follows [not computable for 28S rRNA since different fragments were sequenced in Jørgensen *et al.* (2011) and in the present study]:

- 18S rRNA: from 0.5% (*H. gladiator*, MT809240) to 3.8% (*H. flavus*, HM193377).
- *COI*: 9.8% (*H. flavus*, HM193410).

Downloaded from https://academic.oup.com/zoolinnean/article/192/3/794/6030998 by guest on 18 April 2022

Genetically verified geographic distribution: Eastern Palaearctic: Japan.

SPECIES: *HYPECHINISCUS GLADIATOR* (MURRAY, 1905)

Echiniscus gladiator; *locus typicus*: Loch Ness (Scotland); Murray (1905)

E. gladiator; Loch Morar, Ben Lawers (Scotland), Faroe Islands; Murray (1907)

E. gladiator; Borðoy, Suðuroy (Faroe Islands); Sellnick (1908)

E. gladiator; Achill Island (Ireland); Murray (1911)

Parechiniscus unispinosus; *locus typicus*: Serra d'Arga, Serra de Estrela (Portugal); da Cunha (1947)

Hypechiniscus gladiator; Nuuk/Godthåb, Kangaamiut, Kangerlussuaq/Søndre Strømfjord (Greenland); Petersen (1951)

E. (*H.*) *gladiator*; Achnasheen, Ben Nevis (Scotland), Cwm Idwal (Wales); Morgan & King (1976)

H. gladiator; Bergen (Norway); Kristensen (1987)

H. gladiator; Narssaq (Greenland), Thingvellir (Iceland); Maucci (1996)

H. gladiator; Sierra de Guadarrama (Spain); Guil & Sanchez-Moreno (2013)

H. gladiator; Faroe Islands; Trygvadóttir & Kristensen (2013)

(FIGS 11–15, 26A, B; TABLES 9, 10)

Redescription

Females (i.e. from the third instar onwards; measurements and statistics in Table 9): Body white and stout, with spheroid or ovoid black eyes, persisting also after mounting (Figs 11A, B, 12A). Elongated, dactyloid cephalic papillae (secondary clavae) and (primary) clavae (Figs 11A, B, 12A–D); peribuccal cirri without cirrophores (Figs 11A, B, 12A–C). Cirrus *A* short, with the cirrophore (Figs 11A, B, 12B, D). Long *cirrus dorsalis* with a triangular base inserted after median plate 2 (Figs 11A, 12A, 14A), sometimes flagellum subdivided into two cirri (the '*fissigladii* form'; Fig. 15B) or two cirri with independent bases are present (the '*bigladii* form', Fig. 15C).

Dorsal plates poorly sclerotized, with the *Pseudechiniscus*-type sculpturing, i.e. endocuticular pillars protruding through the epicuticle and visible as densely arranged dark dots in PCM (Fig. 11A), bumps in NCM (Fig. 11D) or weakly elevated protrusions (granules) in SEM (Fig. 26B). No epicuticular ridges

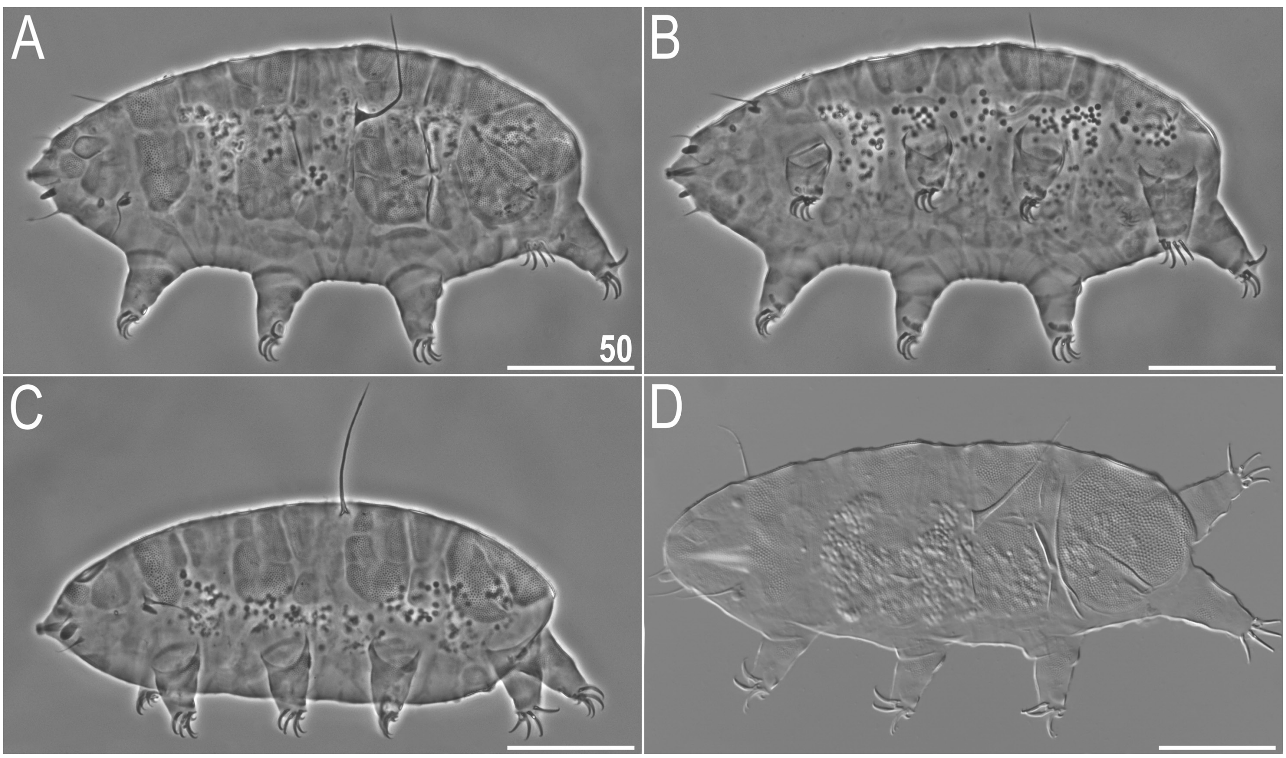

Figure 11. Habitus of *Hypechiniscus gladiator* (Murray, 1905) (LCM): A, neotype (♀), dorsolateral view (PCM); B, neotype (♀), lateroventral view (PCM); C, male from a Scottish population, lateral view (PCM); D, male from an Icelandic population, dorsolateral view (NCM). All scale bars = 50 μm.

Downloaded from https://academic.oup.com/zoolinnean/article/192/3/794/6030998 by guest on 18 April 2022

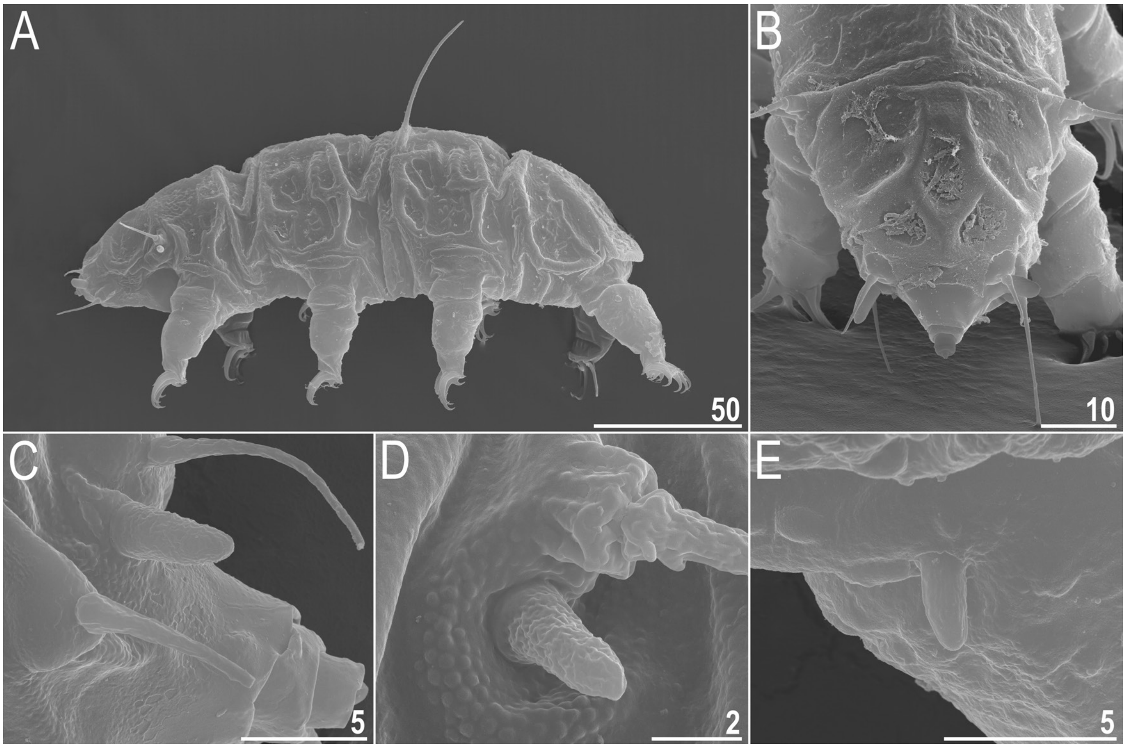

Figure 12. Habitus and morphological details of *Hypechiniscus gladiator* (SEM): A, female, lateral view; B, cephalic region with peribuccal cirri and secondary clavae (cephalic papillae); C, peribuccal cirri and cephalic papilla in close-up; D, primary clava and cirrophore *A* in close-up; E, papilla on leg IV. All scale bars in µm.

(Fig. 26A) or epicuticular ornamentation visible only in SEM (Fig. 26B). Generally, the sculpture is well-developed and evident in LCM. The cephalic plate is large and clearly sexpartite, with three small anterior portions, a central keel-like portion (with the most sclerotized margins) and two significantly larger trapezoid portions (Figs 11A, 12B, 14A). The cervical (neck) plate not visible in LCM, reduced to a thickening anterior to the scapular plate (Figs 12B, 14A). The scapular plate divided in two parts by a central longitudinal suture (Figs 11A, 14A). Three median plates, all weakly outlined and unipartite (Figs 11A, 14A), with three pairs of lateral intersegmental platelets flanking their borders (Figs 11A, 12A, 14A). Two pairs of large segmental plates with short incisions at their anterior and posterior margins (Figs 11A, 12A, 14A). Caudal (terminal) plate large, with long incisions (Figs 11A, 12A, 14A).

Ventral cuticle with a clear species-specific pattern reaching the lateroventral sides of the body (Figs 11A, B, 14B), and composed of endocuticular pillars of variable sizes. The largest and most evident pillars occur in the subcephalic zone (forming a single large pseudoplate), immediately posterior to legs I, at the level of legs II–III, and in the gonoporal zone (Figs 11B, 14B). The remaining pillars are smaller, forming belts on the lateral portions of the venter, a reticulate design between legs I–III and before the gonoporal area, and a column-like shape extending posteriorly from the subcervical zone towards the first aggregation of larger pillars (Fig. 14B). Sexpartite gonopore located anteriorly of legs IV and a trilobed anus between legs IV.

Pedal plates and dentate collar IV absent; instead, large patches of pillars are present centrally on each leg (Fig. 13A). Distinct pulvini on all legs (Fig. 11A). Markedly sclerotized areas present on the inner side of each leg below the claws (Fig. 11B). A spine or papilla on leg I absent (LCM and SEM), and a papilla on leg IV present (Figs 11B, 12A, E). Claws I–IV of equal heights. External claws on all legs spurless (Fig. 13). Internal claws with massive spurs positioned at *c.* one-quarter of the claw height and strongly bent downwards. Upward-directed fragments of epicuticle formed as pseudoaccessory points on all claw branches (visible only in SEM; Fig. 13B, C).

Buccal apparatus (anatomically homogenous in the entire genus) with a rigid, thick-walled tube and a spheroidal pharynx. Pharynx with very short, reduced placoids encrusted with $CaCO_3$ (see figs 29–30 in Kristensen 1987). Stylet supports absent.

Males and sexually dimorphic traits (i.e. from the second instar onwards; measurements and statistics in Table 10): ♂♂ almost identical to ♀♀, i.e. sexual

Downloaded from https://academic.oup.com/zoolinnean/article/192/3/794/6030998 by guest on 18 April 2022

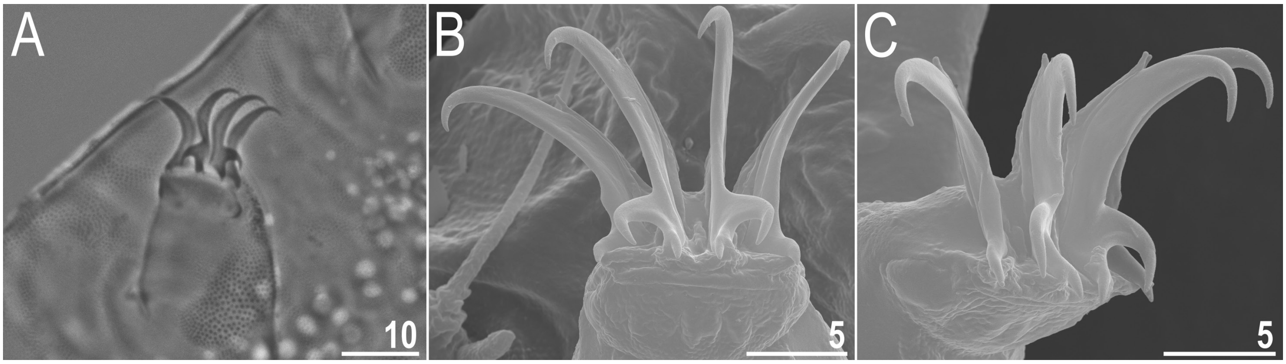

Figure 13. Claws of *Hypechiniscus gladiator*: A, claws III (PCM, paratype); B, claws I (SEM); C, claws III (SEM). Note divergent pseudoaccessory points. All scale bars in μm.

dimorphism is rudimentary, as even clavae are of similar lengths in both sexes (size differences in clavae are typically indicative of sexual dimorphism in echiniscids). Cephalic papillae broader in ♂♂ (Fig. 11C). Of the standardly measured traits, ♂♂ differ significantly from ♀♀ only in body size, estimated both as mean body length ± SD: 200 ± 19 μm vs. 246 ± 25 μm (one-tailed Welch's *t*-test due to unequal variances, with $N_{♀♀} = 30$ and $N_{♂♂} = 30$: $t_{55}=8.06$; $P < 0.001$) and as average scapular plate length: 21.4 ± 1.8 μm vs. 25.4 ± 2.6 μm ($t_{52} = 6.90$; $P < 0.001$). The *bs* ratio ranges, which are usually clearly separate for each sex, also overlap (0.34–0.41 in *N* = 11 ♂♂ vs. 0.37–0.47 in *N* = 10 ♀♀).

Juveniles (i.e. the second instar, sexually immature females): Except for the lack of the gonopore, no qualitative differences with respect to adult females were observed. Shorter than adult females.

Larvae (i.e. the first instar; measurements and statistics in Table 10): Dorsal sculpturing weakly developed. Gonopore and anus absent. Shorter than juveniles.

Eggs: One to four round, white eggs per exuvia were found.

Genetic markers: 18S rRNA was characterized by three haplotypes with minor differences between them (*p*-distances = 0.1–0.3%), but one haplotype was detected for 28S rRNA, and four in ITS1 (0.3–1.6%); see Table 3 for details.

Neotype material: Neotype (adult female, slide GB.058.12), 105 individuals (25♀♀, 28♂♂, 11 juveniles, and one larva on slides GB.033.16–51; 19♀♀, 14♂♂, 4 juveniles on slides GB.058.11–17), including the form *bigladii*, and four exuvia. Slides GB.033.16–46 (22♀♀, 22♂♂, 8 juveniles, 1 larva, 2 exuvia) + GB.058.11–12 (5♀♀, 4♂♂, 1 juvenile) deposited in UJ, slide GB.058.13 deposited in NHMD (3♀♀, 3♂♂), slide GB.058.14 deposited in NMS (2♀♀, 3♂♂, 1 juvenile), and slides GB.033.47–51 (3♀♀, 6♂♂, 3 juveniles, 2 exuvia) + GB.058.15–17 (10♀♀, 4♂♂, 2 juveniles) deposited in CU.

New type (neotype) locality: 56°57'33.03''N, 4°34'04.5"W, 624 m a.s.l.: Scotland, Creag Meagaidh, Lochan a' Choire; mountain grassland; moss from rock. The species was accompanied by other echiniscids: *Bryodelphax parvulus* Thulin, 1928, *Diploechiniscus oihonnae* (Richters, 1903) and *Echiniscus merokensis* Richters, 1904.

Additional locality: 57°08'49"N, 4°40'42"W, 20 m a.s.l.: Scotland, Loch Ness, Fort Augustus; moss from rock off the lake shore. The species was accompanied by other echiniscids: *B. parvulus*, *D. oihonnae* and *E. merokensis*.

Etymology: The name most likely refers to the presence of the *cirrus dorsalis*, which resembles a whip that gladiators (*lorarii*) in the Roman Empire used to goad animals and humans into fighting at arenas. A noun in the nominative singular standing in apposition.

Phenotypic differential diagnosis: The species is separated from the *exarmatus* group by having a *cirrus dorsalis* and it differs from the remaining members of the *gladiator* group:

- *H. papillifer* by having smooth external claws (with secondary spurs directed upwards in *H. papillifer*) and lacking papillae on legs II–III.
- *H. daedalus* and *H. geminus* by only endocuticular pillars visible in LCM (clear epicuticular ridges visible in LCM as grey elements overlapping with pillars in the two new species; compare Figs 3, 8 and 11), the epicuticular portion of the sculpture is similar in all three species under SEM (Fig. 26B, C, E).

Downloaded from https://academic.oup.com/zoolinnean/article/192/3/794/6030998 by guest on 18 April 2022

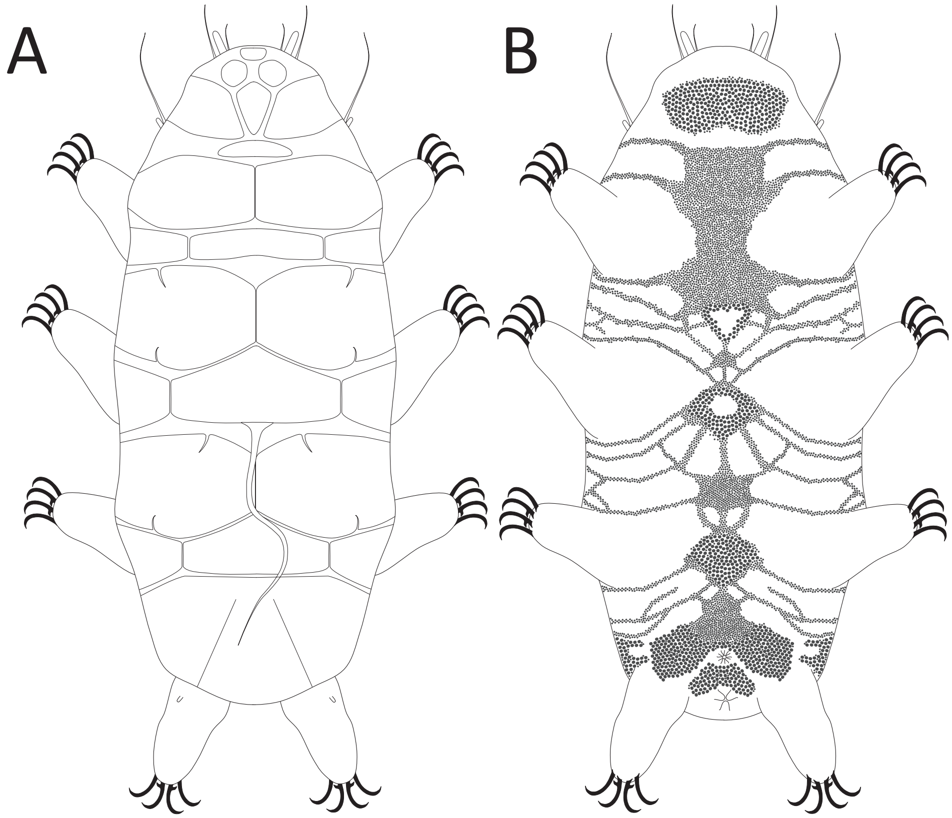

Figure 14. Schematic depiction of morphology of *Hypechiniscus gladiator*: A, dorsum; B, venter.

Genetic differential diagnosis: Uncorrected *p*-distances between *H. gladiator* and other species are as follows:

- 18S rRNA: from 0.2% (*H. daedalus*, MT809237) to 4.3% (*H. flavus*, HM193377).
- 28S rRNA: from 0.5% (*H. daedalus*, MT809199, MT809200) to 4.5% (*H. cataractus*, MT809195–8).
- ITS1: from 2.4% (*H. daedalus*, MT809187, MT809189) to 18.2% (*H. cataractus*, MT809184).

Genetically verified geographic distribution: Western Palaearctic: Iceland, Scotland.

Remarks: Animals found in Italy and the Swedish Öland constitute the first records of this rare species for both countries (Maucci, 1986; Guidetti *et al*., 2015). Both the forms *fissigladii* and *bigladii* [described by Iharos (1973); see Fig. 15; recorded as subspecies in Degma *et al*. (2009–20)] are herein suppressed, because: (1) they fall within the genetic variability of the morphotype of *H. gladiator* with a single *cirrus dorsalis* and (2) similar morphological variability with regard to the *cirrus dorsalis* occurs in the new species of the *gladiator* group (described above). However, the status of the form *spinulosa* (Fig. 15A) is unclear. Originally it was used to separate individuals of '*H. gladiator*' (see the section 'Biogeography') having three projections in the median line and at the posterior edges of the scapular and segmental plates, together with two anterior projections of the caudal plate, from 'typical' individuals with continuous, smooth plate margins (Iharos, 1973). However, as the dorsal armour is thin and easily deformable in the entire genus, it is feasible that such projections could be formed as artefacts resulting from incomplete relaxation of an individual during mounting (the examination of the syntypes deposited in the Hungarian Natural History Museum in Budapest revealed that such projections are absent). Therefore, this form possesses no reliable character, which would substantiate its distinctiveness. The form *spinulosa* should, therefore, be recognized as invalid until *Hypechiniscus* specimens originating from the Korean Peninsula are examined.

SPECIES: *HYPECHINISCUS PAPILLIFER* (ROBOTTI, 1972)

Shortened and corrected version of the original description: Sex not specified: Body 196–227 µm in length, almost translucent. Eyespots black. *Cirrus dorsalis* 52.0–59.0 µm long. Dorsal plates with the fine

Downloaded from https://academic.oup.com/zoolinnean/article/192/3/794/6030998 by guest on 18 April 2022

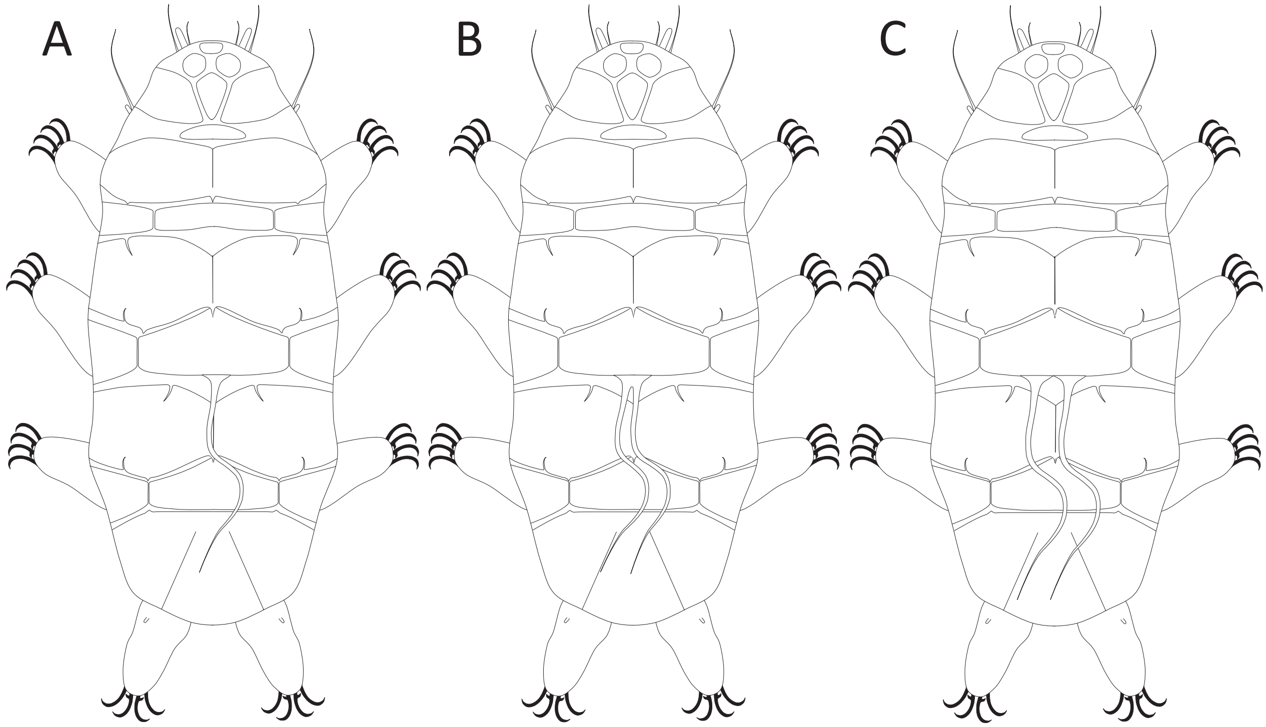

Figure 15. Forms of *Hypechiniscus gladiator* distinguished by Iharos (1973) and suppressed in the present study: A, forma *spinulosa*; B, forma *fissigladii*; C, forma *bigladii*.

Pseudechiniscus-type sculpturing. Ventral sculpturing pattern unknown. Papillae present on legs II–IV. Internal claws with robust spurs directed downwards, and external claws with minute, needle-like spurs at their bases, directed upwards.

Phenotypic differential diagnosis: This is the only *Hypechiniscus* species with papillae on legs II–III.

The *Hypechiniscus exarmatus* morphogroup

Species: Hypechiniscus cataractus Gąsiorek, Oczkowski, Kristensen & Michalczyk, sp. nov.

Zoobank registration: 49CA86F7-0A6E-4909-AC49-8F13A5DE2964.

(Figs 16–19, 26F; Tables 11–13)

Description

Females (i.e. from the third instar onwards; measurements and statistics in Table 11): Body translucent to white, cylindrical (Figs 16A, C, 17A–C), with minute spheroid black eyes present after mounting. Elongated, dactyloid cephalic papillae (secondary clavae) and (primary) clavae (Figs 16A, C, 17A, C, 18A); peribuccal cirri without cirrophores (Fig. 18A). Cirrus *A* short, with cirrophore. *Cirrus dorsalis* absent.

Minute and densely arranged endocuticular pillars present (see the pillars exposed by a fragment of detached epicuticle in Fig. 17B, arrowhead), however their *capituli* (heads) are not visible either under LCM or SEM, thereby giving the cuticle an unsculptured appearance. Dorsal plates are thus uniformly grey in PCM (Fig. 16A), and smooth in NCM and SEM (Figs 16C, 17A, B, 26F). The cephalic plate is large and pentapartite, with two small anterior portions, a central keel-like portion, and two larger trapezoid posterior portions (Figs 16A, 17A, B). The cervical (neck) plate is not visible in LCM and is reduced to an anterior thickening of the scapular plate (Fig. 17A, B). The scapular plate divided into four parts by horizontal and longitudinal sutures (Figs 16A, 19A). Three median plates, all weakly outlined and unipartite, with false secondary sutures dividing them into smaller subparts (Figs 16A, 19A) and five pairs of lateral intersegmental platelets flanking their borders (Fig. 19A). Two pairs of large segmental plates with very short incisions at their anterior and posterior margins, and folds of cuticle that subdivide them into smaller portions (Figs 17A, 19A). Caudal (terminal)

Downloaded from https://academic.oup.com/zoolinnean/article/192/3/794/6030998 by guest on 18 April 2022

Table 9. Measurements (in µm) of selected morphological structures of the adult females of *Hypechiniscus gladiator* (neotype series + population GB.033) mounted in Hoyer's medium. *N*, number of specimens/structures measured; RANGE refers to the smallest and the largest structure among all measured specimens; SD, standard deviation; *sp*, the proportion between the length of a given structure and the length of the scapular plate

CHARACTER	*N*	RANGE						MEAN		SD		Neotype	
		µm			*sp*			µm	*sp*	µm	*sp*	µm	*sp*
Body length	30	194	–	300	*795*	–	*1102*	246	*972*	25	*61*	235	*1022*
Scapular plate length	30	21.1	–	30.8		–		25.4	–	2.6	–	23.0	–
Head appendages lengths													
Cirrus internus	29	8.8	–	15.0	*32.7*	–	*53.6*	11.0	*43.1*	1.4	*5.3*	9.2	*40.0*
Cephalic papilla	30	5.4	–	8.9	*20.1*	–	*35.5*	7.0	*27.9*	0.8	*3.3*	6.7	*29.1*
Cirrus externus	29	13.2	–	21.1	*51.4*	–	*81.4*	17.0	*67.0*	1.7	*7.6*	16.6	*72.2*
Clava	29	4.0	–	6.9	*14.9*	–	*29.5*	5.9	*23.5*	0.7	*3.5*	5.9	*25.7*
Cirrus *A*	30	12.8	–	31.4	*44.6*	–	*115.5*	22.7	*90.3*	4.0	*17.3*	21.8	*94.8*
Cirrus *A*/Body length ratio	30	5%	–	12%		–		9%	–	2%	–	9%	–
Body appendages lengths													
Cirrus C^d	28	40.3	–	77.8	*156.8*	–	*332.2*	60.7	*239.2*	10.1	*44.9*	59.1	*257.0*
Papilla on leg IV length	24	3.3	–	5.3	*13.3*	–	*20.0*	4.2	*16.4*	0.6	*1.6*	4.0	*17.4*
Claw I heights													
Branch	27	10.7	–	13.5	*43.1*	–	*57.6*	12.3	*49.3*	1.0	*3.8*	11.6	*50.4*
Spur	23	2.2	–	3.9	*8.0*	–	*14.3*	2.8	*10.9*	0.4	*1.4*	2.2	*9.6*
Spur/branch height ratio	23	18%	–	29%		–		22%	–	3%	–	19%	–
Claw II heights													
Branch	28	10.1	–	14.8	*42.8*	–	*57.1*	12.7	*50.0*	1.3	*3.6*	10.1	*43.9*
Spur	26	2.4	–	3.7	*8.9*	–	*13.8*	2.9	*11.3*	0.3	*1.2*	?	*?*
Spur/branch height ratio	26	19%	–	25%		–		23%	–	2%	–	?	–
Claw III heights													
Branch	24	10.6	–	15.4	*44.2*	–	*55.2*	12.8	*50.0*	1.2	*3.0*	10.6	*46.1*
Spur	22	2.1	–	3.7	*7.7*	–	*14.6*	2.8	*10.9*	0.5	*1.7*	2.1	*9.1*
Spur/branch height ratio	22	17%	–	27%		–		22%	–	3%	–	20%	–
Claw IV heights													
Branch	27	11.1	–	15.9	*43.1*	–	*63.1*	13.5	*53.2*	1.3	*4.4*	11.9	*51.7*
Spur	21	2.1	–	3.4	*9.0*	–	*12.7*	2.7	*10.8*	0.3	*1.1*	2.1	*9.1*
Spur/branch height ratio	21	16%	–	23%		–		20%	–	3%	–	18%	–

Downloaded from https://academic.oup.com/zoolinnean/article/192/3/794/6030998 by guest on 18 April 2022

Table 10. Measurements (in µm) of selected morphological structures of the adult males and a larva of *Hypechiniscus gladiator* (neotype series + population GB.033) mounted in Hoyer's medium. *N*, number of specimens/structures measured; RANGE refers to the smallest and the largest structure among all measured specimens; SD, standard deviation; *sp*, the proportion between the length of a given structure and the length of the scapular plate

CHARACTER	*N*	RANGE		MEAN		SD		Larva	
		µm	*sp*	µm	*sp*	µm	*sp*	µm	*sp*
Body length	30	150 – 239	*773* – *1072*	200	*936*	19	*68*	124	*984*
Scapular plate length	30	18.6 – 24.6	–	21.4	–	1.8	–	12.6	–
Head appendages lengths									
Cirrus internus	26	6.9 – 14.5	*34.8* – *59.8*	9.9	*46.6*	1.7	*6.9*	4.9	*38.9*
Cephalic papilla	30	5.4 – 9.1	*27.3* – *43.5*	7.3	*34.3*	1.1	*3.8*	3.9	*31.0*
Cirrus externus	29	11.5 – 22.2	*50.0* – *91.4*	15.3	*71.4*	2.4	*10.0*	5.8	*46.0*
Clava	30	4.5 – 8.5	*21.5* – *34.6*	5.8	*27.3*	1.0	*3.3*	3.9	*31.0*
Cirrus *A*	28	12.0 – 24.8	*51.3* – *120.3*	19.3	*91.0*	3.5	*15.4*	10.8	*85.7*
Cirrus *A*/Body length ratio	28	6% – 12%	–	10%	–	2%	–	9%	–
Body appendages lengths									
Cirrus C^d	28	30.3 – 62.3	*138.8* – *302.6*	47.3	*221.5*	10.2	*45.2*	23.2	*184.1*
Papilla on leg IV length	17	2.8 – 5.1	*14.1* – *22.5*	3.9	*18.4*	0.6	*2.4*	?	*?*
Claw I heights									
Branch	25	9.1 – 13.4	*43.0* – *60.1*	11.2	*51.2*	1.0	*3.8*	6.5	*51.6*
Spur	20	1.8 – 3.4	*9.0* – *15.1*	2.7	*12.3*	0.4	*1.8*	2.3	*18.3*
Spur/branch height ratio	20	18% – 28%	–	24%	–	3%	–	35%	–
Claw II heights									
Branch	24	8.5 – 13.1	*44.4* – *56.9*	11.0	*51.5*	1.1	*3.3*	6.5	*51.6*
Spur	23	1.9 – 3.1	*9.2* – *16.2*	2.7	*12.5*	0.4	*1.6*	1.8	*14.3*
Spur/branch height ratio	23	17% – 26%	–	24%	–	3%	–	28%	–
Claw III heights									
Branch	24	8.4 – 12.7	*45.2* – *58.1*	11.1	*51.4*	1.1	*2.9*	6.2	*49.2*
Spur	22	1.8 – 3.2	*9.7* – *16.6*	2.6	*11.9*	0.4	*1.6*	1.9	*15.1*
Spur/branch height ratio	22	19% – 25%	–	23%	–	3%	–	31%	–
Claw IV heights									
Branch	28	10.0 – 13.8	*50.5* – *60.9*	12.0	*55.9*	1.0	*2.8*	7.1	*56.3*
Spur	9	2.2 – 3.2	*10.3* – *14.3*	2.6	*12.0*	0.4	*1.3*	?	*?*
Spur/branch height ratio	9	17% – 26%	–	22%	–	3%	–	?	–

Downloaded from https://academic.oup.com/zoolinnean/article/192/3/794/6030998 by guest on 18 April 2022

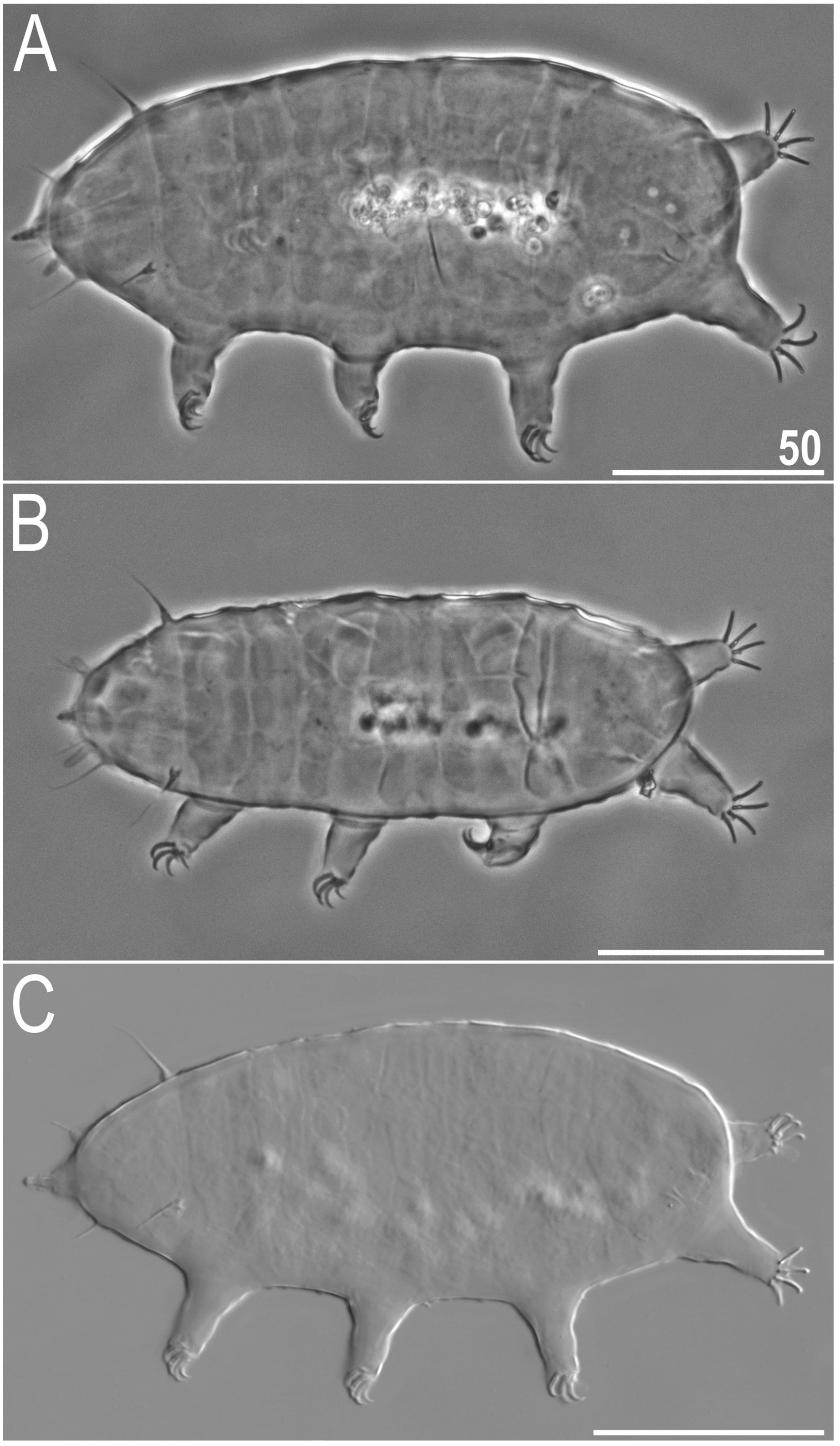

Figure 16. Habitus of *Hypechiniscus cataractus* (LCM): A, holotype (♀), dorsolateral view (PCM); B, allotype (♂), dorsal view (PCM); C, paratype (♀), dorsolateral view (NCM). All scale bars = 50 µm.

Downloaded from https://academic.oup.com/zoolinnean/article/192/3/794/6030998 by guest on 18 April 2022

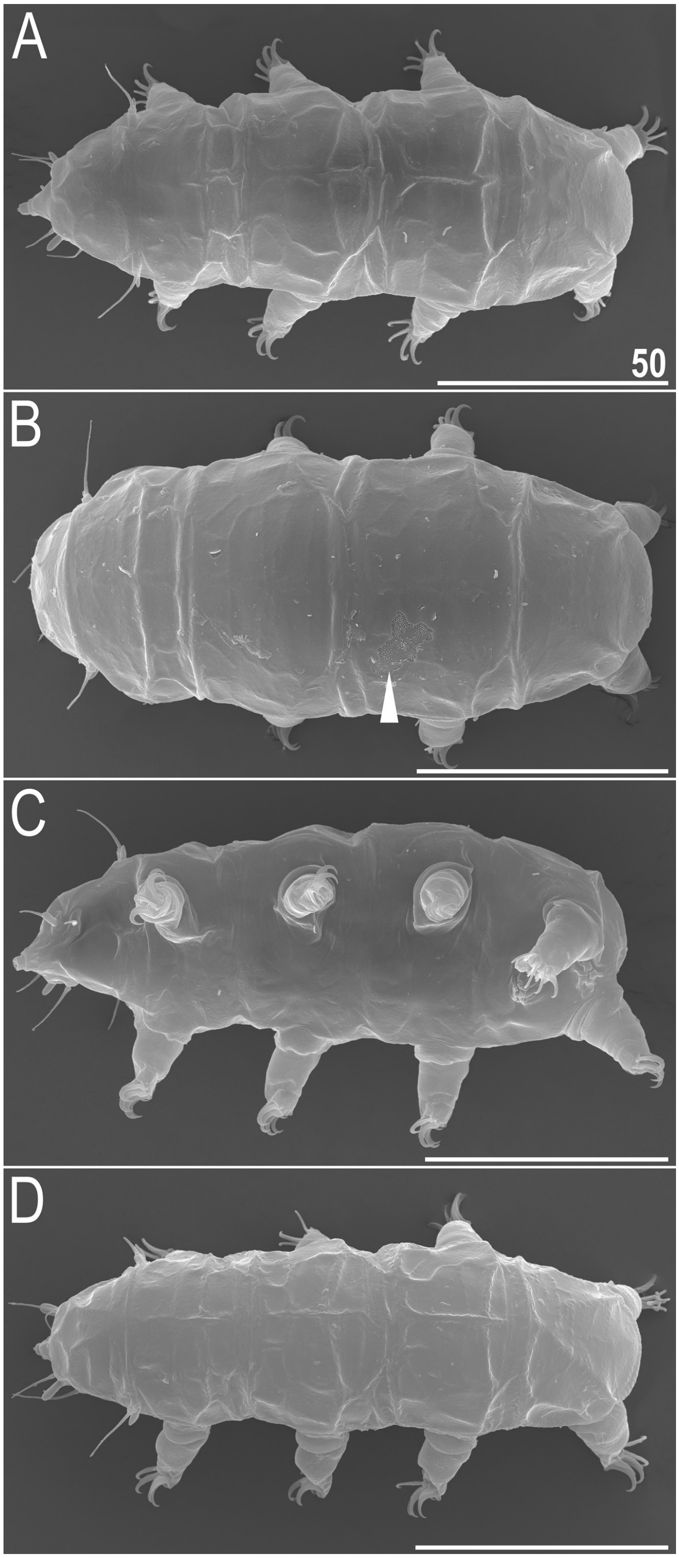

Figure 17. Habitus of *Hypechiniscus cataractus* (SEM): A, paratype (♀), dorsal view; B, paratype (♀), dorsal view, arrowhead indicates an exposed fragment of endocuticle (note the difference in body proportions between the two females); C, paratype (♀), ventral view; D, paratype (♂), dorsal view (note the difference in the body proportions between the members of two sexes). All scale bars = 50 µm.

Downloaded from https://academic.oup.com/zoolinnean/article/192/3/794/6030998 by guest on 18 April 2022

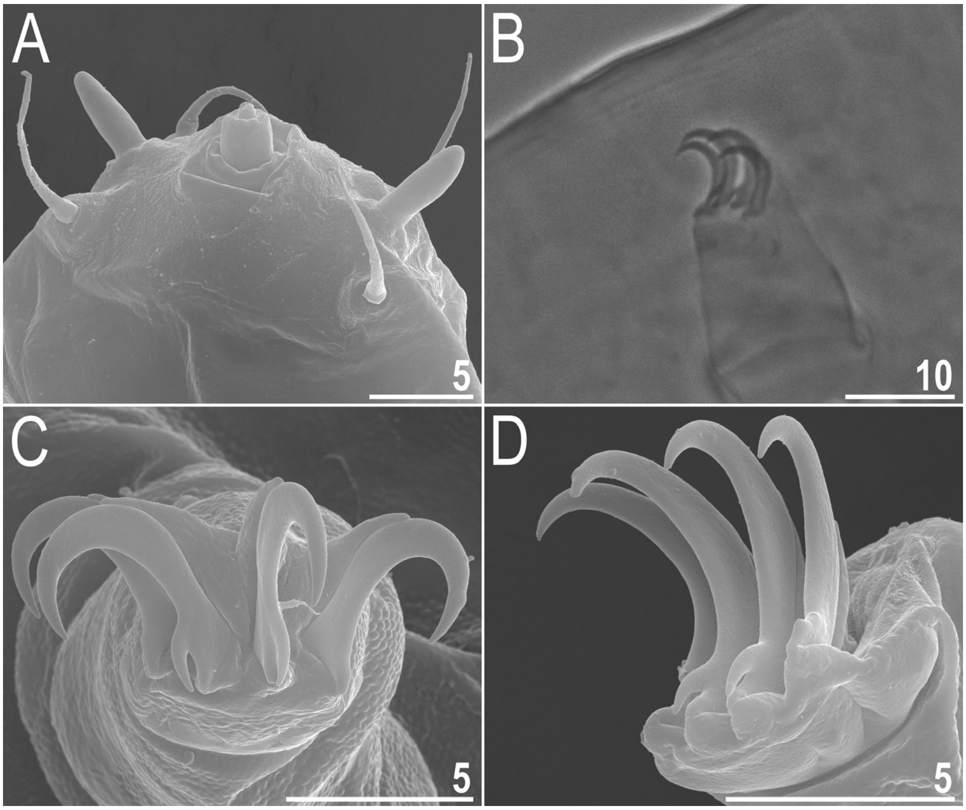

Figure 18. Head appendages and claws of *Hypechiniscus cataractus*: A, peribuccal cirri and secondary clavae (cephalic papillae) in close-up (SEM); B, claws III (PCM, paratype); C, claws II (SEM); D, claws III (SEM). All scale bars in μm.

plate large, with poorly marked incisions (Figs 17A, 19A).

Ventral cuticle with a clear species-specific pattern of ornamentation that extends to the lateroventral margins of the body (Fig. 19B). Ornamentation composed of endocuticular pillars of two sizes: large pillars forming a pseudoplate in the subcephalic zone, at the level of legs I, and a pair of genital pseudoplates; and smaller pillars forming thin stripes and an additional two pseudoplates at the level of legs II–III. Importantly, epicuticular thickenings are absent, thus the venter appears smooth under SEM (Fig. 17C).

Pedal plates, belts of pillars, pulvini, and dentate collar IV absent (Fig. 16A). A small spine or papilla on leg I absent and a papilla on leg IV present (LCM and SEM; Fig. 17A, C). Claws minute and resembling those of *Pseudechiniscus*. Claws IV higher than claws I–III. External claws on all legs smooth. Internal claws with small spurs positioned at *c.* one-quarter of the claw height and strongly bent downwards. Pseudoaccessory points absent (Fig. 18B–D).

Males and sexually dimorphic traits (i.e. from the second instar onwards; measurements and statistics in Table 12): Almost identical to ♀♀, i.e. sexual dimorphism rudimentary, as even the clavae are of similar lengths and shapes in both sexes. The ♂♂ are significantly different from ♀♀ only in body size (see Figs 16B, 17D) estimated as mean body length ± SD: 153 ± 12 μm vs. 179 ± 13 μm (one-tailed Welch's *t*-test with $N_{♀♀} = 15$ and $N_{♂♂} = 10$: $t_{21} = 5.31$; $P < 0.001$); and as average scapular plate length: 15.4 ± 1.5 μm vs. 18.6 ± 1.9 μm ($t_{22} = 4.58$; $P < 0.001$). The *bs* ratios for both sexes overlap (0.32–0.37 in $N = 10$ ♂♂ vs. 0.33–0.43 in $N = 15$ ♀♀).

Juveniles (i.e. the second instar, sexually immature females; measurements and statistics in Table 13): Except for the lack of the gonopore, no qualitative differences with respect to adults were observed. Clearly smaller than adult females.

Larvae and eggs: Unknown.

Genetic markers: Three haplotypes were found for 18S rRNA (*p*-distances = 0.1–0.3%), two for 28S rRNA (0.1%), and six for ITS1 (0.2–0.9%).

Type material: Holotype (adult female, slide MY.802.05), allotype (adult male, slide MY.805.05) and 50 paratypes (21♀♀, 20♂♂, 9 juveniles on slides MY.802.03–6, MY.803.02–3, MY.805.01, 4–7, 11). Slides MY.802.05–6, MY.803.02–3, MY.805.01, 4–6 (15♀♀,

Downloaded from https://academic.oup.com/zoolinnean/article/192/3/794/6030998 by guest on 18 April 2022

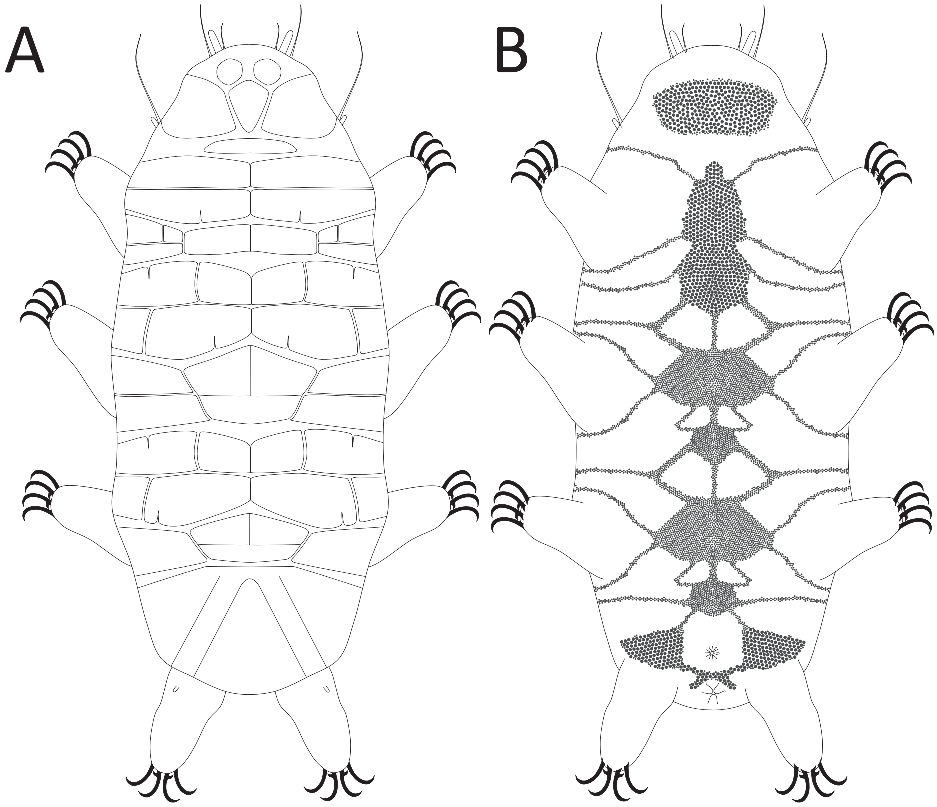

Figure 19. Schematic depiction of morphology of *Hypechiniscus cataractus*: A, dorsum; B, venter.

14♂♂, 5 juveniles) deposited in UJ, slides MY.802.03–4 (3♀♀, 3♂♂, 3 juveniles) deposited in CU, and slides MY.805.07, 11 (3♀♀, 4♂♂, 1 juvenile) deposited in Lee Kong Chian Natural History Museum of Singapore.

Type locality: *c.* 1°43'28"N, 110°28'13"E, 67–90 m a.s.l.: Malaysia, Borneo, Sarawak, Bako Peninsula (see Supporting Information, Fig. S4); Sundaland heath forest (*keranga*) passing into *padang* scrub with dominant *Nepenthes gracilis* Korth. and *N. rafflesiana* Jack pitcher plants, both growing on acidic arenosols; moss from tree bark.

Etymology: From Latin *cataracta* = waterfall. The name signifies the type locality, localised in the vicinity of the waterfall Terjun Tajor. An adjective in the nominative singular.

Phenotypic differential diagnosis: The species is separated from all other known *Hypechiniscus* spp. by the absence of dorsal sculpturing.

Genetic differential diagnosis: Uncorrected *p*-distances between *H. cataractus* and other species are as follows:

- 18S rRNA: from 2.6% (*H. gladiator*, MT809240) to 5.8% (*H. flavus*, HM193377).
- 28S rRNA: from 4.3% (*H. daedalus*, MT809199, MT809200) to 6.4% (*H. exarmatus*, MT809201).
- ITS1: from 16.9% (*H. gladiator*, MT809194) to 18.2% (*H. daedalus*, MT809186, MT809188).

Genetically verified geographic distribution: The Indomalayan realm: Indonesia, Malaysia.

Species: Hypechiniscus exarmatus (Murray, 1907)

Echiniscus gladiator var. *exarmatus*; *locus typicus*: Ronas Hill (Shetland Islands); Murray (1907)

E. gladiator var. *exarmatus*; Achill Island, Clare Island, Inishturk Island, Belclare (Ireland); Murray (1911)

Hypechiniscus gladiator exarmatus; Rocca d'Argimonia (Piedmont, Italy); Bertolani *et al*. (1984)

H. exarmatus; Faroe Islands; Trygvadóttir & Kristensen (2013)

(Figs 20–21; Tables 14, 15)

Downloaded from https://academic.oup.com/zoolinnean/article/192/3/794/6030998 by guest on 18 April 2022

Table 11. Measurements (in µm) of selected morphological structures of the adult females of *Hypechiniscus cataractus* (type series) mounted in Hoyer's medium. *N*, number of specimens/structures measured; RANGE refers to the smallest and the largest structure among all measured specimens; SD, standard deviation; *sp*, the proportion between the length of a given structure and the length of the scapular plate

CHARACTER	*N*	RANGE						MEAN		SD		Holotype	
		µm			*sp*			µm	*sp*	µm	*sp*	µm	*sp*
Body length	15	158	–	206	*823*	–	*1139*	179	*972*	13	*101*	183	*915*
Scapular plate length	15	14.2	–	20.4		–		18.6	–	1.9	–	20.0	–
Head appendages lengths													
Cirrus internus	15	7.0	–	11.5	*35.8*	–	*59.7*	9.0	*48.6*	1.4	*7.8*	8.4	*42.0*
Cephalic papilla	15	4.5	–	6.9	*23.5*	–	*43.0*	5.7	*30.8*	0.7	*4.5*	6.9	*34.5*
Cirrus externus	15	9.4	–	16.8	*48.7*	–	*111.3*	14.1	*76.8*	2.1	*14.8*	13.4	*67.0*
Clava	12	3.2	–	5.6	*16.2*	–	*37.1*	4.2	*22.5*	0.6	*5.2*	4.4	*22.0*
Cirrus *A*	15	14.5	–	20.8	*71.8*	–	*123.2*	17.1	*93.1*	1.8	*13.2*	17.4	*87.0*
Cirrus *A*/Body length ratio	15	8%	–	11%		–		10%	–	1%	–	10%	–
Body appendages lengths													
Papilla on leg IV length	5	1.9	–	2.7	*10.1*	–	*13.2*	2.2	*11.8*	0.3	*1.2*	?	*?*
Claw I heights													
Branch	14	6.5	–	8.5	*32.2*	–	*47.5*	7.3	*39.7*	0.6	*4.8*	7.1	*35.5*
Spur	11	0.7	–	1.5	*4.4*	–	*8.6*	1.2	*6.2*	0.2	*1.2*	1.2	*6.0*
Spur/branch height ratio	11	11%	–	19%		–		16%	–	3%	–	17%	–
Claw II heights													
Branch	13	6.1	–	8.3	*32.0*	–	*43.7*	7.1	*38.6*	0.7	*4.0*	6.4	*32.0*
Spur	10	0.9	–	1.6	*4.4*	–	*8.3*	1.1	*5.7*	0.2	*1.2*	1.2	*6.0*
Spur/branch height ratio	9	12%	–	19%		–		15%	–	3%	–	19%	–
Claw III heights													
Branch	15	6.2	–	8.1	*32.5*	–	*43.7*	7.1	*38.5*	0.6	*3.8*	6.5	*32.5*
Spur	12	0.8	–	1.4	*3.9*	–	*7.7*	1.1	*5.9*	0.2	*1.2*	1.2	*6.0*
Spur/branch height ratio	12	11%	–	20%		–		15%	–	3%	–	18%	–
Claw IV heights													
Branch	14	7.0	–	9.0	*35.6*	–	*53.6*	8.0	*43.5*	0.6	*4.8*	8.3	*41.5*
Spur	9	0.7	–	1.4	*4.1*	–	*7.3*	1.0	*5.5*	0.2	*1.0*	?	*?*
Spur/branch height ratio	9	9%	–	16%		–		13%	–	2%	–	?	–

Downloaded from https://academic.oup.com/zoolinnean/article/192/3/794/6030998 by guest on 18 April 2022

Table 12. Measurements (in µm) of selected morphological structures of the adult males of *Hypechiniscus cataractus* (type series) mounted in Hoyer's medium. *N*, number of specimens/structures measured; RANGE refers to the smallest and the largest structure among all measured specimens; SD, standard deviation; *sp*, the proportion between the length of a given structure and the length of the scapular plate

CHARACTER	*N*	RANGE		MEAN		SD		Allotype	
		µm	*sp*	µm	*sp*	µm	*sp*	µm	*sp*
Body length	10	129 – 175	*877 – 1183*	153	*996*	12	*99*	149	*974*
Scapular plate length	10	12.6 – 17.9	–	15.4	–	1.5	–	15.3	–
Head appendages lengths									
Cirrus internus	10	6.1 – 10.1	*40.7 – 66.7*	8.1	*52.6*	1.4	*8.5*	9.2	*60.1*
Cephalic papilla	10	4.9 – 7.7	*31.6 – 50.0*	6.4	*42.0*	1.0	*6.5*	7.3	*47.7*
Cirrus externus	10	11.8 – 17.6	*76.2 – 110.7*	13.9	*90.8*	1.5	*11.3*	14.0	*91.5*
Clava	10	4.0 – 6.2	*26.5 – 40.5*	5.1	*32.9*	0.8	*4.6*	6.2	*40.5*
Cirrus *A*	10	11.1 – 18.5	*64.5 – 138.1*	14.3	*93.8*	2.6	*22.6*	12.5	*81.7*
Cirrus *A*/Body length ratio	10	7% – 12%	–	9%	–	2%	–	8%	–
Body appendages lengths									
Papilla on leg IV length	8	1.7 – 2.5	*10.7 – 14.5*	2.1	*13.1*	0.3	*1.2*	2.0	*13.1*
Claw I heights									
Branch	9	5.9 – 6.7	*39.0 – 46.8*	6.4	*42.2*	0.3	*2.7*	6.0	*39.2*
Spur	6	0.8 – 1.3	*5.2 – 8.5*	1.1	*6.8*	0.2	*1.2*	1.3	*8.5*
Spur/branch height ratio	6	12% – 22%	–	17%	–	4%	–	22%	–
Claw II heights									
Branch	9	5.8 – 6.5	*35.5 – 48.4*	6.2	*41.1*	0.2	*3.8*	6.0	*39.2*
Spur	8	0.7 – 1.3	*4.5 – 8.7*	1.0	*6.9*	0.2	*1.4*	0.9	*5.9*
Spur/branch height ratio	8	11% – 21%	–	17%	–	3%	–	15%	–
Claw III heights									
Branch	8	6.0 – 7.1	*39.7 – 48.4*	6.4	*42.0*	0.3	*3.1*	?	*?*
Spur	7	0.7 – 1.1	*5.0 – 7.2*	0.9	*6.2*	0.1	*0.9*	?	*?*
Spur/branch height ratio	7	11% – 17%	–	15%	–	2%	–		–
Claw IV heights									
Branch	9	6.2 – 8.0	*40.7 – 52.4*	7.2	*46.1*	0.6	*3.6*	6.5	*42.5*
Spur	9	0.8 – 1.5	*5.1 – 10.2*	1.1	*7.0*	0.2	*1.7*	0.9	*5.9*
Spur/branch height ratio	9	11% – 19%	–	15%	–	3%	–	14%	–

Downloaded from https://academic.oup.com/zoolinnean/article/192/3/794/6030998 by guest on 18 April 2022

Table 13. Measurements (in µm) of selected morphological structures of the juveniles of *Hypechiniscus cataractus* (type series) mounted in Hoyer's medium. *N*, number of specimens/structures measured; RANGE refers to the smallest and the largest structure among all measured specimens; SD, standard deviation; *sp*, the proportion between the length of a given structure and the length of the scapular plate

CHARACTER	*N*	RANGE						MEAN		SD	
		µm			*sp*			µm	*sp*	µm	*sp*
Body length	5	96	–	158	*873*	–	*1065*	134	*954*	25	*73*
Scapular plate length	5	11.0	–	16.2		–		14.0	–	2.2	–
Head appendages lengths											
Cirrus internus	5	4.7	–	7.5	*42.7*	–	*54.7*	6.6	*47.5*	1.1	*5.1*
Cephalic papilla	5	3.9	–	4.9	*26.5*	–	*35.9*	4.4	*32.2*	0.4	*4.7*
Cirrus externus	5	7.0	–	12.9	*63.6*	–	*87.5*	10.6	*75.6*	2.2	*8.8*
Clava	2	3.5	–	4.1	*21.6*	–	*25.3*	3.8	*23.5*	0.4	*2.6*
Cirrus *A*	5	10.0	–	19.5	*79.7*	–	*120.4*	13.6	*96.7*	3.7	*16.0*
Cirrus *A*/Body length ratio	5	7%	–	12%		–		10%	–	2%	–
Body appendages lengths											
Papilla on leg IV length	2	1.8	–	2.2	*11.1*	–	*17.2*	2.0	*14.1*	0.3	*4.3*
Claw I heights											
Branch	5	4.6	–	6.5	*39.5*	–	*44.2*	5.8	*41.7*	0.8	*1.9*
Spur	3	0.7	–	1.0	*4.3*	–	*6.4*	0.8	*5.6*	0.2	*1.1*
Spur/branch height ratio	3	11%	–	15%		–		14%	–	3%	–
Claw II heights											
Branch	5	4.3	–	6.4	*36.4*	–	*46.4*	5.6	*40.4*	0.8	*4.2*
Spur	4	0.5	–	1.0	*4.5*	–	*7.8*	0.8	*5.7*	0.2	*1.5*
Spur/branch height ratio	4	12%	–	18%		–		15%	–	3%	–
Claw III heights											
Branch	5	4.1	–	6.4	*37.3*	–	*46.1*	5.7	*41.1*	0.9	*4.1*
Spur	3	0.7	–	1.0	*6.2*	–	*6.4*	0.9	*6.2*	0.2	*0.1*
Spur/branch height ratio	3	16%	–	17%		–		16%	–	1%	–
Claw IV heights											
Branch	4	5.0	–	7.0	*41.4*	–	*46.1*	6.2	*44.0*	0.9	*2.2*
Spur	4	0.8	–	1.1	*6.2*	–	*8.2*	1.0	*6.8*	0.1	*0.9*
Spur/branch height ratio	4	14%	–	18%		–		16%	–	2%	–

Downloaded from https://academic.oup.com/zoolinnean/article/192/3/794/6030998 by guest on 18 April 2022

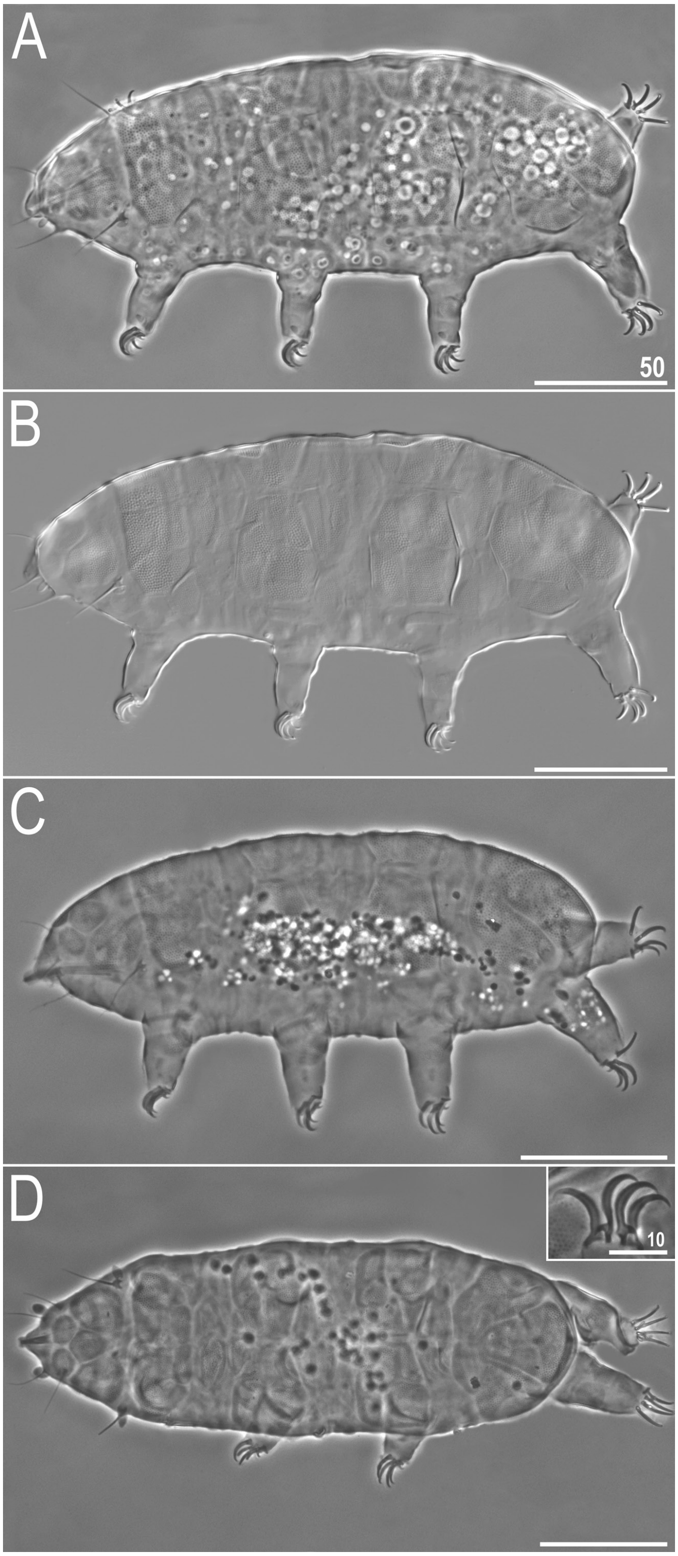

Figure 20. Habitus of *Hypechiniscus exarmatus* (Murray, 1907) (LCM): A, female, dorsolateral view (PCM); B, female, dorsolateral view (NCM); C, male, dorsolateral view (PCM); D, male, dorsal view (PCM). Inset: claws II (PCM). All scale bars = 50 μm (with the exception of the inset).

Downloaded from https://academic.oup.com/zoolinnean/article/192/3/794/6030998 by guest on 18 April 2022

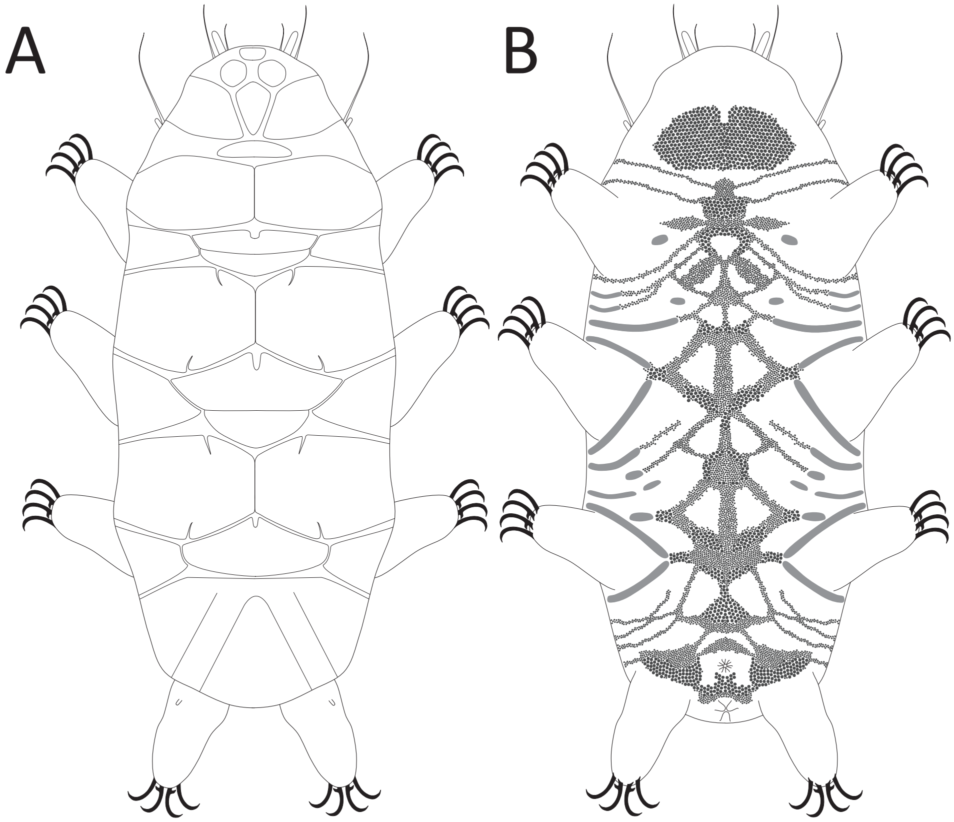

Figure 21. Schematic depiction of morphology of *Hypechiniscus exarmatus*: A, dorsum; B, venter.

Description

Females (i.e. from the third instar onwards; measurements and statistics in Table 14): Body translucent and slender (Fig. 20A, B), with small spheroid black eyes, persisting also after mounting. Elongated, dactyloid cephalic papillae (secondary clavae) and (primary) clavae (Fig. 20A, B); peribuccal cirri without cirrophores. Cirrus *A* short, with the cirrophore (Fig. 20A, B). *Cirrus dorsalis* absent.

Dorsal plates poorly sclerotized, with *Pseudechiniscus*-type sculpturing, i.e. endocuticular pillars protruding through the epicuticle and visible as densely packed dark dots in PCM (Fig. 20A), and bumps in NCM (Fig. 20B). The sculpture is well-developed and evident in LCM. Lacking ornamentation of the epicuticular layer. The cephalic plate is large and clearly sexpartite, with three small anterior portions, a central keel-like portion and two significantly larger trapezoid portions (Figs 20A, B, 21A). The cervical (neck) plate not visible in LCM, presumably reduced to a thickening of the anterior margin of the scapular plate (Fig. 21A). The scapular plate divided in two parts by a central longitudinal suture (Figs 20A, B, 21A). Median plates 1–2 bipartite, and median plate 3 unipartite (Figs 20B, 21A), with three pairs of lateral intersegmental platelets flanking their boarders (Figs 20B, 21A). Two pairs of large segmental plates with short incisions at their anterodorsal and posterodorsal margins (Figs 20A, B, 21A). Caudal (terminal) plate large, with long incisions (Figs 20D, 21A).

Ventral cuticle with a clear species-specific pattern of ornamentation, which extends to the lateroventral sides of the body, composed of epicuticular thickenings and endocuticular pillars of variable size (Fig. 21B). Belts of epicuticular thickenings extending medially from the ventral margin. Belts enclosing legs II and III replaced at their mutual junction by predominantly large endocuticular pillars. The remaining belts, which are of variable length, transition into small endocuticular pillars. Two aggregations of large pillars are present: in the subcephalic zone (pseudoplate with an anterior incision), and in the genital zone, surrounding the gonopore laterally and posteriorly (lateral portions form wing-shaped pseudoplates). Sexpartite gonopore placed anteriorly of legs IV and the trilobed anus placed between legs IV.

Downloaded from https://academic.oup.com/zoolinnean/article/192/3/794/6030998 by guest on 18 April 2022

Table 14. Measurements (in µm) of selected morphological structures of the adult females of *Hypechiniscus exarmatus* (populations GB.061 + GB.110) mounted in Hoyer's medium. *N*, number of specimens/structures measured; RANGE refers to the smallest and the largest structure among all measured specimens; SD, standard deviation; *sp*, the proportion between the length of a given structure and the length of the scapular plate

CHARACTER	*N*	RANGE						MEAN		SD	
		µm			*sp*			µm	*sp*	µm	*sp*
Body length	6	144	–	256	*742*	–	*967*	202	*817*	41	*83*
Scapular plate length	6	18.4	–	31.1		–		24.8	–	5.3	–
Head appendages lengths											
Cirrus internus	5	8.0	–	13.6	*37.9*	–	*55.3*	11.1	*45.4*	2.4	*7.1*
Cephalic papilla	6	3.5	–	4.9	*13.3*	–	*19.6*	4.1	*16.7*	0.6	*2.6*
Cirrus externus	6	13.3	–	19.5	*56.1*	–	*77.2*	16.5	*67.2*	2.8	*8.4*
Clava	6	2.1	–	4.4	*10.8*	–	*17.9*	3.4	*13.9*	0.8	*2.7*
Cirrus *A*	6	20.3	–	25.2	*70.8*	–	*118.5*	22.5	*93.3*	1.8	*16.9*
Cirrus *A*/Body length ratio	6	9%	–	14%		–		11%	–	2%	–
Body appendages lengths											
Papilla on leg IV length	4	1.9	–	2.7	*7.5*	–	*12.0*	2.4	*9.7*	0.4	*2.0*
Claw I heights											
Branch	6	7.8	–	11.7	*37.6*	–	*51.1*	10.2	*41.7*	1.5	*4.8*
Spur	5	1.0	–	1.9	*4.7*	–	*6.1*	1.4	*5.3*	0.3	*0.5*
Spur/branch height ratio	5	11%	–	16%		–		13%	–	2%	–
Claw II heights											
Branch	6	7.6	–	11.6	*34.6*	–	*51.1*	10.0	*40.9*	1.4	*5.9*
Spur	5	1.0	–	2.1	*4.3*	–	*6.8*	1.4	*5.7*	0.4	*0.9*
Spur/branch height ratio	5	11%	–	18%		–		14%	–	3%	–
Claw III heights											
Branch	6	7.3	–	11.7	*37.6*	–	*50.5*	10.2	*41.8*	1.7	*5.3*
Spur	5	1.0	–	2.3	*5.4*	–	*7.6*	1.6	*6.0*	0.5	*0.9*
Spur/branch height ratio	5	11%	–	20%		–		14%	–	4%	–
Claw IV heights											
Branch	6	9.3	–	12.3	*39.2*	–	*56.0*	11.1	*45.8*	1.2	*6.7*
Spur	6	1.1	–	2.0	*4.7*	–	*8.1*	1.6	*6.2*	0.5	*1.1*
Spur/branch height ratio	6	11%	–	16%		–		14%	–	3%	–

Downloaded from https://academic.oup.com/zoolinnean/article/192/3/794/6030998 by guest on 18 April 2022

Table 15. Measurements (in μm) of selected morphological structures of the adult males of *Hypechiniscus exarmatus* (population GB.061) mounted in Hoyer's medium. *N*, number of specimens/structures measured; RANGE refers to the smallest and the largest structure among all measured specimens; SD, standard deviation; *sp*, the proportion between the length of a given structure and the length of the scapular plate

CHARACTER	*N*	RANGE						MEAN		SD	
		μm			*sp*			μm	*sp*	μm	*sp*
Body length	2	205	–	235	*810*	–	*880*	220	*845*	21	*49*
Scapular plate length	2	25.3	–	26.7		–		26.0	–	1.0	–
Head appendages lengths											
Cirrus internus	2	8.9	–	16.8	*35.2*	–	*62.9*	12.9	*49.0*	5.6	*19.6*
Cephalic papilla	2	5.6	–	6.7	*22.1*	–	*25.1*	6.2	*23.6*	0.8	*2.1*
Cirrus externus	2	12.5	–	21.1	*49.4*	–	*79.0*	16.8	*64.2*	6.1	*20.9*
Clava	2	3.4	–	6.6	*13.4*	–	*24.7*	5.0	*19.1*	2.3	*8.0*
Cirrus *A*	2	23.4	–	24.2	*87.6*	–	*95.7*	23.8	*91.6*	0.6	*5.7*
Cirrus *A*/Body length ratio	2	10%	–	12%		–		11%	–	1%	–
Body appendages lengths											
Papilla on leg IV length	2	2.0	–	3.0	*7.9*	–	*11.2*	2.5	*9.6*	0.7	*2.4*
Claw I heights											
Branch	2	10.6	–	12.3	*41.9*	–	*46.1*	11.5	*44.0*	1.2	*2.9*
Spur	2	1.3	–	1.6	*5.1*	–	*6.0*	1.5	*5.6*	0.2	*0.6*
Spur/branch height ratio	2	12%	–	13%		–		13%	–	1%	–
Claw II heights											
Branch	2	10.6	–	12.6	*41.9*	–	*47.2*	11.6	*44.5*	1.4	*3.7*
Spur	2	1.5	–	1.6	*5.6*	–	*6.3*	1.6	*6.0*	0.1	*0.5*
Spur/branch height ratio	2	12%	–	15%		–		13%	–	2%	–
Claw III heights											
Branch	2	10.9	–	12.2	*43.1*	–	*45.7*	11.6	*44.4*	0.9	*1.8*
Spur	2	1.8	–	1.8	*6.7*	–	*7.1*	1.8	*6.9*	0.0	*0.3*
Spur/branch height ratio	2	15%	–	17%		–		16%	–	1%	–
Claw IV heights											
Branch	2	11.8	–	14.8	*46.6*	–	*55.4*	13.3	*51.0*	2.1	*6.2*
Spur	1	1.9	–	1.9	*7.5*	–	*7.5*	1.9	*7.5*	?	*?*
Spur/branch height ratio	1	16%	–	16%		–		16%	–	?	–

Downloaded from https://academic.oup.com/zoolinnean/article/192/3/794/6030998 by guest on 18 April 2022

Pedal plates and dentate collar IV absent. Large, centrally placed patches of pillars present on each leg. Weakly developed pulvini on all legs. Markedly sclerotized areas present on the inner side of each leg below the claws (Fig. 20A). A spine or papilla on leg I absent (LCM). Papilla on leg IV present (Fig. 20A, B). Claws I–IV of equal heights. External claws on all legs smooth. Internal claws with small spurs positioned at *c.* one-quarter of the claw height and strongly bent downwards (Fig. 20D, insert).

Males and sexually dimorphic traits (i.e. from the second instar onwards; measurements and statistics in Table 15): Almost identical to ♀♀, i.e. sexual dimorphism is rudimentary, as even the clavae are of similar lengths in both sexes (compare Fig. 20A with Fig. 20C). Cephalic papillae and clavae broader in ♂♂ (Fig. 20D). ♂♂ are slightly slimmer (bs = 0.33–0.35 in N = 2 ♂♂ vs. 0.35–0.40 in N = 6 ♀♀).

Juveniles, larvae and eggs: Unknown.

Genetic markers: All four markers were characterized by single haplotypes (see *Table 3* for details).

Type locality: 60°32'02"N, 1°26'46"W, *c.* 450 m a.s.l.; Ronas Hill, Mainland (Shetland); isolated hill.

Etymology: From Latin *exarmo* = disarm, thus the name most likely refers to the absence of *cirrus dorsalis* in reference to the 'armed' *H. gladiator*. An adjective in the nominative singular.

Phenotypic differential diagnosis: The species is separated from the *gladiator* group based on the absence of the *cirrus dorsalis* and it differs from the remaining members of the *exarmatus* group:

- *H. flavus* by having a translucent body (lemon-yellow body colour in the new species; see Fig. 7).
- *H. cataractus* by endocuticular pillars visible in LCM (greyish dorsal plates with no apparent pillars visible in LCM in the new species; compare Figs 16 and 20).

Genetic differential diagnosis: Uncorrected *p*-distances between *H. exarmatus* and other species are as follows:

- 18S rRNA: from 2.9% (*H. daedalus*, MT809236–7) to 4.4% (*H. cataractus*, MT809233).
- 28S rRNA: from 3.2% (*H. gladiator*, MT809202–3) to 6.4% (*H. cataractus*, MT809195–8).
- ITS1: from 12.5% (*H. gladiator* and *H. daedalus*, MT809191–4, MT809187, MT809189) to 17.7% (*H. cataractus*, MT809184).
- *COI*: from 21.1% (*H. flavus*, HM193410) to 22.9% (*H. geminus*, HM193411).

Genetically verified geographic distribution: Western Palaearctic: Scotland.

Species: Hypechiniscus flavus Gąsiorek, Oczkowski, Suzuki, Kristensen & Michalczyk, sp. nov.

Zoobank registration: 84BD6B3B-8134-45A5-A778-34491DD0100C.

Hypechiniscus exarmatus; Mt. Amigasa (Nagano Prefecture, Japan); Jørgensen *et al.* (2011)

(Figs 7, 22–25, 26D; Tables 16–18)

Description

Females (i.e. from the third instar onwards; measurements and statistics in Table 16): Body lemon-yellow (Fig. 7) and stout (Figs 22A, B, 23), with ovoid black eyes, persisting also after mounting. Elongated, dactyloid cephalic papillae (secondary clavae) and (primary) clavae (Figs 22A, B, 24A); peribuccal cirri without cirrophores. Cirrus *A* short, with cirrophore (Fig. 22A, B). *Cirrus dorsalis* absent.

Dorsal plates poorly sclerotized, with an indistinct *Pseudechiniscus*-type sculpturing, i.e. endocuticular pillars visible as faint dark densely packed dots in PCM (Fig. 22A) and bumps in NCM (Fig. 22B). *Capituli* (heads) of pillars barely visible in SEM (Fig. 26D). No epicuticular ridges or epicuticular ornamentation visible under SEM; however, irregularly distributed, epicuticular rings (circular and oval structures with thick rims) are visible (Fig. 26D, arrowheads). Generally, the sculpture is poorly developed and barely identifiable in LCM. The cephalic plate is large and pentapartite, with two small anterior portions, a central keel-like portion and two larger trapezoid posterior portions (Figs 22A, B, 25A). The cervical (neck) plate is not visible in LCM and indistinctly merged with the anterior margin of the scapular plate. The scapular plate solid, undivided by sutures (Figs 22A, B, 25A). Three median plates, all weakly outlined and unipartite (Figs 22A, B, 25A), with three pairs of lateral intersegmental platelets flanking their borders (Fig. 25A). Two pairs of large segmental plates without incisions or sutures (Figs 22A, B, 23A, 25A). Caudal (terminal) plate large, without incisions (Figs 22A, B, 23A, 25A).

Downloaded from https://academic.oup.com/zoolinnean/article/192/3/794/6030998 by guest on 18 April 2022

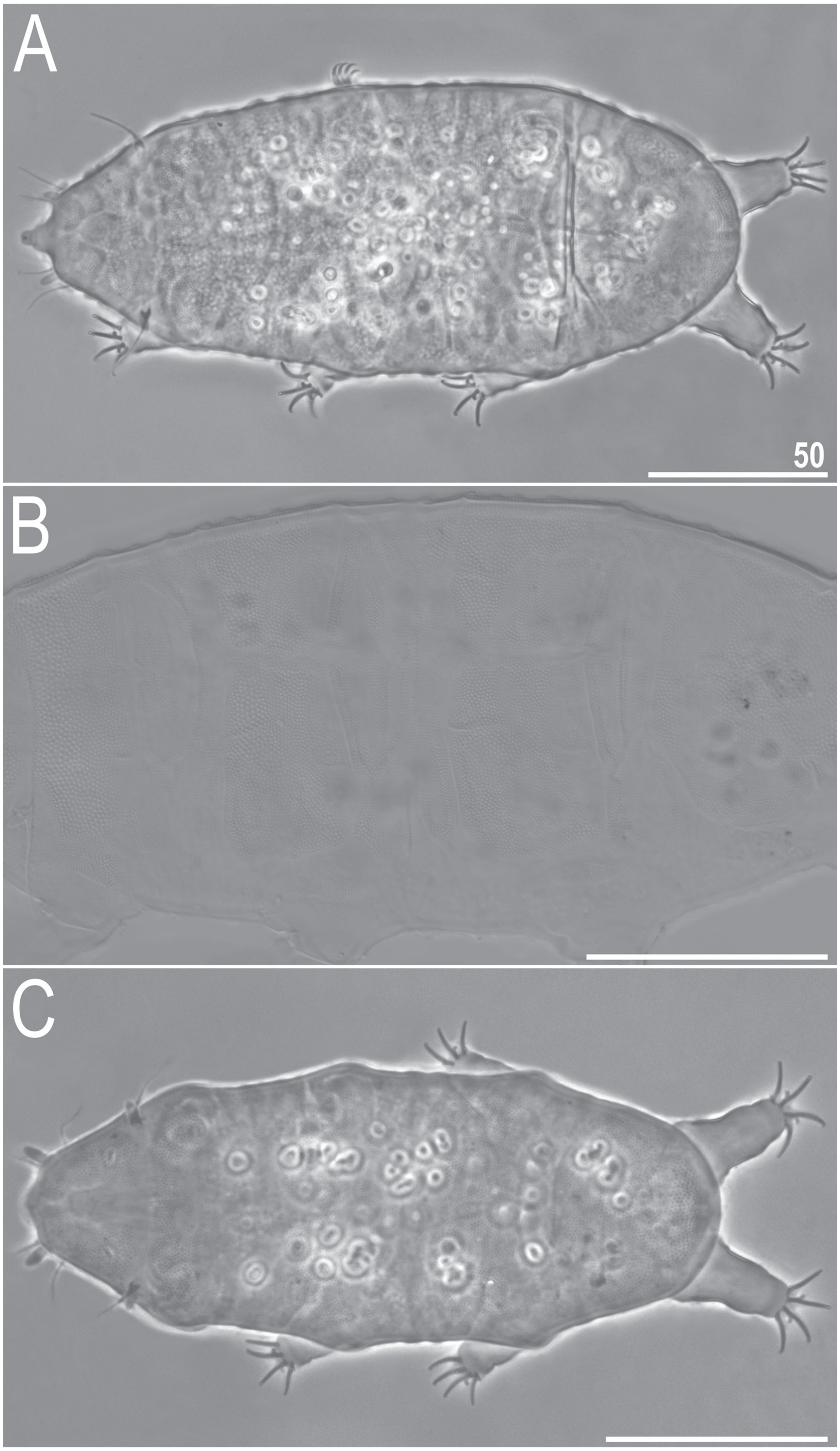

Figure 22. Habitus of *Hypechiniscus flavus* (LCM): A, holotype ♀, dorsal view (PCM); B, holotype ♀, dorsal view (NCM); C, allotype ♂, dorsal view (PCM). All scale bars = 50 μm.

Downloaded from https://academic.oup.com/zoolinnean/article/192/3/794/6030998 by guest on 18 April 2022

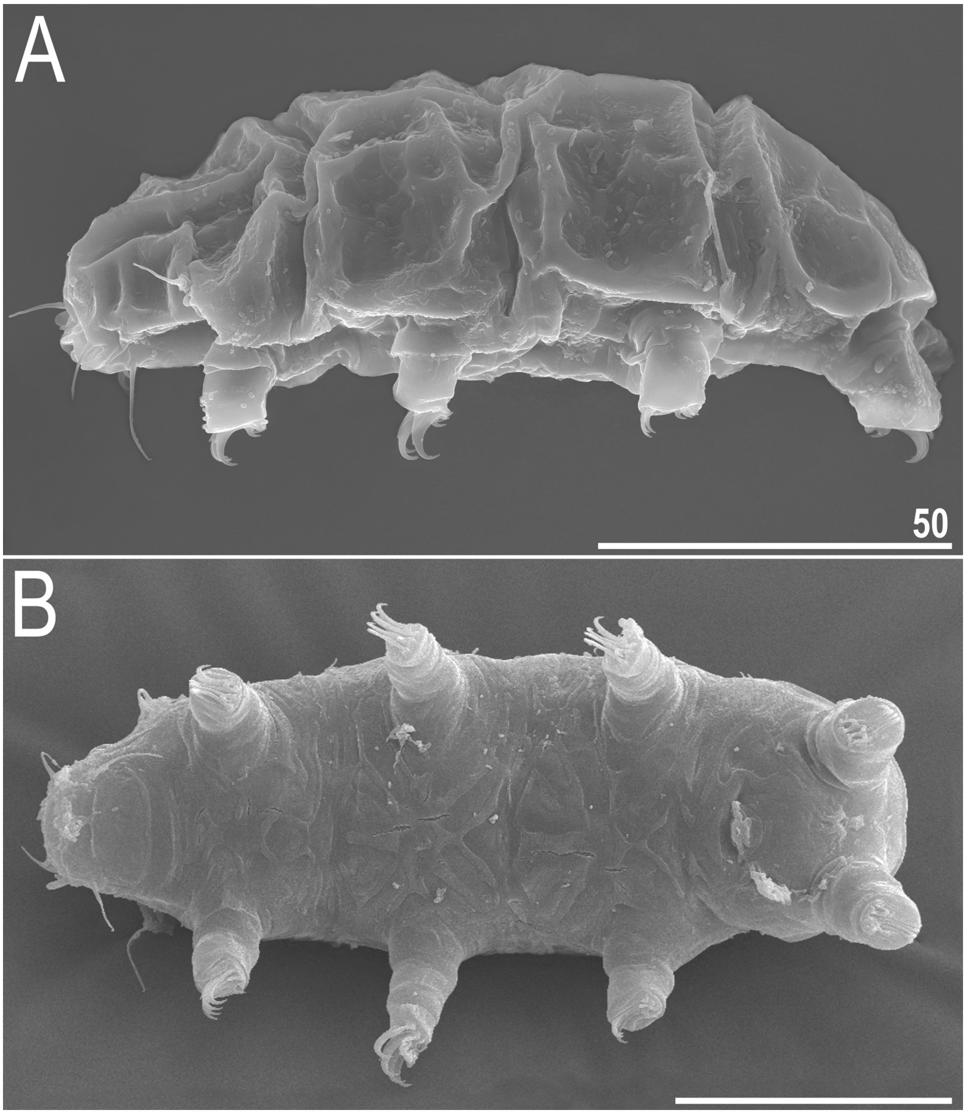

Figure 23. Habitus of *Hypechiniscus flavus* (SEM): A, paratype ♀, lateral view; B, paratype ♀, ventral view. All scale bars = 50 µm.

Ventral cuticle with a clear species-specific pattern of predominantly epicuticular thickenings reaching the lateroventral sides of the body (Figs 23B, 25B). Endocuticular pillars generally overlap with the thickenings, and only occasionally fill the surface between them (Fig. 25B). The largest pillars occur in the centromedian portion of the venter.

Pedal plates, belts of pillars, pulvini and dentate collar IV absent (Fig. 23A). Markedly sclerotized areas at the inner side of all legs below the claws present. A small spine or papilla on leg I absent (LCM and SEM). A papilla on leg IV present (Fig. 23A). Claws on legs I–IV of equal heights. External claws on all legs smooth (Fig. 24). Internal claws with small spurs positioned at *c.* one-quarter of the claw height and strongly bent downwards. Pseudoaccessory points absent (Fig. 24B).

Males and sexually dimorphic traits (i.e. from the second instar onwards; measurements and statistics in Table 17): Males almost identical to ♀♀, i.e. sexual dimorphism is rudimentary, as even clavae are of similar lengths and shapes in both sexes (compare Fig. 22A, B with Fig. 22C). ♂♂ are significantly different from ♀♀ in body size, estimated both as mean body length ± SD: 173 ± 12 µm vs. 205 ± 13 µm (one-tailed Welch's *t*-test with $N_{♀♀} = 15$ and $N_{♂♂} = 15$: $t_{28} = 7.14$; $P < 0.001$) and as average scapular plate length: 18.5 ± 1.5 µm vs. 21.9 ± 1.2 µm ($t_{52} = 6.81$; $P < 0.001$). In contrast to females, claws IV in males are clearly

Downloaded from https://academic.oup.com/zoolinnean/article/192/3/794/6030998 by guest on 18 April 2022

higher than claws I–III (e.g. claw I mean height ± SD: 9.2 ± 0.9 µm vs. claw IV mean height ± SD: 10.7 ± 1.0 µm; $N = 15$; $t_{28} = -4.33$; $P < 0.001$). The *bs* ratio ranges also overlap (0.34–0.41 in $N = 12$ ♂♂ vs. 0.34–0.43 in $N = 12$ ♀♀).

Juveniles (i.e. the second instar, sexually immature females; measurements and statistics in Table 18): Except for the lack of a gonopore, no qualitative differences with respect to females. Smaller than adult females (compare Tables 16 and 18).

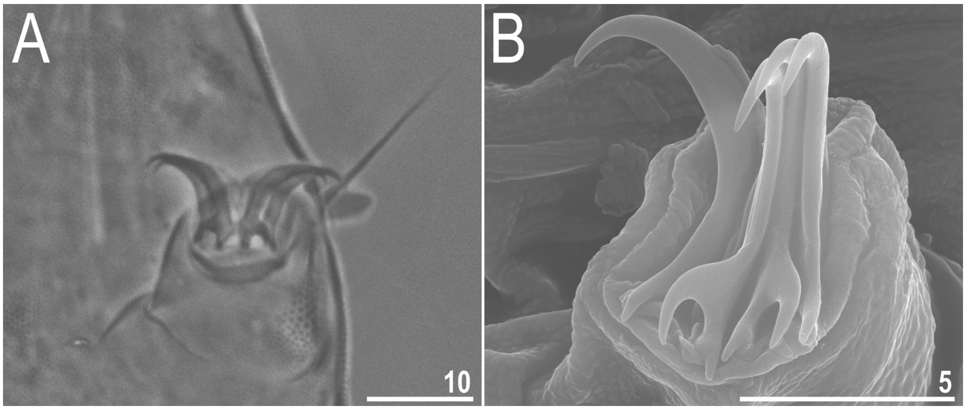

Figure 24. Claws of *Hypechiniscus flavus*: A, claws I (PCM, allotype); B, claws II (SEM). Note that the cuticle margin is tightly adjacent to the claws. All scale bars in µm.

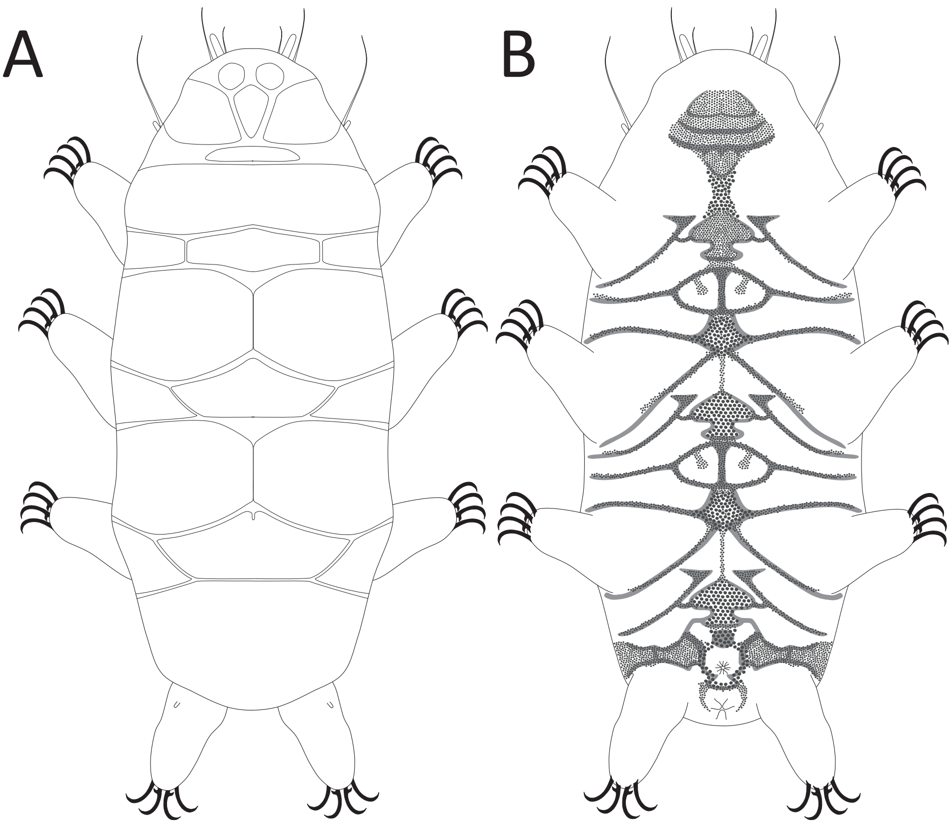

Figure 25. Schematic depiction of morphology of *Hypechiniscus flavus*: A, dorsum; B, venter.

Downloaded from https://academic.oup.com/zoolinnean/article/192/3/794/6030998 by guest on 18 April 2022

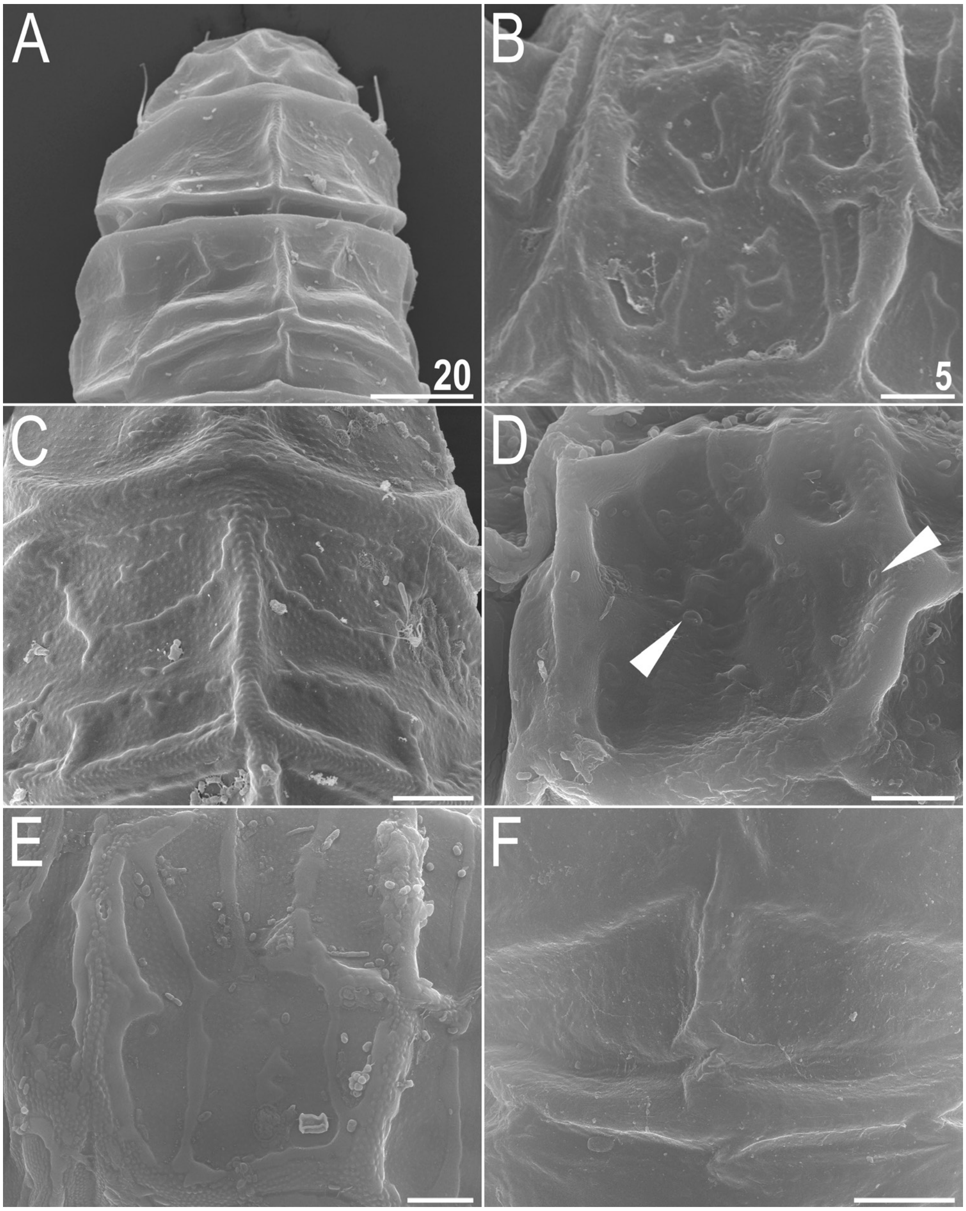

Figure 26. Differences in dorsal plate sculpturing between various members of the genus *Hypechiniscus* Thulin, 1928 (SEM): A, focus in the following microphotographs was on the scapular or the first segmental plates of the body armour (*H. gladiator* here); B, *H. gladiator*; C, *H. daedalus*; D, *H. flavus*, arrowheads indicate epicuticular rings; E, *H. geminus*; F, *Hypechiniscus cataractus.* All scale bars = 5 µm, with the exception of A.

Larvae (i.e. the first instar; measurements and statistics in Table 18): Gonopore and anus absent. Dorsal sculpturing weakly developed. Clearly smaller than juveniles.

Eggs: One to four round, white eggs per exuvia.

Genetic markers: Single haplotypes were presented for 18S rRNA, 28S rRNA and *COI* in Jørgensen *et al.* (2011); see Table 3 for details.

Type material: Holotype (adult female, slide JP.006.13), allotype (adult male, slide JP.008.03) and 87 paratypes (48♀♀, 14♂♂, 24 juveniles, 1 larva on slides JP.006.13–20, JP.008.01–9). Slides JP.006.13–20, JP.008.01–3 (12♀♀, 8♂♂, 5 juveniles) deposited in UJ, slides JP.008.04–5 deposited in NHMD (9♀♀, 1♂, 7 juveniles), slide JP.008.06 (9♀♀) deposited in CU and slides JP.008.07–9 (18♀♀, 5♂♂, 12 juveniles, 1 larva) deposited in NMNS.

Downloaded from https://academic.oup.com/zoolinnean/article/192/3/794/6030998 by guest on 18 April 2022

Table 16. Measurements (in μm) of selected morphological structures of the adult females of *Hypechiniscus flavus* (type series) mounted in Hoyer's medium. *N*, number of specimens/structures measured; RANGE refers to the smallest and the largest structure among all measured specimens; SD, standard deviation; *sp*, the proportion between the length of a given structure and the length of the scapular plate

CHARACTER	*N*	RANGE						MEAN		SD		Holotype	
		μm			*sp*			μm	*sp*	μm	*sp*	μm	*sp*
Body length	15	186	–	229	*810*	–	*1068*	205	*936*	13	*69*	208	*920*
Scapular plate length	15	20.0	–	23.7		–		21.9	–	1.2	–	22.6	–
Head appendages lengths													
Cirrus internus	13	7.9	–	11.0	*35.3*	–	*49.8*	9.5	*43.0*	0.9	*4.3*	10.6	*46.9*
Cephalic papilla	15	4.9	–	8.5	*20.7*	–	*37.6*	5.9	*26.9*	0.9	*4.0*	8.5	*37.6*
Cirrus externus	14	12.6	–	19.3	*59.2*	–	*81.5*	16.0	*72.5*	1.7	*6.4*	16.5	*73.0*
Clava	15	3.7	–	6.0	*17.5*	–	*26.5*	4.7	*21.5*	0.6	*2.7*	6.0	*26.5*
Cirrus *A*	15	17.3	–	24.8	*78.2*	–	*107.8*	20.3	*92.4*	2.3	*9.8*	21.8	*96.5*
Cirrus *A*/Body length ratio	15	8%	–	13%		–		10%	–	1%	–	10%	–
Body appendages lengths													
Papilla on leg IV length	13	2.2	–	3.6	*9.5*	–	*17.6*	2.9	*13.5*	0.5	*2.5*	2.4	*10.6*
Claw I heights													
Branch	15	8.7	–	10.9	*40.8*	–	*50.2*	9.7	*44.3*	0.6	*2.7*	10.3	*45.6*
Spur	11	1.3	–	2.3	*6.0*	–	*11.5*	1.7	*7.7*	0.3	*1.7*	2.2	*9.7*
Spur/branch height ratio	11	14%	–	25%		–		17%	–	3%	–	21%	–
Claw II heights													
Branch	15	8.3	–	10.7	*39.0*	–	*50.0*	9.7	*44.4*	0.6	*3.4*	10.7	*47.3*
Spur	11	1.2	–	2.0	*5.2*	–	*8.8*	1.5	*7.1*	0.2	*1.1*	2.0	*8.8*
Spur/branch height ratio	11	12%	–	19%		–		16%	–	2%	–	19%	–
Claw III heights													
Branch	15	8.5	–	10.5	*36.9*	–	*51.0*	9.7	*44.3*	0.6	*3.7*	10.5	*46.5*
Spur	9	1.2	–	1.7	*5.6*	–	*8.3*	1.6	*7.3*	0.2	*0.8*	?	*?*
Spur/branch height ratio	9	13%	–	20%		–		17%	–	2%	–	?	–
Claw IV heights													
Branch	15	9.1	–	12.2	*42.7*	–	*56.5*	10.8	*49.2*	0.8	*4.1*	11.6	*51.3*
Spur	4	1.9	–	2.1	*8.2*	–	*9.1*	2.0	*8.5*	0.1	*0.4*	?	*?*
Spur/branch height ratio	4	16%	–	19%		–		18%	–	1%	–	?	–

© 2020 The Linnean Society of London, *Zoological Journal of the Linnean Society*, 2021, **192**, 794–852

Downloaded from https://academic.oup.com/zoolinnean/article/192/3/794/6030998 by guest on 18 April 2022

Table 17. Measurements (in µm) of selected morphological structures of the adult males of *Hypechiniscus flavus* (type series) mounted in Hoyer's medium. *N*, number of specimens/structures measured; RANGE refers to the smallest and the largest structure among all measured specimens; SD, standard deviation; *sp*, the proportion between the length of a given structure and the length of the scapular plate

CHARACTER	*N*	RANGE						MEAN		SD		Allotype	
		µm			*sp*			µm	*sp*	µm	*sp*	µm	*sp*
Body length	15	153	–	201	*785*	–	*1175*	173	*937*	12	*92*	201	*1005*
Scapular plate length	15	16.0	–	20.9		–		18.5	–	1.5	–	20.0	–
Head appendages lengths													
Cirrus internus	12	7.0	–	9.6	*35.9*	–	*52.7*	8.3	*44.8*	0.8	*5.0*	8.4	*42.0*
Cephalic papilla	15	4.8	–	9.0	*25.6*	–	*43.5*	6.5	*35.2*	1.1	*4.5*	7.0	*35.0*
Cirrus externus	14	9.8	–	18.8	*61.3*	–	*93.5*	14.7	*79.4*	2.4	*10.9*	14.8	*74.0*
Clava	15	3.4	–	7.0	*21.0*	–	*34.8*	5.4	*28.9*	0.9	*4.0*	5.8	*29.0*
Cirrus *A*	12	15.0	–	21.4	*85.2*	–	*123.8*	18.2	*99.1*	1.7	*12.5*	18.5	*92.5*
Cirrus *A*/Body length ratio	12	8%	–	13%		–		10%	–	1%	–	9%	–
Body appendages lengths													
Papilla on leg IV length	12	2.1	–	3.6	*12.8*	–	*18.5*	2.8	*15.1*	0.4	*2.0*	?	*?*
Claw I heights													
Branch	15	7.2	–	10.7	*36.9*	–	*56.4*	9.2	*49.9*	0.9	*4.5*	9.9	*49.5*
Spur	10	1.3	–	1.7	*7.3*	–	*8.7*	1.5	*7.9*	0.1	*0.5*	1.5	*7.5*
Spur/branch height ratio	10	15%	–	18%		–		16%	–	1%	–	21%	–
Claw II heights													
Branch	14	6.9	–	10.2	*43.1*	–	*56.0*	9.1	*48.8*	0.9	*3.1*	10.2	*51.0*
Spur	11	1.0	–	2.0	*6.3*	–	*9.9*	1.5	*7.9*	0.3	*1.2*	1.3	*6.5*
Spur/branch height ratio	11	13%	–	21%		–		16%	–	2%	–	19%	–
Claw III heights													
Branch	13	6.6	–	10.3	*41.3*	–	*55.1*	9.1	*48.7*	1.0	*4.1*	10.3	*51.5*
Spur	7	1.0	–	2.0	*5.1*	–	*9.9*	1.6	*8.0*	0.3	*1.7*	1.6	*8.0*
Spur/branch height ratio	7	12%	–	21%		–		16%	–	3%	–	16%	–
Claw IV heights													
Branch	15	8.1	–	12.0	*47.7*	–	*63.6*	10.7	*58.1*	1.0	*4.2*	11.4	*57.0*
Spur	3	1.9	–	2.1	*9.9*	–	*10.5*	2.0	*10.2*	0.1	*0.3*	2.1	*10.5*
Spur/branch height ratio	3	16%	–	18%		–		18%	–	1%	–	18%	–

Downloaded from https://academic.oup.com/zoolinnean/article/192/3/794/6030998 by guest on 18 April 2022

Table 18. Measurements (in µm) of selected morphological structures of the juveniles and a larva of *Hypechiniscus flavus* (type series) mounted in Hoyer's medium. *N*, number of specimens/structures measured; RANGE refers to the smallest and the largest structure among all measured specimens; SD, standard deviation; *sp*, the proportion between the length of a given structure and the length of the scapular plate

CHARACTER	*N*	RANGE						MEAN		SD		Larva	
		µm			*sp*			µm	*sp*	µm	*sp*	µm	*sp*
Body length	4	137	–	152	*856*	–	*968*	143	*901*	7	*54*	114	*1009*
Scapular plate length	4	15.5	–	16.2		–		15.9	–	0.3	–	11.3	–
Head appendages lengths													
Cirrus internus	4	6.1	–	6.2	*38.3*	–	*39.5*	6.2	*39.0*	0.1	*0.6*	4.8	*42.5*
Cephalic papilla	4	4.5	–	5.5	*27.8*	–	*35.0*	4.9	*30.9*	0.4	*3.0*	4.0	*35.4*
Cirrus externus	4	9.7	–	10.9	*61.8*	–	*68.1*	10.2	*64.3*	0.5	*2.7*	8.5	*75.2*
Clava	3	3.7	–	4.2	*22.8*	–	*26.8*	3.9	*24.4*	0.3	*2.0*	?	*?*
Cirrus *A*	4	15.5	–	17.4	*97.5*	–	*110.8*	16.2	*102.1*	0.9	*5.9*	9.6	*85.0*
Cirrus *A*/Body length ratio	4	11%	–	12%		–		11%	–	0%	–	8%	–
Body appendages lengths													
Papilla on leg IV length	1	2.3	–	2.3	*14.8*	–	*14.8*	2.3	*14.8*	?	*?*	1.6	*14.2*
Claw I heights													
Branch	4	7.1	–	8.3	*44.4*	–	*52.9*	7.7	*48.4*	0.6	*4.0*	6.4	*56.6*
Spur	2	1.1	–	1.2	*7.1*	–	*7.6*	1.2	*7.4*	0.1	*0.4*	0.9	*8.0*
Spur/branch height ratio	2	14%	–	15%		–		15%	–	1%	–	14%	–
Claw II heights													
Branch	4	7.4	–	7.9	*45.7*	–	*51.0*	7.7	*48.5*	0.2	*2.3*	6.2	*54.9*
Spur	1	1.1	–	1.1	*7.1*	–	*7.1*	1.1	*7.1*	?	*?*	0.9	*8.0*
Spur/branch height ratio	1	14%	–	14%		–		14%	–	?	–	15%	–
Claw III heights													
Branch	4	7.4	–	7.8	*45.7*	–	*48.8*	7.5	*47.5*	0.2	*1.4*	6.6	*58.4*
Spur	2	0.9	–	1.1	*5.7*	–	*7.1*	1.0	*6.4*	0.1	*1.0*	1.0	*8.8*
Spur/branch height ratio	2	12%	–	15%		–		13%	–	2%	–	15%	–
Claw IV heights													
Branch	4	7.6	–	9.3	*46.9*	–	*59.2*	8.5	*53.5*	0.7	*5.3*	7.4	*65.5*
Spur	2	1.0	–	1.3	*6.2*	–	*8.4*	1.2	*7.3*	0.2	*1.6*	1.1	*9.7*
Spur/branch height ratio	2	13%	–	15%		–		14%	–	1%	–	15%	–

Downloaded from https://academic.oup.com/zoolinnean/article/192/3/794/6030998 by guest on 18 April 2022

Type locality: 35°56'32"N, 138°20'46"E, 2510 m a.s.l.: Japan, Honshu, Mount Amigasa (see Supporting Information, Fig. S3); Japanese stone pine (*Pinus pumila*) zone; moss from rocks and fallen tree trunks. The species was accompanied by *H. geminus*, *Stellariscus pseudelegans* and a *Pilatobius* sp. nov.

Additional locality: 36°03'31"N, 138°20'43"E, 2127 m a.s.l.: Japan, Honshu, Mugikusa Pass; mixed forest composed of Northern Japanese hemlock [*Tsuga diversifolia* (Maxim.) Mast.] and Maries' fir (*Abies mariesii* Mast.), with the admixture of Japanese larch [*Larix kaempferi* (Lamb.) Carrière] and Erman's birch (*Betula ermanii* Cham.); moss from rocks and fallen tree trunks. The new species was found with *Echiniscus clevelandi* Beasley, 1999, *Echiniscus laterosetosus* Ito, 1993, *Adorybiotus granulatus* (Richters, 1903) and a *Pilatobius* sp. nov.

Etymology: From Latin *flavus* = yellow. Underlining the unusual body colour of the new species. An adjective in the nominative singular.

Phenotypic differential diagnosis: The species is separated from all other known *Hypechiniscus* spp. based on the intensively yellow body colour (Fig. 7), which is atypical for this genus. Moreover, the species is separated from the *gladiator* group by the absence of the *cirrus dorsalis* and it differs from the remaining members of the *exarmatus* group:

- *H. cataractus* by endocuticular pillars visible in LCM (greyish dorsal plates with no apparent pillars visible in LCM in *H. cataractus*; compare Figs 16 with 22).
- *H. exarmatus* by median plates m1–2 undivided (both plates divided by a longitudinal suture in *H. exarmatus*).

Genetic differential diagnosis: Uncorrected *p*-distances between *H. flavus* and other species are as follows [not computable for 28S rRNA since different fragments were sequenced in Jørgensen *et al.* (2011) and in the present study]:

- 18S rRNA: from 3.8% (*H. exarmatus* and *H. geminus*, MT809238, HM193378) to 5.8% (*H. cataractus*, MT809233).

Genetically verified geographic distribution: Eastern Palaearctic: Japan.

Morphometric diversity in *Hypechiniscus*

The first and the second principal components explained a significant portion of the variance (65% for ♀♀ and 63% for ♂♂), whereas each of the subsequent components explained < 10% of the variance. The PC1 (composed mainly of claw and claw spurs dimensions) and PC2 (comprising predominantly lengths of peribuccal appendages, primary clavae and cirri *A*) suggested that ♀♀ of *H. cataractus* are significantly different from the remaining *Hypechiniscus* spp. (Fig. 27A), whereas ♂♂ of *H. cataractus* and *H. gladiator* are distinct both from each other and from the remaining *Hypechiniscus* spp. (Fig. 27B). The variability in morphometric traits largely overlapped for ♀♀ of *H. flavus* and *H. geminus* (Fig. 27A) and for ♂♂ of *H. daedalus* and *H. flavus* (Fig. 27B). All traits constituting PC1 and PC2 were subjected to

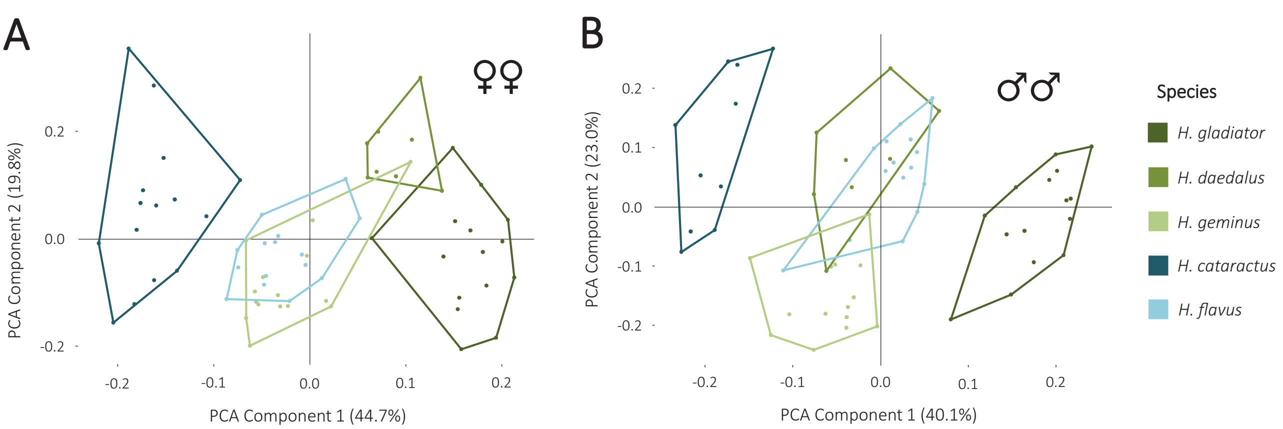

Figure 27. Graphs illustrating the relationships between the first two principal components (PC1–PC2) revealed by the PCA for five *Hypechiniscus* spp. Polygonal shapes indicate the range of variability found in a given species, each represented by a neotype/type population. Colours correspond to those in Figure 1.

Downloaded from https://academic.oup.com/zoolinnean/article/192/3/794/6030998 by guest on 18 April 2022

ANOVA tests, which revealed that differences in lengths of primary clavae and cirri *A* between ♀♀ of *Hypechiniscus* spp. were non-significant, and thus were excluded from Tukey's testing, and the variances of *cirrus internus* lengths for ♂♂ were heterogeneous ($P < 0.05$ in Levene's test), so this trait was not taken into consideration in ANOVA for this sex. The results of the ANOVAs (A) and Tukey's tests (T) for the remaining traits are discussed in the next paragraphs.

Hypechiniscus spp. are not homogenous in terms of the body size (A: body length: ♀♀: $F_{63,4} = 25.53$, ♂♂: $F_{57,4} = 11.11$, $P << 0.001$ in both cases). *Hypechiniscus gladiator* is the largest species, as the post-hoc Tukey's tests revealed that ♀♀ and ♂♂ of the species are always statistically longer than its congeners (T: $P < 0.002$). ♀♀ of *H. cataractus* were found to be smaller than ♀♀ of *H. flavus* (T: $P < 0.01$). Apart from the above, no further disparities were found. In the case of ♂♂ of the remaining four species, no differences were revealed.

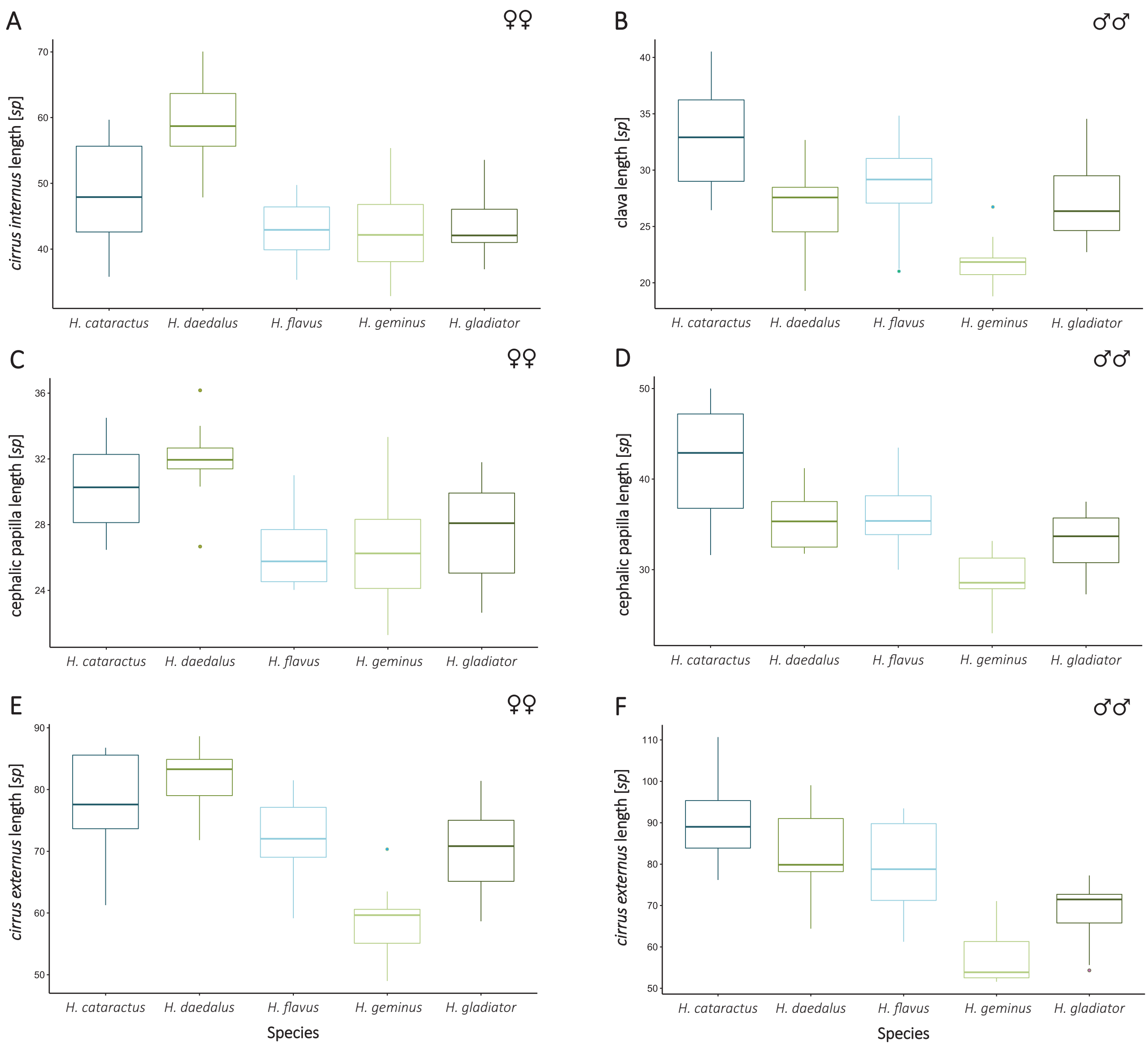

Figure 28. Box plot charts for the relative values (*sp*) of four cephalic appendages in five *Hypechiniscus* spp.: A, *cirrus internus* (♀); B, clava (♂); C, cephalic papilla (♀); D, cephalic papilla (♂); E, *cirrus externus* (♀); F, *cirrus externus* (♂). Boxes represent the interquartile range, whereas the intersection in each box is the median. The whiskers present the variability range of each morphometric trait, excluding outliers marked by filled circles. Population colour codes correspond to those in Figure 1.

Downloaded from https://academic.oup.com/zoolinnean/article/192/3/794/6030998 by guest on 18 April 2022

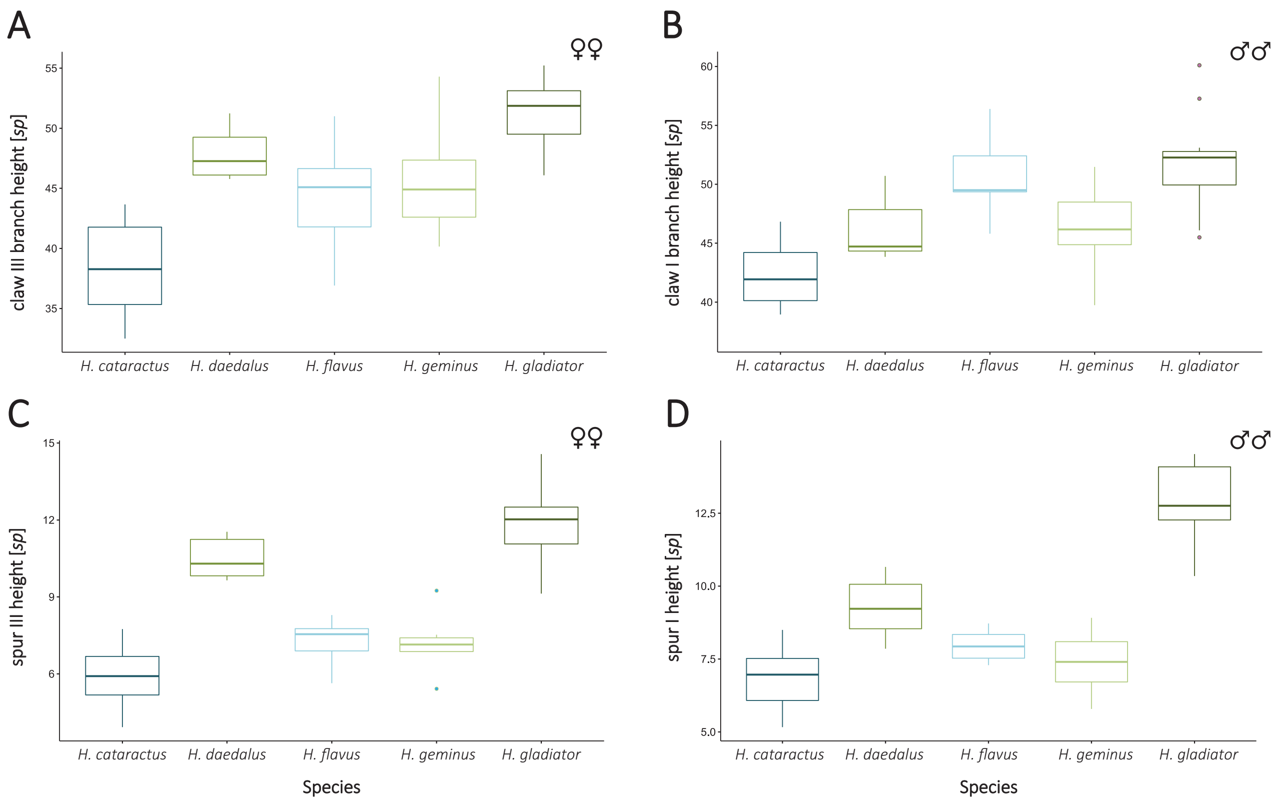

Figure 29. Box plot charts for the relative values (*sp*) of claws in five *Hypechiniscus* spp.: A, claw III branches (♀); B, claw I branches (♂); C, spur III (♀); D, spur I (♂). Boxes represent the interquartile range, whereas the intersection in each box – the median. The whiskers illustrate the variability range of each morphometric trait, excluding outliers marked by filled circles. Population colour codes correspond to those in Figure 1.

In relative terms (i.e. *sp* index values), the lengths of cephalic appendages were highly discriminative for some of the analysed *Hypechiniscus* spp. Specifically, *cirrus internus* was always the longest in ♀♀ of *H. daedalus* (A: $F_{53,4} = 9.68$, $P << 0.001$; T: $P << 0.01$; Fig. 28A), cephalic papilla was always the longest in ♂♂ of *H. cataractus* (A: $F_{53,4} = 14.57$, $P << 0.001$; T: $P < 0.02$; Fig. 28D), and *cirrus externus* was always the shortest in ♀♀ of *H. geminus* (A: $F_{55,4} = 17.67$, $P << 0.001$; T: $P << 0.001$; Fig. 28E). The relative clava length (A: $F_{54,4} = 11.69$, $P << 0.001$) differentiates ♂♂ of *H. cataractus* from all remaining spp. (T: $P < 0.01$) with the exception of ♂♂ of *H. flavus* (Fig. 28B). The clava length is also useful for separating ♂♂ of *H. geminus* from the remaining spp. (T: $P < 0.001$) except for ♂♂ of *H. daedalus* (Fig. 28B). The relative length of the cephalic papilla is useful for the separation of ♀♀ of *H. daedalus* (A: $F_{60,4} = 8.04$, $P << 0.01$; T: $P << 0.001$; Fig. 28C), except for the pair *H. daedalus*–*H. cataractus*, which overlap significantly (T: $P > 0.05$). Finally, ♂♂ of *H. gladiator* and *H. geminus* have relatively the shortest *cirri externi* (A: $F_{51,4} = 20.87$, $P << 0.01$; T: $P < 0.05$; Fig. 28F).

The relative heights of claws and spurs exhibited a slightly different pattern of interspecific variability between sexes. In the case of ♀♀, *H. cataractus* had the shortest claws (e.g. claws III – A: $F_{59,4} = 24.82$, $P << 0.001$; T: $P << 0.001$; Fig. 29A) and *H. gladiator* – the longest (T: $P << 0.001$), except for the pair *H. gladiator*–*H. daedalus* (T: $P > 0.05$). There were no such disparities for ♂♂ (e.g. claws I – A: $F_{52,4} = 11.20$, $P << 0.001$; Fig. 29B), in which Tukey's tests revealed *H. cataractus* has shorter claws than *H. gladiator* and *H. flavus* (T: $P << 0.001$), and *H. gladiator* has longer claws than *H. cataractus* and *H. daedalus* (T: $P << 0.02$). Claw spurs, in turn, are consistently longer in ♀♀ of *H. gladiator* and *H. daedalus* (e.g. spurs III – A: $F_{41,4} = 46.92$, $P << 0.001$; T: $P << 0.001$; Fig. 29C) than in the three other species. In ♂♂, *H. gladiator* has relatively longer spurs than the other species (e.g. spurs I – A: $F_{35,4} = 43.16$, $P << 0.001$; T: $P << 0.001$; Fig. 29D).

Downloaded from https://academic.oup.com/zoolinnean/article/192/3/794/6030998 by guest on 18 April 2022

DISCUSSION

Species diversity and intrageneric phylogeny

Tardigrade taxonomy is progressively entering its 'golden age' since many of the old nominal taxa have been integratively redescribed (e.g. see Gąsiorek *et al.*, 2017, 2018b, 2019b; Grobys *et al.*, 2020 for heterotardigrade cases) and, as a consequence, an extraordinarily rich and undescribed diversity in each lineage of this phylum is being uncovered. Considering this, the doubling of the number of *Hypechiniscus* spp. in the present study is not startling. Although limno-terrestrial tardigrade diversity had been estimated to be mostly delineated (Bartels *et al.*, 2016), the key assumption that the number of known higher taxa is stable turned out to be wrong, as it has increased dramatically in recent years. There are two counteracting factors that influence the number of recognized water bear species: (1) a high number of synonymies or dubious taxa that remain unidentifiable due to inadequate descriptions, especially in the most speciose genera, such as *Echiniscus* or *Isohypsibius* (Degma *et al.*, 2009–20), that lead to taxonomic inflation; (2) recently presented cases of species complexes that can be readily resolved in detail under the integrative taxonomy framework (e.g. Stec *et al.*, 2018; Guidetti *et al.*, 2019). Each of these complexes most likely contain tens of undescribed species, e.g. in *Macrobiotus* (Kaczmarek & Michalczyk, 2017), *Milnesium* (Morek & Michalczyk, 2020) or *Pseudechiniscus* (Cesari *et al.*, 2020). Consequently, the total number of tardigrade species awaits new estimations with improved taxonomic data, i.e. excluding dubious taxa and including the recently uncovered candidate species.

The addition of statistical delimitation of species to the nowadays more commonly applied combination of molecular and morphological methods seems needed not only in the case of *Hypechiniscus*, but for other taxa too (Morek *et al.*, 2019). Crucially, as phenotypic differences between the *Hypechiniscus* spp. exist, the genus is a classic example of pseudocryptic speciation (Sáez *et al.*, 2003). In contrast to the representatives of the paraphyletic *exarmatus* morphogroup, the members of the crown *gladiator* group are more difficult to tell apart, likely because they are the youngest species and the divergence between them is not as deep as between *H. flavus*, *H. exarmatus* and *H. cataractus* (see: Aguilée *et al.*, 2018). The morphological homogeneity within the *gladiator* group, contrasting with evident variability in the *exarmatus* morphogroup, is demonstrated, for example, by identical dorsal patterns in SEM in *H. gladiator*, *H. daedalus* and *H. geminus* versus divergent cuticle phenotypes in *H. flavus* and *H. cataractus* observed in SEM. On the other hand, ventral patterns are species-specific and no general trend for either simplification or additional reinforcement of the venter by epicuticular thickenings is seen, as species equipped with these structures are phylogenetically intermingled with species devoid of such thickenings (Fig. 1). The presence of these thickenings seems to be plesiomorphic, whereas the loss of epicuticular elements on the ventral surface represents advanced convergence, e.g. as found in *H. gladiator* and *H. cataractus* (this hypothesis is strongly supported by the absence of such epicuticular thickenings in other genera, with the exception of *Pseudechiniscus*).

Morphometry constitutes one of the cornerstones of tardigrade taxonomy (Kristensen & Hallas, 1980; Pilato 1981; Bartels *et al.*, 2011; Fontoura & Morais, 2011; Kosztyła *et al.*, 2016; Morek *et al.*, 2019; Santos *et al.*, 2019; Surmacz *et al.*, 2020). Morphometric delimitation of the sexes of different *Hypechiniscus* spp. is sufficient to delineate all currently known species (Figs 27–29). The traits used in the ANOVAs and post hoc tests corroborate the recent analyses of the genus *Nebularmis* (Gąsiorek *et al.*, 2019b), which also utilized claw heights. Interestingly, claw spurs, which were pointed out by Murray (1907) and Kristensen (1987) as relevant in the distinction between *H. exarmatus* and *H. gladiator*, are consistently higher (and more massive) in the latter than in the four other species analysed in this study. Moreover, spur heights separate the sexes in the similar species *H. gladiator* and *H. geminus*. Finally, there are no differences between members of the *gladiator* group in the length of the *cirrus dorsalis*, making this trait, together with the cirrus *A* length, taxonomically uninformative.

Morphology in the context of echiniscid phylogeny

Hypechiniscus is a unique echiniscid genus in terms of morphological characters (Thulin, 1928; Kristensen, 1987). Specifically, the *Pseudechiniscus*-type sculpturing in a genus without pseudosegmental plates, the autapomorphic development of *cirrus dorsalis* in some of its members and an unusual claw curvature distinguish *Hypechiniscus* from other echiniscids. The majority of *Hypechiniscus* spp. have hyaline white or grey-white body, but *H. flavus* is intensely yellow because of a carotenoid pigment, the presence of which is typical for echiniscids. Thanks to the untangling of the *Hypechiniscus* phylogeny, *H. flavus* would appear to be basal with regard to the rest of the *Hypechiniscus* spp., indicating that translucence or white colour is a derived character, a synapomorphy of the remaining species, whereas yellow is a retained plesiomorphy of *H. flavus.* With the odd exception of *H. cataractus*, which exhibits

Downloaded from https://academic.oup.com/zoolinnean/article/192/3/794/6030998 by guest on 18 April 2022

minute claws with a classic echiniscid curvature similar to *Pseudechiniscus* (which may be an example of regressive evolution caused by an adaptation to a specific habitat of the tropical rainforest), the shape of claws and claw spurs also represents an advanced trait in the genus. Of particular interest is the presence of pseudoaccessory points, identifiable only in SEM, which are upwardly directed extensions of the epicuticle on the back side of claw branches (Figs 5C, 9B, 13C) in the three species of the *gladiator* group analysed in this study (a state unknown in *H. papillifer* and *H. fengi*). In contrast, *H. flavus* and *H. cataractus* do not exhibit these structures; thus the examination of *H. exarmatus* in SEM is also needed to confirm the synapomorphic character of this trait in the *gladiator* group. Another trait associated with limbs is the presence of papillae, which can often be tricky to determine in *Hypechiniscus* spp. due to their small size. All species, apart from *H. fengi*, have papillae on leg IV (Sun & Li, 2013), although sometimes these structures can be difficult to identify in LCM. Given that *H. fengi* has not been examined under SEM, the lack of papilla IV needs to be treated as uncertain. The rudimentary papilla I in *H. daedalus*, detectable only in SEM, supports the hypothesis regarding the plesiomorphic nature of the presence of papillae, or triangular spines, on legs I in echiniscids (Tumanov, 2020). Notably, *H. papillifer*, recorded from the Alps, exhibits papillae on legs II–IV (Robotti, 1972), which suggests that preservation of these receptors on legs I–III in the course of evolution may be a conservative trait in *Hypechiniscus*.

The position of *Hypechiniscus* in echiniscid phylogeny has been independently confirmed several times, with the overall congruent placement of this genus as a sister-taxon of the remaining *Echiniscus*-like genera (Jørgensen *et al*., 2011; Cesari *et al*., 2020). Gąsiorek *et al*. (2018c) inferred *Stellariscus*, an endemic East-Asian genus for which genetic data are yet to be obtained, as sister to *Hypechiniscus*, using morphological traits. Both genera share many characters with *Pseudechiniscus*, which, however, belongs to the echiniscid lineage defined by the presence of the pseudosegmental plate IV'. First, *Hypechiniscus* possesses a type of sculpturing that is highly atypical for *Echiniscus*-like genera, i.e. having only endocuticular pillars that are visible as dark dots in PCM and small bumps/granules in NCM and SEM, and lacking pores. This is a character common to all three genera, although in *Stellariscus* and *Pseudechiniscus* the *capituli* (heads) of these pillars are often connected by *striae* (Gąsiorek *et al*., 2018c; Tumanov, 2020), which are absent in *Hypechiniscus*. All three genera exhibit black crystalline eye spots, although it seems that they can dissolve in the smallest representatives and juvenile stages after mounting in Hoyer's medium. Dorsal plates are very weakly sclerotized in *Hypechiniscus* and in the majority of *Pseudechiniscus* spp., thus they are prone to deformation during mounting or preparation for SEM. This property has the potential to give rise to a number of various artefacts, such as 'spines' formed at the edges of dorsal plates in the form *spinulosa* (Iharos, 1973), or false divisions of some plates, such as the scapular plate (Tumanov, 2020). Moreover, our study showed that, similarly to *Pseudechiniscus* (Grobys *et al*., 2020; Tumanov, 2020), the ventral ornamentation pattern is one of the most discriminative taxonomic criteria in *Hypechiniscus*. Whereas *Stellariscus* has the typical spine I, the evidence shown herein, and by Tumanov (2020) for *Pseudechiniscus*, suggests that this receptor was present on legs I in ancestors of both *Hypechiniscus* and *Pseudechiniscus*, and that it was later reduced.

In light of the described novel characters found in *Hypechiniscus*, the generic diagnosis is amended as follows: Small to medium-sized (< 300 µm) echiniscids with black ovoid or rectangular eyes. Cephalic plate subdivided into five or six portions. Other dorsal plates regularly subdivided into smaller portions by sutures or incisions, which may result in pseudodivisions (e.g. of median plates). Dorsal sculpturing of the *Pseudechiniscus* type, i.e. composed solely of endocuticular pillars that may protrude through epicuticle, forming small granules. Ventral sculpturing always present, but ventral plates absent. Clavae elongated (dactyloid). Rigid buccal tube without stylet supports, pharynx with short calcified placoids. Dioecious.

Reproduction and sexual dimorphism

Although males developing directly from larvae, in contrast to females that eclose from juveniles, were first observed in *Hypechiniscus* (Bertolani *et al*., 1984), such heterochrony in sexual maturation does not occur exclusively in this genus. This phenomenon was further described in *Antechiniscus*, *Pseudechiniscus* and *Bryodelphax* by Kristensen (1987). The morphometric data shown herein, and in Claxton (2001), corroborate this supposition for the first two genera, however data are lacking for *Pseudechiniscus* and the only available descriptions of dioecious *Bryodelphax* species with separate measurements for all instars, *B. instabilis* Gąsiorek & Degma, 2018 and *B. nigripunctatus* Degma *et al*., 2020 in Gąsiorek *et al*. (2020), do not allow for drawing a conclusion whether males develop directly from larvae or from juveniles. Conversely, the recent erection of *Stellariscus* contributes to this issue, again highlighting that males probably develop from larvae (Gąsiorek *et al*., 2018c). All above-mentioned genera (except for *Hypechiniscus*) share an important

Downloaded from https://academic.oup.com/zoolinnean/article/192/3/794/6030998 by guest on 18 April 2022

characteristic: their average body size is considerably below or around 200 µm, making them one of the smallest echiniscids. Finally, although *Testechiniscus meridionalis* (Murray, 1906) was treated as having males developing faster than females in Gąsiorek *et al*. (2018c), the data from Gąsiorek *et al*. (2018b) indicate that both sexes develop from juveniles. Accelerated sexual maturation of males, or male progenesis, in microscopic animals has been documented in other representatives of microfauna, e.g. rotifers (Ricci & Melone, 1998) and copepods (Østergaard *et al*., 2005). Progenesis in such *r*-selected microinvertebrates is usually considered to be a side-effect of short generation time and increasing reproduction rate, in which longer lived females are inseminated by their faster developing offspring (Lewontin, 1965). Another hypothesis was postulated for benthic polychaetes, namely that progenesis is an adaptation to counteract high mate search costs (Westheide, 1984), which can be a good explanation for tardigrades, which are often characterized by low population sizes (when a population is defined as a group of conspecific individuals inhabiting a single moss/lichen cushion) and patchy distribution.

Sexual dimorphism in *Hypechiniscus* is rudimentary, but not uniformly reduced. Specifically, three levels of reduction can be distinguished: (I) moderate attenuation of secondary dimorphic traits, where a number of qualitative and quantitative criteria separate males from females (e.g. slender body shape, usually weaker/less discernible ventral sculpturing pattern, swollen cephalic papillae and/or shorter claws in males of *H. gladiator*, *H. flavus* and *H. cataractus*); (II) strong attenuation of secondary dimorphic traits, where a few qualitative and quantitative criteria separate males and females (e.g. slender body shape and swollen cephalic papillae in males of *H. exarmatus*); and (III) only primary sexual dimorphism differentiates the sexes (i.e. the presence of a circular gonopore in males and a sexpartite rosette in females in *H. daedalus* and *H. geminus*). The reduction of sexual dimorphism in *Hypechiniscus* is intriguing given that the genus is characterized by heterochrony – males develop directly from larvae, whereas there is a typical juvenile (second) stage between larvae and sexually mature females (Bertolani *et al*., 1984; Kristensen, 1987). Also, the morphometric data presented in this revision support the earlier observations, as there are clear morphometric gaps between juveniles and females but the body size ranges for juveniles and males overlap (compare relevant morphometric tables above). Progenetic males are usually anatomically simplified (Ricci & Melone, 1998), thus the faster sexual maturation of males should entail the elaboration

Taxonomic key

The key provided below is based solely on qualitative traits of sexually mature (adult) specimens that are readily detectable *in vivo* or under LCM. While this is the usual practice in modern echiniscid taxonomy, previous authors did not distinguish between different life stages, therefore larvae and juveniles are excluded from the key since they are not known for every species.

1. *Cirrus dorsalis* present .... 2 (the *gladiator* group)
–. *Cirrus dorsalis* absent .... 6 (the *exarmatus* group)
2(1). External claws with secondary spurs directed upwards, papillae present on legs II–III .... *H. papillifer*
–. External claws smooth, papillae absent on legs II–III 3
3(2). Papillae not detectable in LCM on any legs .... *H. fengi*
–. Papillae detectable in LCM on legs IV only 4
4(3). Only dorsal endocuticular pillars visible in LCM .... *H. gladiator*
–. Both dorsal endocuticular pillars and epicuticular ornamentation visible in LCM 5
5(4). Ventral endocuticular pillars concentrated in the central portion of the body, forming roughly uniform shape .... *H. geminus* sp. nov.
–. Ventral endocuticular pillars concentrated in the central portion of the body, but clearly subdivided into regular areas joined by only thin strips of pillars .... *H. daedalus* sp. nov.
6(1). Yellow body colour, epicuticular thickenings on ventral cuticle overlap with belts of endocuticular pillars in most parts .... *H. flavus* sp. nov.
–. Translucent or whitish body colour, epicuticular thickenings on ventral cuticle do not overlap with belts of endocuticular pillars or thickenings absent 7
7(6). Endocuticular pillars on the dorsal side visible in LCM .... *H. exarmatus*
–. Endocuticular pillars on the dorsal side absent in LCM .... *H. cataractus* sp. nov.

Downloaded from https://academic.oup.com/zoolinnean/article/192/3/794/6030998 by guest on 18 April 2022

of sexual dimorphism. Interestingly, however, this is not the case in *Hypechiniscus*, whereas in the gonochoristic *Echiniscus* spp., in which both sexes develop from juveniles, the dimorphism is evident mainly in qualitative traits (Claxton, 1996; Claxton & Dastych, 2017; Gąsiorek & Michalczyk, 2020b). This interesting conundrum remains temporarily unexplained. Although there are differences in ventral ornamentation patterns between the sexes, pillars are usually faint in males, thus the resulting patterns are difficult to determine.

BIOGEOGRAPHY

For decades, tardigrade biogeography was not a subject of research as tardigrade species were assumed to be cosmopolitan (Artois *et al*., 2011) under the 'Everything is everywhere but environment selects' hypothesis (Beijerinck, 1913), thus no biogeographic patterns were expected to be uncovered and scrutinized. However, tardigrade biogeography is nowadays a field of lively debate with some studies reporting limited genus/species distributions (Kristensen, 1987; Pilato & Binda, 2001; Gąsiorek *et al*., 2016, 2020; Guidetti *et al*., 2017; Morek & Michalczyk, 2020), while others suggest more complex patterns, both because of the undersampling of many regions of the globe and the patchy distribution of tardigrades in many microhabitats (Meyer, 2006; Degma *et al*., 2011; Gąsiorek *et al*., 2019a, b; Guidetti *et al*., 2019). The presence of many similar (pseudocryptic or cryptic) species further impedes unravelling real faunal composition of a given area and blurs the biogeographic and phylogeographic patterns, which have been observed in various groups [e.g. in insects by Gill *et al*. (2016); crustaceans by Terossi *et al*. (2017); annelids by Cerca *et al*. (2020) and in tardigrades by Gąsiorek *et al*. (2019a) or Morek & Michalczyk (2020)]. The present study questions the majority of the old records of *H. gladiator* and *H. exarmatus* and explicitly shows that some of the earlier records of these two taxa represent new species [*H. geminus* reported as *H. gladiator* and *H. flavus* reported as *H. exarmatus* by Jørgensen *et al*. (2011)]. Moreover, there are further questions regarding the potential extent of geographic distributions of both species. As *H. gladiator* appears to exhibit a preference for cold, mountainous locales of the Western Palaearctic, it is somewhat surprising that this species has not been found in the Polish Tatras (Gąsiorek & Degma, 2018), where climate conditions are similar to those in the Alps. Currently, the locality in Öland reported in this study constitutes the easternmost trustworthy record of this species. The records of *H. gladiator* from the Korean Peninsula (Iharos, 1973) are likely erroneous and are more likely to represent *H. geminus* (described from Japan), *H. fengi* (known from south-eastern China; Sun & Li, 2013) or perhaps they may be yet another new species. Similar caution should be applied to records from North America (Meyer, 2013; Kaczmarek *et al*., 2016), as they potentially represent *H. daedalus*. Analogously, records of *H. exarmatus* from South America (Grigarick *et al*., 1983, *Oreella breviclava* therein), Australia (Claxton, 2004) and New Zealand (Horning *et al*., 1978), most likely belong to new taxa. To summarize, current data suggest limited distributions and weak dispersal abilities of *Hypechiniscus* species. This, combined with an apparent absence of species in environments that should support them, indicate that species in the genus *Hypechiniscus* are not cosmopolitan, but seem to be geographically structured.

ACKNOWLEDGEMENTS

Sample collectors are gratefully acknowledged (alphabetically): Nate Gross, Mackenzie McClay, Małgorzata Mitan and Małgorzata Osielczak. Brent McGuirt kindly allowed the use of the photograph showing the habitat of *Hypechiniscus daedalus*. Two reviewers and the Editor in Chief, Dr Maarten Christenhusz, are thanked for improving the manuscript. The study was supported by the Polish Ministry of Science and Higher Education via the Diamond Grant (DI2015 014945 to PG, supervised by ŁM), by the Preludium grant funded by the National Science Centre (grant no. 2019/33/N/NZ8/02777 to PG, supervised by ŁM), the SYNTHESYS programme (grants no. HU-TAF-2224 to ŁM and DK-TAF-6332 to PG) and by the Carlsberg Foundation (grant no. CF16-0236 to RMK, from which the short internship of PG at NHMD was financed). Some of the analyses were carried out with the equipment purchased from the Sonata Bis programme of the Polish National Science Centre (grant no. 2016/22/E/NZ8/00417 to ŁM). PG was supported by the START stipend from the Foundation for Polish Science (FNP) and the Etiuda stipend (2020/36/T/NZ8/00360) from the National Science Centre. Open-access publication of this article was funded by the BioS Priority Research Area under the programme "Excellence Initiative – Research University" at the Jagiellonian University in Kraków, Poland. The authors declare no conflict of interest.

REFERENCES

Aguilée R, **Gascuel F**, **Lambert A**, **Ferriere R. 2018.** Clade diversification dynamics and the biotic and abiotic controls of speciation and extinction rates. *Nature Communications* **9:** 3013.

Artois T, **Fontaneto D**, **Hummon WD**, **McInnes SJ**, **Todaro MA**, **Sørensen MV**, **Zullini A. 2011.** Ubiquity of microscopic animals? Evidence from the morphological

Downloaded from https://academic.oup.com/zoolinnean/article/192/3/794/6030998 by guest on 18 April 2022

approach in species identification. In: Fontaneto D, ed. *Biogeography of microscopic organisms: is everything small everywhere?* Cambridge: Cambridge University Press, Chapter 13, 244–283.

Bartels PJ, **Nelson DR. 2007.** An evaluation of species richness estimators for tardigrades of the Great Smoky Mountains National Park, Tennessee and North Carolina, USA. *Journal of Limnology* **66:** 104–110.

Bartels PJ, **Nelson DR**, **Exline RP. 2011.** Allometry and the removal of body size effects in the morphometric analysis of tardigrades. *Journal of Zoological Systematics and Evolutionary Research* **49:** 17–25.

Bartels PJ, **Apodaca JJ**, **Mora C**, **Nelson DR. 2016.** A global biodiversity estimate of a poorly known taxon: phylum Tardigrada. *Zoological Journal of the Linnean Society* **178:** 730–736.

Beasley CW. 1999. A new species of *Echiniscus* (Tardigrada, Echiniscidae) from northern Yunnan Province, China. *Zoologischer Anzeiger* **238:** 135–138.

Beijerinck MW. 1913. *De infusies en de ontdekking der backteriën. Jaarboek van de Koninklijke Akademie van Wetenschappen.* Amsterdam: Müller.

Bertolani R, **Rebecchi L. 1993.** A revision of the *Macrobiotus hufelandi* group (Tardigrada, Macrobiotidae), with some observations on the taxonomic characters of eutardigrades. *Zoologica Scripta* **22:** 127–152.

Bertolani R, **Grimaldi de Zio S**, **d'Addabbo Gallo M**, **Morone de Lucia MR. 1984.** Postembryonic development in heterotardigrades. *Monitore Zoologico Italiano* **18:** 307–320.

Casquet J, **Thebaud C**, **Gillespie RG. 2012.** Chelex without boiling, a rapid and easy technique to obtain stable amplifiable DNA from small amounts of ethanol-stored spiders. *Molecular Ecology Resources* **12:** 136–141.

Cerca J, **Meyer C**, **Purschke G**, **Struck TH. 2020.** Delimitation of cryptic species drastically reduces the geographical ranges of marine interstitial ghost-worms (*Stygocapitella*; Annelida, Sedentaria). *Molecular Phylogenetics and Evolution* **143:** 106663.

Cesari M, **Bertolani R**, **Rebecchi L**, **Guidetti R. 2009.** DNA barcoding in Tardigrada: the first case study on *Macrobiotus macrocalix* Bertolani & Rebecchi 1993 (Eutardigrada, Macrobiotidae). *Molecular Ecology Resources* **9:** 699–706.

Cesari M, **Guidetti R**, **Rebecchi L**, **Giovannini I**, **Bertolani R. 2013.** A DNA barcoding approach in the study of tardigrades. *Journal of Limnology* **72:** 182–198.

Cesari M, **McInnes SJ**, **Bertolani R**, **Rebecchi L**, **Guidetti R. 2016.** Genetic diversity and biogeography of the south polar water bear *Acutuncus antarcticus* (Eutardigrada: Hypsibiidae) – evidence that it is a truly pan-Antarctic species. *Invertebrate Systematics* **30:** 635–649.

Cesari M, **Montanari M**, **Kristensen RM**, **Bertolani R**, **Guidetti R**, **Rebecchi L. 2020.** An integrated study of the biodiversity within the *Pseudechiniscus suillus–facettalis* group (Heterotardigrada: Echiniscidae). *Zoological Journal of the Linnean Society* **188:** 717–732.

Chernomor O, **von Haeseler A**, **Minh BQ. 2016.** Terrace aware data structure for phylogenomic inference from supermatrices. *Systematic Biology* **65:** 997–1008.

Claxton SK. 1996. Sexual dimorphism in Australian *Echiniscus* (Tardigrada, Echiniscidae) with descriptions of three new species. *Zoological Journal of the Linnean Society* **116:** 13–33.

Claxton SK. 1998. A revision of the genus *Minibiotus* (Tardigrada: Macrobiotidae) with descriptions of eleven new species from Australia. *Records of the Australian Museum* **50:** 125–160.

Claxton SK. 2001. *Antechiniscus* in Australia: Description of *Antechiniscus moscali* sp. n. and redescription of *Antechiniscus parvisentus* (Horning & Schuster, 1983) (Heterotardigrada: Echiniscidae). *Zoologischer Anzeiger* **240:** 281–289.

Claxton SK. 2004. *The taxonomy and distribution of Australian terrestrial tardigrades.* Unpublished Ph.D. Thesis, Macquarie University, Australia, 618 + 182.

Claxton SK, **Dastych H. 2017.** A new bisexual species of *Echiniscus* C.A.S. Schultze, 1840 (Heterotardigrada: Echiniscidae) from Tasmania, Australia. *Entomologie heute* **29:** 105–119.

da Cunha AX. 1947. Description d'un tardigrade nouveau de la faune portugaise, *Parechiniscus unispinosus* sp. n. *Memórias e Estudos do Museu Zoológico da Universidade de Coimbra* **180:** 1–6.

Dastych H. 1999. A new species of the genus *Mopsechiniscus* Du Bois-Reymond Marcus, 1944 (Tardigrada) from the Venezuelan Andes. *Acta Biologica Benrodis* **10:** 91–101.

Dastych H, **McInnes SJ**, **Claxton SK. 1998.** *Oreella mollis* Murray, 1910 (Tardigrada): a redescription and revision of *Oreella*. *Mitteilungen aus dem Hamburgischen Zoologischen Museum und Institut* **95:** 89–113.

Degma P, **Bertolani R**, **Guidetti R. 2009–20.** *Actual checklist of Tardigrada species, v.38: 18-08-2020.* Available at: https://doi.org/10.25431/11380_1178608 (accessed 18 August 2020).

Degma P, **Katina S**, **Sabatovičová L. 2011.** Horizontal distribution of moisture and Tardigrada in a single moss cushion. *Journal of Zoological Systematics and Evolutionary Research* **49:** 71–77.

Faurby S, **Jørgensen A**, **Kristensen RM**, **Funch P. 2011.** Phylogeography of North Atlantic intertidal tardigrades: refugia, cryptic speciation and the history of the Mid-Atlantic Islands. *Journal of Biogeography* **38:** 1613–1624.

Folmer O, **Black M**, **Hoeh W**, **Lutz R**, **Vrijenhoek R. 1994.** DNA primers for amplification of mitochondrial cytochrome c oxidase subunit I from diverse metazoan invertebrates. *Molecular Marine Biology and Biotechnology* **3:** 294–299.

Fontoura P, **Morais P. 2011.** Assessment of traditional and geometric morphometrics for discriminating cryptic species of the *Pseudechiniscus suillus* complex (Tardigrada, Echiniscidae). *Journal of Zoological Systematics and Evolutionary Research* **49:** 26–33.

Fox J, **Weisberg S. 2011.** *An {R} companion to applied regression, 2nd edn.* Thousand Oaks: Sage. Available at: https://socsery.socsci.mcmaster.ca/jfox/Books/Companion (accessed 01 March 2020).

Gąsiorek P, **Degma P. 2018.** Three Echiniscidae species (Tardigrada: Heterotardigrada) new to the Polish fauna, with the description of a new gonochoristic *Bryodelphax* Thulin, 1928. *Zootaxa* **4410:** 77–96.

Downloaded from https://academic.oup.com/zoolinnean/article/192/3/794/6030998 by guest on 18 April 2022

Gąsiorek P, **Michalczyk Ł. 2020a.** Revised *Cornechiniscus* (Heterotardigrada) and new phylogenetic analyses negate echiniscid subfamilies and tribes. *Royal Society Open Science* **7:** 200581.

Gąsiorek P, **Michalczyk Ł. 2020b.** *Echiniscus siticulosus* (Echiniscidae: *spinulosus* group), a new tardigrade from Western Australian scrub. *New Zealand Journal of Zoology* **47:** 87–105.

Gąsiorek P, **Stec D**, **Morek W**, **Zawierucha K**, **Kaczmarek Ł**, **Lachowska-Cierlik D**, **Michalczyk Ł. 2016.** An integrative revision of *Mesocrista* Pilato, 1987 (Tardigrada: Eutardigrada: Hypsibiidae). *Journal of Natural History* **50:** 2803–2828.

Gąsiorek P, **Stec D**, **Morek W**, **Michalczyk Ł. 2017.** An integrative redescription of *Echiniscus testudo* (Doyère, 1840), the nominal taxon for the class Heterotardigrada (Ecdysozoa: Panarthropoda: Tardigrada). *Zoologischer Anzeiger* **270:** 107–122.

Gąsiorek P, **Stec D**, **Morek W**, **Michalczyk Ł. 2018a.** An integrative redescription of *Hypsibius dujardini* (Doyère, 1840), the nominal taxon for Hypsibioidea (Tardigrada: Eutardigrada). *Zootaxa* **4415:** 45–75.

Gąsiorek P, **Stec D**, **Zawierucha K**, **Kristensen RM**, **Michalczyk Ł. 2018b.** Revision of *Testechiniscus* Kristensen, 1987 (Heterotardigrada: Echiniscidae) refutes the polar-temperate distribution of the genus. *Zootaxa* **4472:** 261–297.

Gąsiorek P, **Suzuki AC**, **Kristensen RM**, **Lachowska-Cierlik D**, **Michalczyk Ł. 2018c.** Untangling the *Echiniscus* Gordian knot: *Stellariscus* gen. nov. (Heterotardigrada: Echiniscidae) from Far East Asia. *Invertebrate Systematics* **32:** 1234–1247.

Gąsiorek P, **Jackson KJ**, **Meyer HA**, **Zając K**, **Nelson DR**, **Kristensen RM**, **Michalczyk Ł. 2019a.** *Echiniscus virginicus* complex: the first case of pseudocryptic allopatry and pantropical distribution in tardigrades. *Biological Journal of the Linnean Society* **128:** 789–805.

Gąsiorek P, **Blagden B**, **Michalczyk Ł. 2019b.** Towards a better understanding of echiniscid intraspecific variability: a redescription of *Nebularmis reticulatus* (Murray, 1905) (Heterotardigrada: Echiniscoidea). *Zoologischer Anzeiger* **283:** 242–255.

Gąsiorek P, **Vončina K**, **Degma P**, **Michalczyk Ł. 2020.** Small is beautiful: the first phylogenetic analysis of *Bryodelphax* Thulin, 1928 (Heterotardigrada, Echiniscidae). *Zoosystematics and Evolution* **96:** 217–236.

Gill BA, **Kondratieff BC**, **Casner KL**, **Encalada AC**, **Flecker AS**, **Gannon DG**, **Ghalambor CK**, **Guayasamin JM**, **Poff NL**, **Simmons MP**, **Thomas SA**, **Zamudio KR**, **Funk WC. 2016.** Cryptic species diversity reveals biogeographic support for the 'mountain passes are higher in the tropics' hypothesis. *Proceedings of the Royal Society B: Biological Sciences* **283:** 20160553.

Grigarick AA, **Schuster RO**, **Nelson DR. 1983.** Heterotardigrada of Venezuela (Tardigrada). *Pan-Pacific Entomologist* **59:** 64–77.

Grobys D, **Roszkowska M**, **Gawlak M**, **Kmita H**, **Kepel A**, **Kepel M**, **Parnikoza I**, **Bartylak T**, **Kaczmarek Ł. 2020.** High diversity in the *Pseudechiniscus suillus–facettalis* complex (Heterotardigrada; Echiniscidae) with remarks on the morphology of the genus *Pseudechiniscus*. *Zoological Journal of the Linnean Society* **188:** 733–752.

Guidetti R, **Bertolani R**, **Nelson DR. 1999.** Ecological and faunistic studies on tardigrades in leaf litter of beech forests. *Zoologischer Anzeiger* **238:** 215–223.

Guidetti R, **Jönsson KI**, **Kristensen RM. 2015.** Tardigrades of Sweden; an updated check-list. *Zootaxa* **3981:** 491–507.

Guidetti R, **Rebecchi L**, **Bertolani R**, **Jönsson KI**, **Kristensen RM**, **Cesari M. 2016.** Morphological and molecular analyses on *Richtersius* (Eutardigrada) diversity reveal its new systematic position and lead to the establishment of a new genus and a new family within Macrobiotoidea. *Zoological Journal of the Linnean Society* **178:** 834–845.

Guidetti R, **McInnes SJ**, **Cesari M**, **Rebecchi L**, **Rota-Stabelli O. 2017.** Evolutionary scenarios for the origin of an Antarctic tardigrade species based on molecular clock analyses and biogeographic data. *Contributions to Zoology* **86:** 97–110.

Guidetti R, **Cesari M**, **Bertolani R**, **Altiero T**, **Rebecchi L. 2019.** High diversity in species, reproductive modes and distribution within the *Paramacrobiotus richtersi* complex (Eutardigrada, Macrobiotidae). *Zoological Letters* **5:** 1.

Guil N, **Sanchez-Moreno S. 2013.** Fine-scale patterns in micrometazoans: tardigrade diversity, community composition and trophic dynamics in leaf litter. *Systematics and Biodiversity* **11:** 181–193.

Higgins RP. 1960. Some tardigrades from the Piedmont of North Carolina. *Journal of the Elisha Mitchell Scientific Society* **76:** 29–35.

Hoang DT, **Chernomor O**, **von Haeseler A**, **Minh BQ**, **Vinh LS. 2018.** UFBoot2: Improving the ultrafast bootstrap approximation. *Molecular Biology and Evolution* **35:** 518–522.

Horning DS, **Schuster RO**, **Grigarick AA. 1978.** Tardigrada of New Zealand. *New Zealand Journal of Zoology* **5:** 185–280.

ICZN. **1999.** *International code of zoological nomenclature, fourth ed.* London: The International Trust for Zoological Nomenclature, 306.

Iharos G. 1973. Angaben zur geographischen Verbreitung der Tardigraden. *Opuscula Zoologica, Budapest* **12:** 73–86.

Ito M. 1993. Taxonomic study on the class Heterotardigrada (Tardigrada) from the Northern Slope of Mt. Fuji, Central Japan. *Edaphologia* **50:** 1–13.

Jackson KJA, **Meyer HA. 2019.** Morphological and genetic analysis of *Milnesium* cf. *granulatum* (Tardigrada: Milnesiidae) from Northeastern North America. *Zootaxa* **4604:** 497–510.

Jørgensen A, **Møbjerg N**, **Kristensen RM. 2011.** Phylogeny and evolution of the Echiniscidae (Echiniscoidea, Tardigrada) – an investigation of the congruence between molecules and morphology. *Journal of Zoological Systematics and Evolutionary Research* **49:** 6–16.

Jørgensen A, **Kristensen RM**, **Møbjerg N. 2018.** Phylogeny and integrative taxonomy of Tardigrada. In: Schill RO, ed. *Water bears: the biology of tardigrades. Zoological monographs.* New York: Springer, 95–114.

Downloaded from https://academic.oup.com/zoolinnean/article/192/3/794/6030998 by guest on 18 April 2022

Kaczmarek Ł, **Michalczyk Ł**, **McInnes SJ. 2016.** Annotated zoogeography of non-marine Tardigrada. Part III: North America and Greenland. *Zootaxa* **4203:** 1–249.

Kaczmarek Ł, **Michalczyk Ł. 2017.** The *Macrobiotus hufelandi* group (Tardigrada) revisited. *Zootaxa* **4363:** 101–123.

Kalyaanamoorthy S, **Minh BQ**, **Wong TKF**, **von Haeseler A**, **Jermiin LS. 2017.** ModelFinder: fast model selection for accurate phylogenetic estimates. *Nature Methods* **14:** 587–589.

Katoh K, **Toh H. 2008.** Recent developments in the MAFFT multiple sequence alignment program. *Briefings in Bioinformatics* **9:** 286–298.

Katoh K, **Misawa K**, **Kuma K**, **Miyata T. 2002.** MAFFT: a novel method for rapid multiple sequence alignment based on fast Fourier transform. *Nucleic Acids Research* **30:** 3059–3066.

Kendall-Fite K, **Nelson DR. 1996.** Two new species of tardigrades from Short Mountain, Tennessee, U.S.A. *Zoological Journal of the Linnean Society* **116:** 205–214.

Kosztyła P, **Stec D**, **Morek W**, **Gąsiorek P**, **Zawierucha K**, **Michno K**, **Ufir K**, **Małek D**, **Hlebowicz K**, **Laska A**, **Dudziak M**, **Frohme M**, **Prokop ZM**, **Kaczmarek Ł**, **Michalczyk Ł. 2016.** Experimental taxonomy confirms the environmental stability of morphometric traits in a taxonomically challenging group of microinvertebrates. *Zoological Journal of the Linnean Society* **178:** 765–775.

Kristensen RM. 1987. Generic revision of the Echiniscidae (Heterotardigrada), with a discussion of the origin of the family. In: Bertolani R, ed. *Biology of Tardigrades. Selected Symposia and Monographs U.Z.I.* **1:** 261–335.

Kristensen RM, **Hallas TE. 1980.** The tidal genus *Echiniscoides* and its variability, with erection of Echiniscoididae fam. n. (Tardigrada). *Zoologica Scripta* **9:** 113–127.

Lanfear R, **Frandsen PB**, **Wright AM**, **Senfeld T**, **Calcott B. 2016.** PartitionFinder 2: new methods for selecting partitioned models of evolution for molecular and morphological phylogenetic analyses. *Molecular Biology and Evolution* **34:** 772–773.

Lewontin RC. 1965. Selection for colonizing ability. In: Baker HG, Stebbins GL, eds. *The genetics of colonizing species: Proceedings of the First International Union of Biological Sciences Symposia on General Biology.* New York and London: Academic Press, 77–94.

Lisi O. 2011. Remarks on *Doryphoribius flavus* (Iharos, 1966), and description of three new species (Tardigrada, Hypsibiidae). *Zootaxa* **2834:** 17–32.

Maucci W. 1986. *Tardigrada. Fauna d`Italia.* Bologna: Edizioni Calderini.

Maucci W. 1996. Tardigrada of the Arctic tundra with descriptions of two new species. *Zoological Journal of the Linnean Society* **116:** 185–204.

McInnes SJ. 1994. Zoogeographic distribution of terrestrial/freshwater tardigrades from current literature. *Journal of Natural History* **28:** 257–352.

Meyer HA. 2006. Small-scale spatial distribution variability in terrestrial tardigrade populations. *Hydrobiologia* **558:** 133–139.

Meyer HA. 2013. Terrestrial and freshwater Tardigrada of the Americas. *Zootaxa* **3747:** 1–71.

Michalczyk Ł, **Kaczmarek Ł. 2013.** The Tardigrada Register: a comprehensive online data repository for tardigrade taxonomy. *Journal of Limnology* **72:** 175–181.

Michalczyk Ł, **Wełnicz W**, **Frohme M**, **Kaczmarek Ł. 2012.** Redescriptions of three *Milnesium* Doyère, 1840 taxa (Tardigrada: Eutardigrada: Milnesiidae), including the nominal species for the genus. *Zootaxa* **3154:** 1–20.

Mironov SV, **Dabert J**, **Dabert M. 2012.** A new feather mite species of the genus *Proctophyllodes* Robin, 1877 (Astigmata: Proctophyllodidae) from the long-tailed tit *Aegithalos caudatus* (Passeriformes: Aegithalidae): morphological description with DNA barcode data. *Zootaxa* **3253:** 54–61.

Morek W, **Michalczyk Ł. 2020.** First extensive multilocus phylogeny of the genus *Milnesium* (Tardigrada) reveals no congruence between genetic markers and morphological traits. *Zoological Journal of the Linnean Society* **188:** 681–693.

Morek W, **Stec D**, **Gąsiorek P**, **Michalczyk Ł. 2019.** *Milnesium tardigradum* Doyère, 1840: the first integrative study of interpopulation variability in a tardigrade species. *Journal of Zoological Systematics and Evolutionary Research* **57:** 1–23.

Morgan CI. 1977. An annotated catalogue of Tardigrada in the collections of the Royal Scottish Museum, Edinburgh. *Natural History* **5:** 1–29.

Morgan CI, **King PE. 1976.** British tardigrades. *Synopses of the British Fauna* **9:** 1–133.

Morikawa K. 1951. Notes on four interesting *Echiniscus* (Tardigrada) from Japan. *Annotationes Zoologicae Japonenses* **24:** 108–110.

Murray J. 1905. The Tardigrada of the Scottish Lochs. *Transactions of the Royal Society of Edinburgh* **41:** 677–698.

Murray J. 1906. Scottish national Antarctic expedition: Tardigrada of the South Orkneys. *Transactions of the Royal Society of Edinburgh* **45:** 323–334.

Murray J. 1907. Scottish Tardigrada, collected by the lake survey. *Transactions of the Royal Society Edinburgh* **45:** 641–668.

Murray J. 1911. Clare Island survey. Arctiscoida. *Proceedings of the Royal Irish Academy* **31:** 1–16.

Nelson DR. 1975. Ecological distribution of tardigrades on Roan Mountain, Tennessee - North Carolina. In: Higgins RP, ed. *Proceedings of the first international symposium on Tardigrades. Memorie dell'Istituto Italiano di Idrobiologia, Pallanza* **Supplement 32:** 225–276.

Nelson DR, **Bartels PJ. 2007.** 'Smoky bears' – tardigrades of the Great Smoky Mountains National Park. *Southeastern Naturalist* **6:** 229–238.

Nelson DR, **Bartels PJ. 2013.** Species richness of soil and leaf litter tardigrades in the Great Smoky Mountains National Park (North Carolina/Tennessee, USA). *Journal of Limnology* **72:** 144–151.

Nelson DR, **Bartels PJ**, **Fegley SR. 2020.** Environmental correlates of tardigrade community structure in mosses

Downloaded from https://academic.oup.com/zoolinnean/article/192/3/794/6030998 by guest on 18 April 2022

and lichens in the Great Smoky Mountains National Park (Tennessee and North Carolina, USA). *Zoological Journal of the Linnean Society* **188:** 913–924.

Nguyen L-T, **Schmidt HA**, **von Haeseler A**, **Minh BQ. 2015.** IQ-TREE: a fast and effective stochastic algorithm for estimating maximum likelihood phylogenies. *Molecular Biology and Evolution* **32:** 268–274.

Østergaard P, **Boxshall GA**, **Quicke DLJ. 2005.** Dwarfs or giants? Sexual size dimorphism in Chondracanthidae (Copepoda, Poecilostomatoida). *Crustaceana* **78:** 397–408.

Petersen B. 1951. The tardigrade fauna of Greenland. *Meddelelser om Grønland* **150:** 1–94.

Pilato G. 1981. Analisi di nuovi caratteri nello studio degli Eutardigradi. *Animalia* **8:** 51–57.

Pilato G, **Binda MG. 2001.** Biogeography and limno-terrestrial tardigrades: Are they truly incompatible binomials? *Zoologischer Anzeiger* **240:** 511–516.

Ramazzotti G. 1956. Tre nuove specie di tardigradi ed altre specie poco comuni. *Atti della Società Italiana di Scienze Naturali e del Museo Civico di Storia Naturale in Milano* **95:** 284–291.

Rambaut A, **Suchard MA**, **Xie D**, **Drummond AJ. 2014.** *Tracer v.1.6.* Available at: https://beast.bio.ed.ac.uk/Tracer (accessed 01 February 2020).

Refaat M. 2007. Treatment of missing values. Chapter 11. In: Refaat M, ed. *Data preparation for data mining using SAS.* San Franisco: Morgan Kaufmann Publishers, 171–206.

Ricci C, **Melone G. 1998.** Dwarf males in monogonont rotifers. *Aquatic Ecology* **32:** 361–365.

Richters F. 1903. Nordische Tardigraden. *Zoologischer Anzeiger* **27:** 168–172.

Richters F. 1904. Arktische Tardigraden. *Fauna Arctica* **3:** 495–511.

Riggin GT. 1962. Tardigrada of southwest Virginia: with the addition of a description of a new marine species from Florida. *Virginia Agricultural Experiment Station Technical Bulletin* **152:** 1–147.

Robotti C. 1972. Secondo contributo alla conoscenza dei tardigradi del Piemonte, con la descrizione di *Echiniscus* (*Hyp.*) *papillifer* spec. nov. e di *Hexapodibius pseudomicronyx* spec. nov. *Atti della Società Italiana di Scienze Naturali e del Museo Civico di Storia Naturale in Milano* **133:** 153–162.

Ronquist F, **Huelsenbeck JP. 2003.** MrBayes 3: Bayesian phylogenetic inference under mixed models. *Bioinformatics* **19:** 1572–1574.

RStudio Team. **2015.** *RStudio.* Boston: Integrated Development for R. RStudio, Inc. Available at: https://www.rstudio.com (accessed 01 March 2020).

Sáez AG, **Probert I**, **Geisen M**, **Quinn P**, **Young JR**, **Medlin LK. 2003.** Pseudo-cryptic speciation in coccolithophores. *Proceedings of the National Academy of Sciences of the USA* **100:** 7163–7168.

Santos E, **Veiga P**, **Rubal M**, **Bartels PJ**, **da Rocha CMC**, **Fontoura P. 2019.** *Batillipes pennaki* Marcus, 1946 (Arthrotardigrada: Batillipedidae): deciphering a species complex. *Zootaxa* **4648:** 549–567.

Sellnick M. 1908. Beitrag zur Moosfauna der Faröer. *Zoologischer Anzeiger* **33:** 208–212.

Séméria Y. 1994. Une espèce nouvelle de tardigrade de Taiwan: *Echiniscus pseudelegans*, n. sp. (Heterotardigrada Echiniscidae). *Bulletin Mensuel de la Société Linnéenne de Lyon* **63:** 28–30.

Stec D, **Smolak R**, **Kaczmarek Ł**, **Michalczyk Ł. 2015.** An integrative description of *Macrobiotus paulinae* sp. nov. (Tardigrada: Eutardigrada: Macrobiotidae: *hufelandi* group) from Kenya. *Zootaxa* **4052:** 501–526.

Stec D, **Gąsiorek P**, **Morek W**, **Kosztyła P**, **Zawierucha K**, **Michno K**, **Kaczmarek Ł**, **Prokop ZM**, **Michalczyk Ł. 2016.** Estimating optimal sample size for tardigrade morphometry. *Zoological Journal of the Linnean Society* **178:** 776–784.

Stec D, **Zawierucha K**, **Michalczyk Ł. 2017.** An integrative description of *Ramazzottius subanomalus* (Biserov, 1985) (Tardigrada) from Poland. *Zootaxa* **4300:** 403–420.

Stec D, **Morek W**, **Gąsiorek P**, **Michalczyk Ł. 2018.** Unmasking hidden species diversity within the *Ramazzottius oberhaeuseri* complex, with an integrative redescription of the nominal species for the family Ramazzottiidae (Tardigrada: Eutardigrada: Parachela). *Systematics and Biodiversity* **16:** 357–376.

Sun X, **Li X. 2013.** A new species of genus *Hypechiniscus* (Heterotardigrada: Echiniscidae) from China. *Proceedings of the Biological Society of Washington* **126:** 240–244.

Surmacz B, **Morek W**, **Michalczyk Ł. 2020.** What to do when ontogenetic tracking is unavailable: a morphometric method to classify instars in *Milnesium* (Tardigrada). *Zoological Journal of the Linnean Society* **188:** 797–808.

Tang Y, **Horikoshi M**, **Li W. 2016.** Ggfortify: unified interface to visualize statistical result of popular R packages. *R Journal* **8:** 474–485.

Tarter DC, **Nelson DR. 1990.** An altitudinal comparison of the tardigrade fauna (phylum Tardigrada) from mosses on Spruce Mountain, West Virginia. *Proceedings of the West Virginia Academy of Science* **62:** 134–150.

Tarter DC, **Nelson DR. 1994.** Preliminary list of tardigrades (phylum: Tardigrada) from mosses and liverworts in the Monongahela National Forest. *Proceedings of the West Virginia Academy of Science* **66:** 34.

Terossi M, **De Grave S**, **Mantellato FL. 2017.** Global biogeography, cryptic species and systematic issues in the shrimp genus *Hippolyte* Leach, 1814 (Decapoda: Caridea: Hippolytidae) by multimarker analyses. *Scientific Reports* **7:** 6697.

Thulin G. 1911. Beiträge zur Kenntnis der Tardigradenfauna Schwedens. *Arkiv för Zoologi* **7:** 1–60.

Thulin G. 1928. Über die Phylogenie und das System der Tardigraden. *Hereditas* **11:** 207–266.

Trifinopoulos J, **Nguyen L-T**, **von Haeseler A**, **Minh BQ. 2016.** W-IQ-TREE: a fast online phylogenetic tool for maximum likelihood analysis. *Nucleic Acids Research* **44:** 232–235.

Trygvadóttir BV, **Kristensen RM. 2013.** A zoogeographic study of the limnoterrestrial tardigrade fauna on the Faroe Islands. *Journal of Limnology* **72:** 113–122.

Downloaded from https://academic.oup.com/zoolinnean/article/192/3/794/6030998 by guest on 18 April 2022

Tumanov DV. 2020. Analysis of non-morphometric morphological characters used in the taxonomy of the genus *Pseudechiniscus* (Tardigrada: Echiniscidae). *Zoological Journal of the Linnean Society* **188:** 753–775.

Utsugi K, **Hiraoka T. 1997.** The relationship between mosses and tardigrades from Tanzawa Mountains. *Bryological Research* **7:** 83–84.

Utsugi K, **Nunomura N**, **Hiraoka T**, **Nanai N. 1995.** On terrestrial tardigrades and mosses in Toyama Prefecture. *Proceedings of the Japanese Society of Systematic Zoology* **54:** 85–86.

Wełnicz W, **Grohme MA**, **Kaczmarek Ł**, **Schill RO**, **Frohme M. 2011.** ITS-2 and 18S rRNA data from *Macrobiotus polonicus* and *Milnesium tardigradum* (Eutardigrada, Tardigrada). *Journal of Zoological Systematics and Evolutionary Research* **49:** 34–39.

Westheide W. 1984. The concept of reproduction in polychaetes with small body size: adaptations in interstitial species. *Fortschritte der Zoologie* **29:** 265–287.

Zeller C. 2010. *Untersuchung der Phylogenie von Tardigraden anhand der Genabschnitte 18S rDNA und Cytochrom c Oxidase Untereinheit 1 (COX I)*. Unpublished M.Sc. Thesis, Technische Hochschule Wildau, Wildau, 105.

SUPPORTING INFORMATION

Additional Supporting Information may be found in the online version of this article at the publisher's web-site.

Figure S1. The type locality of ***H. daedalus* sp. nov.** in Purchase Knob (North Carolina).
Figure S2. The additional locality of ***H. daedalus* sp. nov.** in Roan Mountain (Tennessee).
Figure S3. The type locality of ***H. geminus* sp. nov.** and ***H. flavus* sp. nov**. in Mount Amigasa (Honshu).
Figure S4. The type locality of ***H. cataractus* sp. nov.** in Bako Peninsula (Borneo).

Downloaded from https://academic.oup.com/zoolinnean/article/192/3/794/6030998 by guest on 18 April 2022